Methodology for developing reduced reaction mechanisms, and their use in combustion simulations

Zettervall, Niklas

2021

Document Version:
Publisher's PDF, also known as Version of record

Methodology for developing reduced reaction mechanisms, and their use in combustion simulations

NIKLAS ZETTERVALL
DIVISION OF COMBUSTION PHYSICS | DEPARTMENT OF PHYSICS | LUND UNIVERSITY

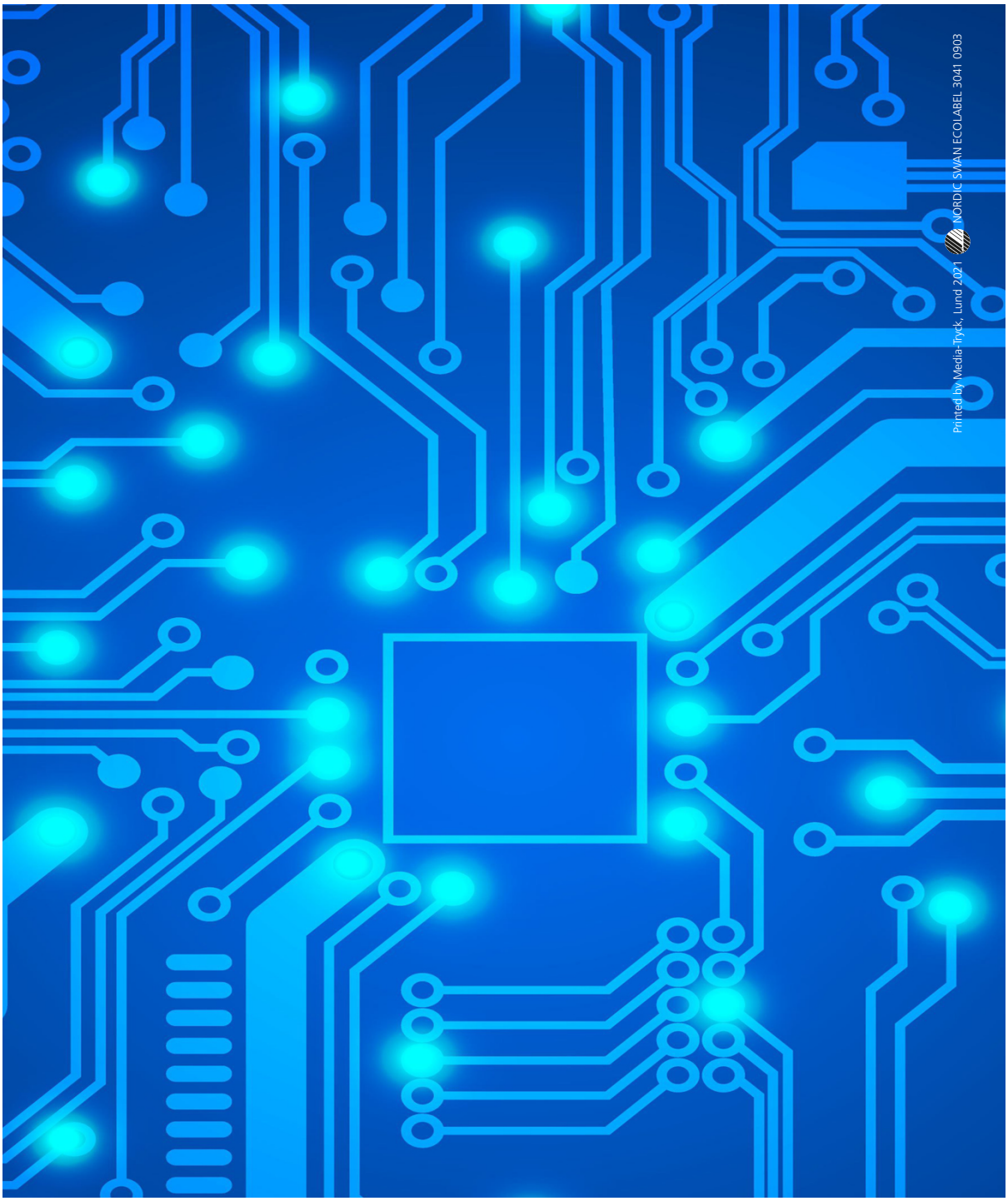

Printed by Media-Tryck, Lund 2021 NORDIC SWAN ECOLABEL 3041 0903

Faculty of Engineering
Department of Physics
Division of Combustion Physics

Lund Reports on Combustion Physics, LRCP 228
ISRN LUTFD2/TFCP-228-SE
ISBN 978-91-7895-729-3
ISSN 1102-8718

Methodology for developing reduced reaction mechanisms, and their use in combustion simulations

Methodology for developing reduced reaction mechanisms, and their use in combustion simulations

by Niklas Zettervall

LUND
UNIVERSITY

Thesis for the degree of Doctor of Philosophy
Thesis advisors: Associate Prof. Elna Heimdal Nilsson,
Prof. Christer Fureby
Faculty opponent: Associate Prof. Alexei Poludnenko

To be presented, with the permission of the Faculty of Engineering of Lund University, for public criticism at Rybergsalen, Fysicum, Professorsgatan 1, on Friday the 26th of March 2021 at 13:15.

Organization	Document name
LUND UNIVERSITY Department of Combustion Physics Box 118 SE–221 00 LUND Sweden	DOCTORAL DISSERTATION Date of disputation 2021-03-26 Sponsoring organization
Author(s) Niklas Zettervall	

Title and subtitle

Methodology for developing reduced reaction mechanisms, and their use in combustion simulations

Abstract

Combustion, present in a vast majority of energy and material production as well as in transportation, represents a foundation of our modern society. To improve and optimize the applications relying on combustion demand a high level of knowledge, and an ability to simulate the combustion process. To do so three-dimensional Computational Fluid Dynamic (CFD) combustion simulations can be used, where a reaction mechanism is used for describing the chemical process. The aim of this thesis is to develop more accurate and compact reaction mechanisms using a new development technique, and to implement these reaction mechanisms into CFD simulations. Because of the high computational cost associated with using reaction mechanisms the new development technique aim at creating reaction mechanisms that balances predictability and computational cost as efficiently as possible. Previous cheaper, simpler reaction mechanisms are often unable to capture key flame parameters, hence compromising the final CFD simulation results. The new, more chemically correct reaction mechanisms presented in this thesis enables the modelling of a wider array of flame parameters, without demanding a too high computational cost. The development technique builds on the idea of dividing the chemistry into sections, or blocks. The chemical complexity of each individual block depends on its importance to the overall combustion process. By individualizing the chemistry of each block only the most important species and reactions can be included, optimizing the size and predictability. By combining several blocks a complete reaction mechanism can then be produced. With the use of the newly developed improved reaction mechanisms in combustion CFD flame parameters such as flame position, decomposition and final products, ignition time, burning velocity, flame-flame interaction and temperature and pressure distributions can all be improved compared to if simpler reaction mechanisms are used.

Key words

Reduced mechanism, block structure, finite rate chemistry, LES

Classification system and/or index terms (if any)

Supplementary bibliographical information	Language
	English
ISSN and key title 1102-8718	ISBN 978-91-7895-729-3(print) 978-91-7895-730-9(pdf)
Recipient's notes	Number of pages 241 Price
	Security classification

Methodology for developing reduced reaction mechanisms, and their use in combustion simulations

by Niklas Zettervall

LUND
UNIVERSITY

Funding information: The thesis work was financially supported by the Swedish Defence Research Agency FOI, the Swedish Defence Materiel Administration FMV, Siemens Energy, foreign partners, the EU project STRATOFLY, and the EFFECT 1 and EFFECT 2 projects supported by the Swedish Energy Agency.

Cover illustration: graffiti showing "$C_{12}H_{23} \rightarrow C_2 \rightarrow C_1$", written on a circuit board.

Department of Combustion Physics
Faculty of Engineering
Lund University
Box 118
SE–221 00 LUND
Sweden

ISBN: 978-91-7895-729-3 (print)
ISBN: 978-91-7895-730-9 (pdf)
ISSN: 1102-8718
ISRN: LUTFD2/TFCP-228-SE

Printed in Sweden by Media-Tryck, Lund University, Lund 2021

Contents

Populärvetenskaplig sammanfattning

I dagens energikrävande värld kommer 85% av all tillgänglig energi från kol, olja och gas, oräknat alkoholer, vätgas, biomassa och biobränslen [1]. Att förbränna ett bränsle för att utvinna energi är således en grundbult i det moderna samhället, och kommer så vara ett bra tag framöver. För att minimera de negativa effekterna från förbränningen, minska bränsleförbrukningen och för att kunna utveckla bättre att utvinna energi ur olika bränsle måste exakta simuleringsmetoder utvecklas och användas. Arbetet som denna avhandling bygger på handlar om att utveckla nya beräkningsmodeller som beskriver bränslespecifika egenskaper vid förbränning, så kallade reaktionsmekanismer, och använda dessa modeller i tredimensionella CFD-simuleringar (Computational Fluid Dynamics). CFD-simuleringarna kan, tillsammans med välutvecklade reaktionsmekanismer, noggrant modellera ett förbränningsförlopp och dess fysikaliska egenskaper.

De reaktionsmekanismer som tidigare använts i CFD har varit alltför förenklade, ofta med grova felpredikteringar av specifika förbränningsparametrar. Resultatet av detta medför att en CFD-simulering kan misslyckas med att prediktera nyckelparametrar i förbränningsprocessen och därmed göra stora delar av simuleringen oanvändbar. För att undvika detta krävs ofta mer exakta reaktionsmekanismer, som dock fortfarande måste vara beräkningsmässigt tillräckligt billiga för att kunna användas i tredimensionella simuleringar. Den utvecklingsmetodik som presenteras i denna avhandling syftar till ta fram kemiskt mer kompletta reaktionsmekanismer specifikt ämnade för att användas i CFD-simuleringar. Metodiken grundar sig på att dela upp kemin i olika kategorier baserat på den specifika kemins innehåll. Varje kategori kommer sedan att ha en individuell kemisk komplexitet beroende på dess vikt för den övergripande förbränningsprocessen. Genom att kombinera flera kategorier kan en komplett reaktionmekanism byggas från grunden, där endast de ämnen och reaktioner som är nödvändiga för den tilltänkta modelleringen används. På så sätt nås en kompromiss mellan storlek, som påverkar beräkningskostnad, och prediktionsförmåga. Samtliga reaktionsmekanismer som presenteras i denna avhan-

dling modellerar någon kolväte-luftblandning även om utvecklingsmetodiken i sig inte är begränsad till denna typ av bränslen.

De nyutvecklade reaktionsmekanismerna används sedan i CFD-simuleringar i alltifrån enklare labbrännare till flamhållare och annulära förbränningskammare i gasturbiner. I flera av studierna görs även jämförelser mellan de nyutvecklade reaktionsmekanismerna mot både enklare och mer komplexa reaktionsmekanismer från litteraturen. Flamposition, komposition av nedbrytnings- och slutprodukter, antändningstid, flamhastighet, interaktion mellan flammor, temperaturfördelning och tryckfördelning är alla exempel på flamparametrar som blir bättre predikterade när de mer nya reaktionsmekanismerna används. Det ökade antalet ämnen i modelleringen som kommer med de komplexa reaktionsmekanismerna möjliggör även jämförelser mot fler typer av experimentella data, vilket i sig hjälper till att koppla ihop experimentell verksamhet med simuleringar.

Abstract

Combustion, present in a vast majority of energy and material production as well as in transportation, represents a foundation of our modern society. To improve and optimize the applications relying on combustion demand a high level of knowledge, and an ability to simulate the combustion process. To do so three-dimensional Computational Fluid Dynamic (CFD) combustion simulations can be used, where a reaction mechanism is used for describing the chemical process. The aim of this thesis is to develop more accurate and compact reaction mechanisms using a new development technique, and to implement these reaction mechanisms into CFD simulations. Because of the high computational cost associated with using reaction mechanisms the new development technique aim at creating reaction mechanisms that balances predictability and computational cost as efficiently as possible. Previous cheaper, simpler reaction mechanisms are often unable to capture key flame parameters, hence compromising the final CFD simulation results. The new, more chemically correct reaction mechanisms presented in this thesis enables the modelling of a wider array of flame parameters, without demanding a too high computational cost.

The development technique builds on the idea of dividing the chemistry into sections, or blocks. The chemical complexity of each individual block depends on its importance to the overall combustion process. By individualizing the chemistry of each block only the most important species and reactions can be included, optimizing the size and predictability. By combining several blocks a complete reaction mechanism can then be produced.

With the use of the newly developed improved reaction mechanisms in combustion CFD flame parameters such as flame position, decomposition and final products, ignition time, burning velocity, flame-flame interaction and temperature and pressure distributions can all be improved compared to if simpler reaction mechanisms are used.

List of Publications

Thesis publications

I **Large Eddy Simulation of a premixed bluff body stabilized flame using global and skeletal reaction mechanisms**

N. Zettervall, K. Nordin-Bates, E. J. K. Nilsson, C. Fureby (2017) Combustion & Flame, vol. 179, pp. 1–22.

II **Skeletal Methane–Air Reaction Mechanism for Large Eddy Simulation of Turbulent Microwave-Assisted Combustion**

A. Larsson, N. Zettervall, T. Hurtig, E. J. K. Nilsson, A. Ehn, P. Peterson, M. Alden, J. Larfeldt, C. Fureby (2017) Energy & Fuels, vol. 31(2), pp. 1904–1926.

III **Combustion LES of a Multi-Burner Annular Aeroengine Combustor using a Skeletal Reaction Mechanism for Jet-A Air Mixtures**

N. Zettervall, E. Fedina, K. Nordin-Bates, E. Heimdal Nilsson, C. Fureby (2015) 51st AIAA/SAE/ASEE Joint Propulsion Conference, 2015, Orlando, Florida, AIAA - 4020.

IV **Small Skeletal Kinetic Mechanism for Kerosene Combustion**

N. Zettervall, C. Fureby, E. J. K. Nilsson (2016)
Energy & Fuels, vol. 30(11), pp. 9801–9813.

V **Small Skeletal Kinetic Reaction Mechanism for Ethylene-Air Combustion**

N. Zettervall, C. Fureby, E. J. K. Nilsson, (2017)
Energy & Fuels, vol. 31(12), pp. 14138–14149.

VI **Large eddy simulation of CH_4-air and C_2H_4-air combustion in a model annular gas turbine combustor**

N. Zettervall, N.A. Worth, M. Mazur,
J.R. Dawson, C. Fureby (2019)
Proceedings of the Combustion Institute,
vol. 37(4), pp. 5223—5231.

VII **A reduced chemical kinetic reaction mechanism for kerosene-air combustion**

N. Zettervall, C. Fureby, E. J. K. Nilsson, (2020)
Fuel, vol. 269, pp. 117446.

Other Publications

Journal publications

- N. Zettervall; 2020, "Reduced Chemical Kinetic Reaction Mechanism for JP-10-Air Combustion", Energy & Fuels, 34(12), 16624-16635. DOI: 10.1021/acs.energyfuels.0c02971.
- A.J. Aspden, N. Zettervall & C. Fureby; 2019, "An a priori analysis of a DNS database of turbulent lean premixed methane flames for LES with finite-rate chemistry", Proceedings of the Combustion Institute, 37(2), 2601-2609.
- A. Vincent-Randonnier, V. Sabelnikov, A. Ristori, N. Zettervall & C. Fureby; 2019, "An experimental and computational study of hydrogen–air combustion in the LAPCAT II supersonic combustor", Proceedings of the Combustion Institute, 37(3), 3703-3711.
- A. Ehn, P. Petersson, J.J. Zhu, Z.S. Li, M. Aldén, E.J.K., Nilsson, J. Larfeldt, A. Larsson, T. Hurtig, N. Zettervall & C. Fureby; 2017, "Investigations of microwave stimulation of a turbulent low-swirl flame", Proceedings of the Combustion Institute, 36(3), 4121-4128.
- A. Ehn, J.J. Zhu, P. Petersson, Z.S. Li, M. Aldén, C. Fureby, T. Hurtig, N. Zettervall, A. Larsson & J. Larfeldt; 2015, "Plasma assisted combustion: Effects of O_3 on large scale turbulent combustion studied with laser diagnostics and Large Eddy Simulations", Proceedings of the Combustion Institute, 35(3), 3487-3495.

Conference publications

- K. Danel, N. Zettervall & C. Fureby; 2019, "A Combined Experimental and Computational Study of Jet Engine Combustion–Baseline Engine Operation", AIAA – 4328.

- K. Danel, N. Zettervall, T.E. Carlsson & C. Fureby; 2019, "A Combined Experimental and Computational Study of Jet Engine Combustion – Baseline Engine Operation", 8$^{\text{th}}$ European Conference for Aeronautics and Space Sciences (EUCASS). DOI: 10.13009/EUCASS2019-328.

- N. Zettervall & C. Fureby; 2018, "A Computational Study of Ramjet, Scramjet and Dual-mode Ramjet Combustion in Combustor with a Cavity Flameholder", AIAA 2018 – 1146.

- A. Vincent-Randonnier, V. Sabelnikov, A. Ristori, N. Zettervall & C. Fureby; 2018, "A Combined Experimental and Computational Study of the LAPCAT II Supersonic Combustor", AIAA – 5208.

- C. Fureby, A. Ehn, E. Nilsson, P. Petterson, M. Aldén, T. Hurtig, N. Zettervall, Z. Li & J. Larfeldt; 2017, "Investigations of Microwave Stimulation of Turbulent Flames with Implications to Gas Turbine Combustors", AIAA – 1779.

- N. Zettervall, K. Nordin-Bates & C. Fureby; 2015, "Understanding Scramjet Combustion using LES of the HyShot II Combustor", AIAA – 3615.

- C. Fureby, N. Zettervall, S. Kim & S. Menon; 2015, "Large eddy simulation of a simplified lean premixed gas turbine combustor", TSFP-9, P-33. Presented at the 9$^{\text{th}}$ International Symposium on Turbulence and Shear Flow Phenomena, Melbourne, Australia.

- A. Ehn, T. Hurtig, P. Petersson, N. Zettervall, B. Zhou, J. Zhu, Z.S. Li, M. Aldén, C. Fureby, A. Larsson & J. Larfeldt; 2015, "Microwave stimulated combustion investigated by laser diagnostics and chemical kinetics", Proceedings of the 7$^{\text{th}}$ European Combustion Meeting.

- O. Parmhed, H. Edefur, C. Fureby, M. Henriksson, S.H. Peng, S. Wallin & N. Zettervall; 2014, "Simulating jet exhaust plumes for optical propagation calculations", AIAA – 2492.

Glossary

As an introduction to the subject of chemical kinetics and combustion fluid dynamics some commonly used terms, concepts and abbreviations are clarified:

Chemical kinetics: a branch of physical chemistry that describes the rate at which chemical reactions occur.

Reaction mechanism: a step-by-step sequence of reactions with corresponding reaction rate parameters.

Reaction rate coefficients: the coefficients used for the mathematical modelling of the rate of a reaction.

Large Eddy Simulation (LES): a mathematical model for turbulence used in computational fluid dynamics.

Laminar burning velocity, s_L: the speed at which an un-stretched laminar flame will propagate through a mixture of unburned reactants.

Ignition delay time, τ_{ig}: the time it takes for a homogeneous fuel-oxidizer mixture to reach a pre-defined state defined as ignition.

Extinction strain rate, σ_{ext}: a flame parameter showing how much heat loss or aerodynamic stretch a flame can withstand before it quenches.

Negative Temperature Coefficient (NTC): the inherent behaviour of large hydrocarbons where an increase in temperature in certain temperature regimes will produce an increase in ignition time, rather than the more common decrease.

Chapter 1

Introduction

Of today's world energy consumption 85% comes from coal, oil and natural gas, with hydro, nuclear and renewable energy sources adding up to the other 15% [1]. When considering that fuels like biomass, hydrogen (H_2), alcohols and biodiesel can be characterized as renewables the total amount of energy coming from combustion is well above 85% of the world energy consumption. The primary energy consumption in the world, calculated as million tonnes oil equivalent, is shown in Figure 1.1. But it is not only in energy production that combustion plays an essential role; global transportation sector (>99% [2]), weapons and material production are examples of areas where the use of combustion is essential.

Because of the uncertainty of which modes of fuels and engine systems will be used in the future the combustion community needs to expand its fundamental knowledge in these areas in order to answer the upcoming combustion issues and alternatives of the future [2]. To aid in the development in the field of combustion science, and in the improved applications resulting from this increased knowledge, combustion modelling is a key tool. This includes solving and modelling the physics controlling the combustion process, including fluid dynamics and chemistry as well as radiation and heat transfer.

The combustion process is connected to a wide range of length and timescales, from the small scales of molecular motion and the short times of chemical reactions to the large length-scales of the fluid flow and the larger turbulent eddies, connected to long fluid flow times. Because of the very small scales associated with the chemical process the reactions and the production and consumption of species cannot be solved for directly and will need to be modelled. This is where the chemistry modelling comes in. This modelling is composed of a set of species and reactions, each with its corresponding mathematical expression for the rate at which it proceeds. This set of species and reactions together with their rate expression is known as a chemical kinetic *reaction mechanism*.

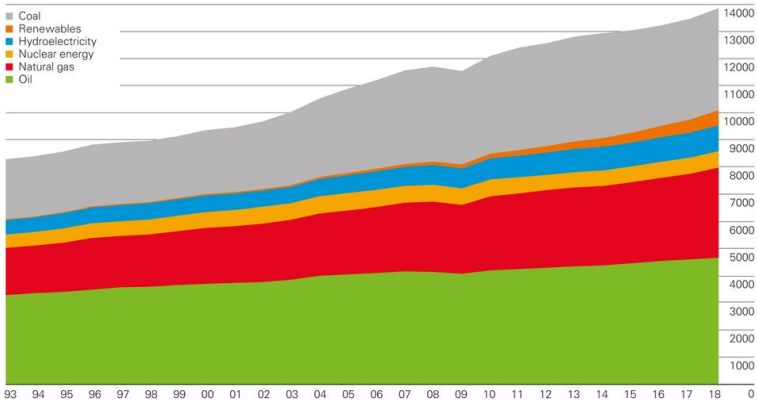

Figure 1.1: Primary world energy consumption [1]. The abscissa shows the year and the ordinate the energy consumption measured in million tonnes oil equivalent.

Due to the high complexity of the combustion process early work in combustion modelling used relatively simple tools, often not resolved in time and with crude models describing the chemical process. As the knowledge of the combustion and modelling fields increased, together with the increases in computational capacities, more accurate and time resolved modelling techniques started to emerge. One such technique is the Large Eddy Simulation [3–6], LES, which has contributed greatly to the understanding of combustion processes. With LES it becomes possible to conduct high-resolved combustion simulations in space and time without the need to solve the governing equations at the smallest length-scales, enabling simulations of complex real-world geometries.

For a long time however the reaction mechanisms used where still relatively simple, implementing only a handful of species and reactions [7–9] to describe what in the real world is a complex physical process involving sometimes hundreds of species and thousands of reactions. If a reaction mechanism is too simple it will not be able to predict key flame characteristics [10–13], and if used in combustion LES' combustion-related processes such as thermoacoustic instabilities, ignition processes, flame position, burning velocities, density variations due to radical species, flame extinction and intermediate and radical species distributions will be challenging, if not to say impossible, to accurately predict. Improved knowledge in the field of chemical kinetics together with increased computational capacities has resulted in the used of more accurate, computationally expensive and chemically complex reaction mechanisms. The LES studies using simple reaction mechanisms in the 1990's [14,15] and 2000's [16–19] are now being replaced by more sophisticated and accurate ones [11, 12, 20–22].

In order for a reaction mechanism to capture key combustion parameters its chemical complexity will need to increase compared to the simpler earlier reaction mechanisms, meaning that more species and reactions need to be included. However, if the reaction mechanism is to be used in combustion LES it also need to be computationally cheap enough, a difficult task since a majority of the computational efforts is spent on solving the chemistry model alone. This creates a delicate balance between chemical complexity, predictability of flame characteristics and computational cost.

With the use of LES coupled to the increase in computational capacity the range of applications possible to simulate increases greatly. Today the applications ranges from gas turbine combustors [12, 20–22], supersonic combustors [10, 13, 23] and two-phase reactive flows [24] to explosions [24] and plasma assisted combustion [25, 26]. Most applications tied to the energy production via gas turbines, and the transportation and propulsion applications are today relying heavily on hydrocarbon fuels of varying molecular sizes. This implies that improved chemical modelling of these fuels can increase the combustion modelling accuracy, impacting large areas of the modern society.

With the need for more accurate reaction mechanisms, and their inclusion into combustion LES, the purpose of this work was to develop a modelling development methodology for creating improved reaction mechanisms of semi-reduced sizes, and to incorporate these models into combustion LES'. These tasks can be summarized as

- Develop a modelling development methodology capable of creating reaction mechanisms with a high accuracy, requiring a computational cost low enough for use in 3D LES';
- Develop reaction mechanisms for a set of hydrocarbon fuels using this new methodology;
- Using these reaction mechanisms in combustion LES.

The research conducted to realize these three tasks are presented in the seven publications, papers I to VII, in this thesis.

In Paper I a chemical model is developed and evaluated for propane-air (C_3H_8-air) combustion. This model is then used in a combustion LES of a flame holder geometry. The results are then compared to experimental data available in the literature.

Paper II creates a reaction mechanism for methane-air (CH_4-air) combustion and couples that to the effect of microwave enhancement of a swirling methane-air flame. This model is evaluated and then used in a combustion LES whose

results are compared to experiments.

Paper III deals with the development and evaluation of a reaction mechanism for kerosene-air ($C_{12}H_{23}$-air) combustion. This reaction mechanism is then used in a combustion LES of a full annular gas turbine combustor.

Paper IV describes the development of an improved version of the kerosene-air reaction mechanism used in Paper III, and here the block structure development routine is described in greater detail.

Paper V is again solely devoted to the chemistry modelling. Here a ethylene-air (C_2H_4-air) reaction mechanism is developed and evaluated. Again an extensive description of the development routine is presented.

Paper VI uses the methane-air and the ethylene-air reaction mechanisms from Papers II and V and incorporates these into combustion LES' of a fully annular premixed combustor, comparing the results to experimental data.

Finally Paper VII further develops the kerosene-air reaction mechanisms presented in Papers III and IV. In Paper VII more accurate fuel breakdown reactions are added in order to capture the specific ignition characteristics of aviation-type hydrocarbons at low temperatures.

Chapter 2 provides an overview of combustion theory and Chapter 3 presents the theory of chemical kinetics. Chapter 4 presents H_2/O_2 and $C_1/H/O$ chemistry theory in detail. This theory is then used when applying the block structure modelling routine in Chapter 5. Chapter 6 provides an overview of combustion modelling. Chapter 7 present key results from the chemistry modelling and the combustion LES'. Finally Chapter 8 summarizes key results and suggests future work.

Chapter 2

Combustion theory

Reactive flows presents a notoriously complicated process which include a broad range of phenomena operating on large ranges of temporal and spatial scales. In most combustion processes there is a close coupling between the fluid dynamics and the chemical reactions and their subsequent heat release [27]. Added to the complexity of reactive flows are phenomena such as possible formation of soot particles, injection of liquid spray and its subsequent gasification, the interaction between electrical fields and the flame, or radiation. Regardless of what type of combustion system is present generally all are dynamic and unsteady [27].

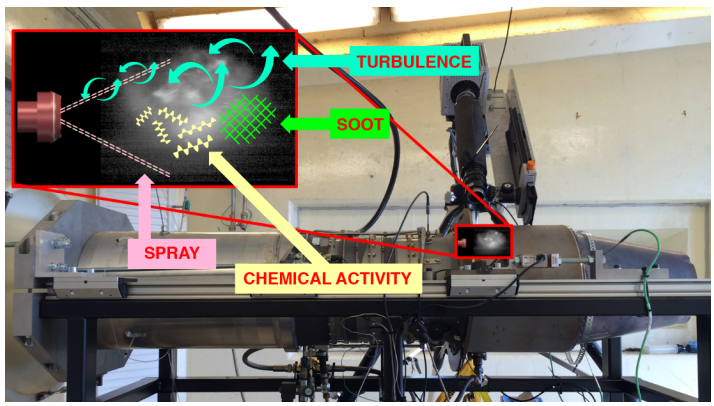

Figure 2.1: Image of a gas turbine test rig, adopted from the work by Danel et al. [22], with an extracted image of the flame chemiluminescence together with a model of the injector. Indicated in the flame image are possible characteristic features present in combustion.

The equations describing the combustion processes are highly complicated, operating on large ranges of time and length scales, from molecular scales where

the chemical kinetics and soot formation takes place to the scale of the device of interest. Computational studies of combustion are usually based on the balance equations of mass, momentum and energy, together describing diffusion, convection and chemical reactions. Due to the unsteady nature of combustion, and to be able to capture many of the effects of this unsteadiness, computational studies most often require a time-resolved method when simulating the process. This, in combination with the wide ranges of scales, requires model simplifications which yet often result in computationally expensive simulations.

2.1 Premixed and non-premixed combustion

Combustion occurs when fuel and oxidizer are mixed and ignited. If the fuel and oxidizer are first perfectly mixed and then burned the flame is categorized as a *premixed* flame, and if the mixing and combustion occurs simultaneously it is classified as a *non-premixed* flame. Each of these two flame categories can then also be categorized by the fluid motion, if the flow is *laminar* or *turbulent* [28]. Consider the reaction between methane and oxygen, represented by the overall reaction

$$\mathrm{CH_4} + 2\,\mathrm{O_2} \longrightarrow \mathrm{CO_2} + 2\,\mathrm{H_2O}. \tag{2.1}$$

Reaction 2.1 is said to be *balanced*, or the ratio between the fuel and oxidizer within the system is said to be *stoichiometric*, if all of the reactants (CH_4 and O_2) are being converted to the final products (CO_2 and H_2O).

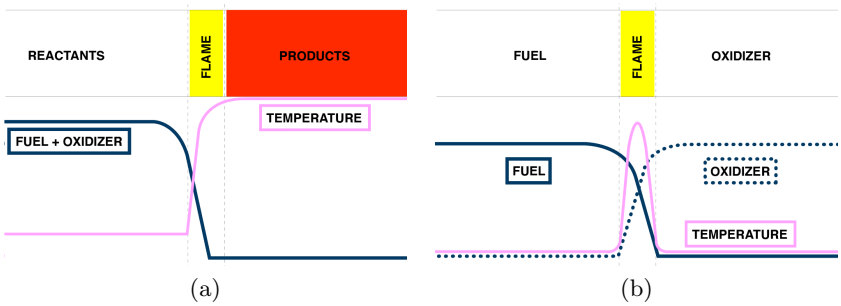

(a) (b)

Figure 2.2: A schematic image of a one-dimensional (a) premixed flame and (b) non-premixed flame.

In a premixed system where the velocity of the flow is low enough to be laminar the flame, schematically shown in Figure 2.2(a), will propagate through the fuel-air mixture with the velocity s_L. Fuel will start to break down and a

sequence of reactions will initiate, eventually resulting in an increase in temperature. When the combustion process is approaching completion the temperature has increased significantly and final products, and some intermediate species and radicals, have been formed. Their individual concentrations produced is heavily dependent on fuel type, fuel-oxidizer ratio and initial gas temperature and pressure.

In non-premixed systems, where the fuel and oxidizer is separated, schematically illustrated in Figure 2.2(b), the burn rate is controlled by the rate at which these are mixed. Here the maximum temperature and reaction activity is found in the reaction zone between the fuel and oxidizer. If the flow is turbulent the mixing of species will be considerably higher, increasing the rate of combustion. In general, the non-premixed systems are more sensitive to mixing and flame stretching, and the flame stretching can quench the flame locally or globally when the turbulent motion exceeds the diffusion rate of reactants.

2.2 Equivalence ratio

In combustion, the fuel (F) and oxidizer (O), described by either mole- or mass fractions, and their ratio, are important quantities when characterizing a flame. This ratio between the fuel and oxidizer, known as the *equivalence ratio*, has different definitions depending if the system is non-premixed or premixed [3]. Here only the latter condition will be described.
Consider a stoichiometric premixed system

$$\psi_F F + \psi_O O \rightarrow Products \tag{2.2}$$

where ψ_F and ψ_O are the stoichiometric coefficients of the fuel and oxidizer, respectively.

The equivalence ratio of a given mixture is

$$\phi = \left(\frac{Y_F}{Y_O}\right) \Big/ \left(\frac{Y_F}{Y_O}\right)_{st} = \left(\frac{Y_F}{Y_O}\right) \Big/ \left(\frac{\psi_F W_F}{\psi_O W_O}\right)_{st} \tag{2.3}$$

where the subscript st corresponds to the stoichiometric condition. The equivalence ratio can be divided into three regions:

- *fuel lean* conditions ($\phi < 1$) where there is an excess of oxidizer within the reacting mixture;
- the *stoichiometric* condition ($\phi = 1$) where the fuel and oxidizer ratio is in balance;
- *fuel rich* conditions ($\phi > 1$) where there is an excess of fuel in the mixture.

The maximum flame temperature is achieved at conditions slightly above stoichiometric conditions. If the mixture is fuel lean some of the excess oxidizer will be heated to the product temperature, lowering the temperature. If too little oxidizer is present, i.e. at fuel rich conditions, there is not enough oxidizer to convert all the species in the fuel into final products, inhibiting some of the energy release, resulting in a lower temperature.

2.3 Turbulence

Turbulent flows, a three-dimensional phenomenon, varies irregularly in both position and time. Turbulence is dissipative, and the structures in a turbulent flow lose their energy to smaller structures. This is occurring until the viscous forces dissipate the energy into heat [4].

The effectiveness of the turbulent motion for mixing and transport of different fluids is of prime importance in many real-world applications [4]. With an increase in turbulence comes an increase in heat and mass transfer which greatly can affect a flame, effectively increasing the rate of consumption of fuel and oxidizer. The topic of turbulence is therefore key in many combustion processes.

The eddies in a turbulent flow have certain length, time and velocity scales [4]. In a flame these scales can be used to classify the structure of a flame (see Sections 2.3.3 and 2.3.4), which is important when determining how to model that flame. The level of turbulence is hence key for the structure of the flame, but also when choosing how to model the flame.

2.3.1 Energy cascade

The view of the energy cascade, proposed in 1922 by Richardson et al. [29], states that turbulence is composed of eddies of different sizes. Eddies are typically characterized by different scales of the flow, and an eddy can have specific length, velocity and time scales. There is no distinct definition of an 'eddy', but it can be viewed as a turbulent motion that is at least moderately coherent within a region of size l [4]. Eddies with size l has the characteristic velocity, v_l, and time, τ_l, scales. Large eddies are unstable and breaks up, transferring their energy to smaller eddies. This break-up of eddies and their following transfer of energy to smaller eddies continues until the motion of eddies is stable. This occurs when the eddies are so small that the viscous forces of the flow cannot be overcome. Figure 2.3 shows the energy cascade as a function of the wave number.

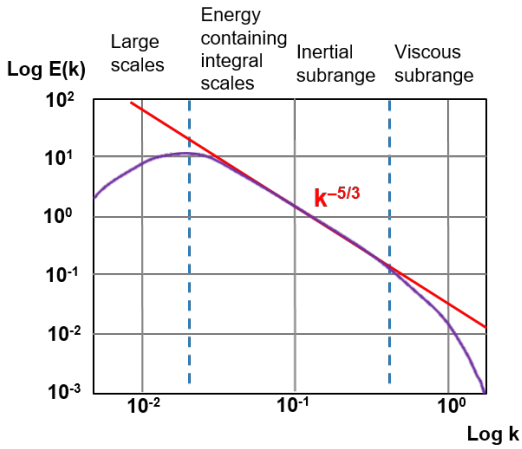

Figure 2.3: Schematic image of the energy cascade. The abscissa shows the wavenumber and the ordinate the kinetic energy.

A range of scales in the turbulent energy cascade can be represented by specific length, time and velocity scales. Such scales can be found for any range in the cascade. The length scales for example ranges from the integral length scales of the flow, l_I, representing the scale of the most energetic eddies in the turbulent cascade [4], down to the smallest scale found in the turbulent flow, the Kolmogorov length scale, η [3]. The Kolmogorov length scale, $\eta \equiv (\nu^3/\epsilon)^{1/4}$ [3, 4], with ν being the viscosity and ϵ the dissipation rate of turbulent kinetic energy, characterize the scales small enough for dissipation to become effective [4]. The Taylor micro scale, λ_T, is an intermediate length scale which at high flow velocities is intermediate in size between η and l_I [4], i.e. between the large scale eddies and the small scale eddies.
The large difference between the integral and Kolmogorov scales indicate the wide range of scales present in the turbulent flow. Capturing scales on such a large range represent great challenges when modelling a turbulent flow, and this has resulted in the development of several different modelling techniques (see Chapter 6).

2.3.2 Non-dimensional numbers in turbulent flow

The length, time and velocity scales can be used to express characteristic dimensionless numbers of the flow. The (turbulent) Reynolds number,

$$Re_t = l_I v'/\mu, \tag{2.4}$$

where μ is the kinematic viscosity, $\mu = \nu/\rho$, ρ the density, and v' the velocity of the turbulent eddies, is a representative velocity of the eddies with the integral length scale l_I. The turbulent Reynolds number represents the ratio of inertia to viscous forces of the largest and most energetic scales but the Reynolds number can be used to describe any scale in the cascade. The Reynolds number decrease with decreasing scale, until it reaches the Kolmogorov length scale, and it can be used to predict the transition from laminar to turbulent flow.
Another key non-dimensional number is the Schmidt number for species i, Sc_i, describing the diffusive to viscous transport;

$$Sc_i = \mu/D_i, \tag{2.5}$$

where D_i is the characteristic molecular diffusivity of species i.

The third non-dimensional number introduced here is the Prandtl number, Pr, which compares the momentum and heat transport,

$$Pr = \mu/\varkappa, \tag{2.6}$$

where $\varkappa$ is the thermal diffusivity. The Sc_i and Pr numbers hence describe the molecular transport of species and heat.

2.3.3 Different scales in premixed combustion

Premixed flames can be associated by the different scales present in the flame. Ranging from the integral length scale of the flow, l_I, to the flame length scale of the laminar flame thickness, δ_v, and down to the Kolmogorov length scale, η [3]. Similarly the velocities are associated by the the laminar burning velocity, s_L, and the velocity of turbulent eddies, v'. Finally, the time scales are associated with the chemical time scale, τ_c, representing the time scales for the chemical reactions, the Kolmogorov time, τ_η, representing the time scale of the smallest eddies, and the integral time scale, τ_l, representing the flow time scales [3].

The Damköhler number, $D_a = \tau_l/\tau_c$, corresponds to the ratio of the integral time scale to the chemical time scale. The Karlovitz number is the ratio of the chemical time scale to the Kolmogorov time, $K_a = \tau_c/\tau_\eta$ [3]. By using characteristic non-dimensional numbers various flame regimes can be identified [3] and plotted in for example Borghi [30] or Williams [31] diagrams. These diagrams indicate whether the flow contains distributed reaction zones, pockets, thin reaction sheets or any kind of flamelet (thin reaction zones) [3]. The different regimes in these diagrams illustrates which mechanisms are controlling the turbulent combustion [24]. Knowledge about which regime a flame belongs to is important when choosing how to model that flame. Figure 2.4 illustrates the Borghi diagram, divided into sections characterizing specific combustion regimes.

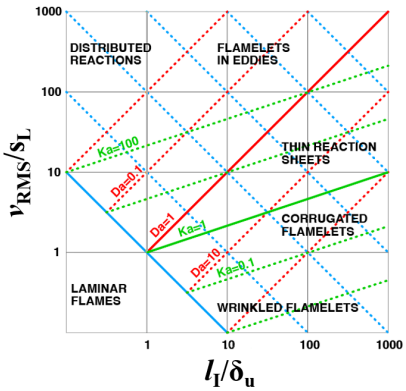

Figure 2.4: The Borghi diagram with regions of different flame structures indicated [30].

2.3.4 Different scales in non-premixed combustion

Non-premixed flames are more difficult to characterize than premixed flames since non-premixed flames do not propagate, hence they do not have a characteristic speed. Also, the flame thickening is governed by the mixing layers between fuel and oxidizer, and there is no obvious length scale [3]. To start a regime classification of non-premixed flames a set of relevant variables that influences the flame structure must be identified. To start a Da number can be specified as $Da_\chi = \tau_\chi/\tau_c$, where τ_χ is a representative time-scale of the mixing, defined as the inverse of the scalar dissipation rate. τ_c is a chemical time scale defined in the same way as for premixed flames. However, Da_χ is not associated with the same length and velocity scales as usually involved in the Reynolds number characterizing the flow, Re_I. By defining a new Da number $Da_I = Da_\chi Re_I^{1/2}$ it is possible to create a combustion regime diagram for non-premixed flames, as shown in Figure 2.5. Here three different regimes can be classified; the extinction regime, with the Da extinction number Da_χ^{ext}, the unsteady regime and the flamelet (LFA, laminar flamelet assumption) regime, with the Da number Da_χ^{LFA}. If $Da_\chi \geq Da_\chi^{LFA}$ the regime has a laminar structure, where large eddies distorts the laminar flame front. Here the chemistry is sufficiently fast to follow changes in the flow introduced by the vortices. For $Da_\chi^{ext} < Da_\chi < Da_\chi^{LFA}$ the eddy size and the mixing length are smaller than the flame front thickness, and the flow changes are faster than the chemistry, and unsteady effects becomes important. Finally if $Da_\chi \leq Da_\chi^{ext}$ extinction events occur because the strain rate induced by the flame front vortex becomes too strong, quenching the flame [3].

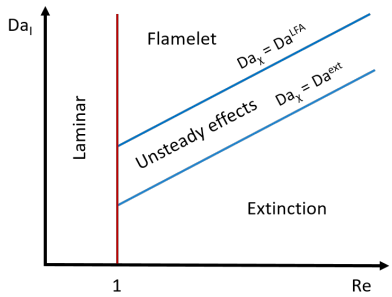

Figure 2.5: Regimes for non-premixed turbulent combustion [3].

2.4 Governing equations

In chemically reacting flows the system can, at each point in space and time, be described by a given pressure, density, temperature, velocity of the flow and the concentrations of the species present [28]. The properties of mass, momentum, and energy are conserved, constituting *the conservation equations* [28, 32].

In the general case of a reacting flow the conservation equations, known as the Reactive Navier-Stokes Equations (RNSE), may be written as [24]

$$\begin{cases} \partial_t(\rho) + \nabla \cdot (\rho \mathbf{v}) = 0, \\ \partial_t(\rho \mathbf{v}) + \nabla \cdot (\rho \mathbf{v} \otimes \mathbf{v}) = -\nabla p + \nabla \cdot \Big(2\mu \mathbf{D} - \frac{2}{3}\mu(\nabla \cdot \mathbf{v})\mathbf{I} \Big), \\ \partial_t(\rho E) + \nabla \cdot (\rho \mathbf{v} E) = \nabla \cdot \Big(- p\mathbf{v} + 2\mu \mathbf{D}\mathbf{v} - \frac{2}{3}\mu(\nabla \cdot \mathbf{v})\mathbf{v} + \varkappa \nabla T \Big) + Q_{rad}, \\ \partial_t(\rho Y_i) + \nabla \cdot (\rho \mathbf{v} Y_i) = \nabla \cdot (D_i \nabla Y_i - \mathbf{b}_i) + \dot{w}_i, \end{cases} \tag{2.7}$$

where ρ is the density, p the pressure, T the temperature, $\mathbf{v}$ the velocity vector, μ the kinematic viscosity, $\mathbf{I}$ the unity tensor, $\mathbf{D}$ the rate-of-strain tensor $\mathbf{D} = \frac{1}{2}(\nabla \mathbf{v} + \nabla \mathbf{v}^T)$, Q_{rad} the radiative heating, and D_i and $\varkappa$ are the species and thermal diffusivities, respectively. The energy is expressed in the form of total energy, $E = e_{in} + \frac{1}{2}\mathbf{v}^2$, a sum of the internal and kinetic energy. The mass fraction of species i is expressed by Y_i and the rate of production of species i by $\dot{w}_i$ [24]. The chemical kinetics enters through $\dot{w}_i$.

Equations 2.7 are then closed by the thermal and caloric equations of state (EoS) and constitutive equations. The thermal EoS describes the relation between density, temperature and pressure [24]. In the present research the EoS used is the ideal gas law, defined by

$$p = \rho R \sum_{i}^{N} (Y_i / M_i) T, \tag{2.8}$$

where M_i is the molar mass of species i, and R is the ideal gas constant. The caloric EoS describes the relation between the energy and the specific heats. The caloric EoS used is

$$e_{in} = \sum_{i}^{N} \left(Y_i h_{f,i}^{\theta} \right) + \sum_{i}^{N} \left(Y_i \int_{T_0}^{T} c_{v,i}(T) \mathrm{d}T \right), \tag{2.9}$$

where e_{in} is the internal energy, $h_{f,i}^{\theta}$ is the enthalpy of formation at standard temperature and pressure of species i, and $c_{v,i}$ the specific heat at a constant volume. T_0 is the temperature of the surroundings. Due to limited maximum temperatures (<3000 K) in the combustion processes in the present research, together with the dominance of nitrogen in hydrocarbon-air flames, the specific heats vary by only small amounts [3] and can be assumed to be linear functions of T, $c_{v,i} = a + bT$, with a and b being species specific constants.

The constitutive equations describe how external forces affect the response of the fluid mixture. All of the fluids in the present research are assumed to be Newtonian fluids with Fourier heat condition and Fickian diffusion. The viscosity, ν, is modelled using Sutherland's law.

Chapter 3

Chemical kinetics

A chemical reaction is the exchange and/or rearrangement of atoms, often occurring when molecules and/or atoms collide. Reactant molecules are rearranged to become product molecules, accompanied by an increase or decrease of heat [28]. Consider the following general reaction between a moles of species A and b moles of species B, forming c moles of species C and d moles of species D;

$$\mathrm{a\,A} + \mathrm{b\,B} \longrightarrow \mathrm{c\,C} + \mathrm{d\,D}. \tag{3.1}$$

It is possible for reaction 3.1 to be reversed, i.e. where A and B become the products and not the reactants. The *rate law* of reaction 3.1, describing its empirical formulation of the *reaction rate*, can be written as [32]

$$\frac{1}{\mathrm{a}}\frac{d[\mathrm{A}]}{dt} = -\kappa[\mathrm{A}]^{\mathrm{a}}[\mathrm{B}]^{\mathrm{b}} = \frac{1}{\mathrm{b}}\frac{d[\mathrm{B}]}{dt} = -\frac{1}{\mathrm{c}}\frac{d[\mathrm{C}]}{dt} = -\frac{1}{\mathrm{d}}\frac{d[\mathrm{D}]}{dt}, \tag{3.2}$$

where the constant κ represents a *reaction rate constant*. The reaction rate describes the formation or consumption of a species in a chemical reaction. a and b are the *reaction orders* with respect to species A and B, respectively, and the sum of the reaction orders denotes the *overall reaction order* [28].

3.1 Global and elementary reactions

A reaction describing the overall combustion system is often written using one reaction where all initial reactants are consumed and forming the final products, such as the following reaction between hydrogen and oxygen molecules forming water,

$$2\,\mathrm{H_2} + \mathrm{O_2} \longrightarrow 2\,\mathrm{H_2O}. \tag{3.3}$$

Such a reaction is known as a net reaction, or a *global reaction* [28]. The rate laws for these global reactions are sometimes complex with reaction orders often being non-integers, and can even be negative. More importantly however, most reacting systems do not progress in such a straightforward manner but rather progresses in a sequence of reactions, together constituting the reacting process. These reactions are where one or more species reacts directly to form intermediate and/or final products in a single reaction step. This type of reaction is known as an *elementary reaction* [28, 33], exemplified by

$$\mathrm{OH} + \mathrm{H_2} \longrightarrow \mathrm{H_2O} + \mathrm{H}. \tag{3.4}$$

3.2 Molecularity

The reaction order of elementary reactions is always constant and is determined by the *molecularity of the reaction* [28]. The molecularity is the number of species forming the reaction complex, consisting of one, two or three reactants. *Unimolecular reactions*, having first-order time behaviour (a reaction order of one), describe either rearrangement or dissociation of a molecule;

$$\mathrm{A} \longrightarrow \text{Products}. \tag{3.5}$$

Bimolecular reactions, the most common type of reactions, have second-order rate laws (a reaction order of two) and are of the form

$$\mathrm{A} + \mathrm{B} \longrightarrow \text{Products}. \tag{3.6}$$

Termolecular reactions, with third-order rate laws (a reaction order of three), are usually recombination reactions, recombining radicals into more stable species,

$$\mathrm{A} + \mathrm{B} + \mathrm{C} \longrightarrow \text{Products}. \tag{3.7}$$

3.3 Reaction rate

All chemical reactions take place at a definite rate that is dependent on the conditions of the system, such as the temperature, concentrations of reactants and the pressure within the system [32]. The rate of the reactions can be expressed using the concentrations of the reactants and a rate constant, as exemplified in equation 3.2.

Consider a chemical system of N species reacting through $\mathcal{M}$ reactions, giving the general equation [33]

$$\sum_{k=1}^{N} \psi'_{kj} X_k = \sum_{k=1}^{N} \psi''_{kj} X_k, \tag{3.8}$$

where X_k represents species k in reaction j, ψ'_{kj} is the molar stoichiometric coefficients of the reactants and ψ''_{kj} is the molar stoichiometric coefficients of the products.

The rate of progress of reaction j is written as

$$q_j = \kappa_{fj} \prod_{k=1}^{N} [X_k]^{\psi'_{kj}} - \kappa_{rj} \prod_{k=1}^{N} [X_k]^{\psi''_{kj}}, \tag{3.9}$$

where κ_{fj} and κ_{rj} are the forward and backward reaction rate constants of reaction j, respectively, and $[X_k]$ denotes the concentrations of species X_k [32, 33]. The *rate of production*, $\dot{w}_k$, of species k can then be computed using

$$\dot{w}_k = \sum_{j=1}^{\mathcal{M}} (\psi''_{kj} - \psi'_{kj}) q_j. \tag{3.10}$$

When considering the arbitrary reaction above, reaction 3.1, described by the reaction rate in equation 3.2, it is important to note that describing the reaction rate in this manner does not infer that every collision of the reactants (A and B) leads to products. Arrhenius put forth a theory that gives a temperature dependence of κ, resulting in that only molecules that possess energy greater than a certain amount, E_a, will react [34, 35]. The postulated theory includes a Boltzmann factor, $\exp(-E_a/RT)$, and kinetic theory shows that the Boltzmann factor gives the fraction of all collisions that have an energy greater than E_a.

Today the reaction rate constants are usually expressed through the modified Arrhenius law

$$\kappa = AT^n \exp(-E_a/RT), \tag{3.11}$$

where A and n are the pre-exponential factor and the temperature exponent, respectively, and E_a the activation energy. The original Arrhenius expression, which is obtained when $n = 0$ in equation 3.11, is often adequate for a limited temperature range. However, for large temperature ranges the modified Arrhenius law is a better representation of the rate of most reactions [32]. A reaction type that do not adhere to the modified Arrhenius law is the pressure dependent reaction, such as dissociation reactions (unimolecular), or recombination reactions (termolecular) [28]. The pressure dependent unimolecular decomposition

can be understood by using the *Lindemann model* [36], extensively investigated by Troe et al. [37]. A unimolecular decomposition of species A can only occur if the energy within the molecule is sufficient to break the bond. It is then necessary, prior to the decomposition reaction, that energy is added to species A through collision with another species M [28]. The activated molecule, A^*, can then either deactivate through a collision or decompose into products P;

(1) Activation, with rate constant κ_a,

$$A + M \longrightarrow A^* + M, \tag{3.12}$$

(2) Deactivation, with rate constant κ_{-a},

$$A^* + M \longrightarrow A + M \tag{3.13}$$

and (3) Unimolecular reaction, with rate constant κ_u,

$$A^* \longrightarrow P. \tag{3.14}$$

The rate of reaction of product P can then be expressed by [28]

$$\frac{d[P]}{dt} = \frac{\kappa_u \kappa_a [A][M]}{\kappa_{-a}[M] + \kappa_u}. \tag{3.15}$$

Here two extremes can be distinguished, one where the pressure is very low and one where it is very high. For the low pressure range the concentrations of M are very low hence $\kappa_{-a}[M] \ll \kappa_u$ in which one obtains the second-order rate law

$$\frac{d[P]}{dt} = \kappa_a [A][M]. \tag{3.16}$$

Here the reaction rate is proportional to the concentrations of species A and M meaning that the collisions between species A and M are rate limiting. In the high pressure range the concentration of M is very high giving $\kappa_{-a}[M] \gg \kappa_u$, resulting in the first-order rate law

$$\frac{d[P]}{dt} = \frac{\kappa_u \kappa_a}{\kappa_{-a}}[A] = k_\infty [A]. \tag{3.17}$$

Because the collisions between species A and M often occur when the pressure is high they are not rate limiting. The rate limiting factor will instead be the decomposition of the activated molecule A^*. The units of the rate constant is dependent on the overall reaction order. Units for reaction rates are s^{-1}, $cm^3 mole^{-1} s^{-1}$ and $cm^6 mole^{-2} s^{-1}$ for first, second and third order reactions, respectively [28].

Equations 3.11, 3.16 and 3.17 all requires three input parameters, A, n and E_a, in order to determine κ for each reaction.

3.4 Reaction process

As previously mentioned the combustion progresses through a sequence of elementary reactions. What this means is that the fuel molecule is partially broken down into smaller intermediate species and fast reacting radical species, which in turn are broken down further creating a chain of reactions culminating in end products. These end products consists of a majority of CO_2 and H_2O, and a minority of CO and H_2, when hydrocarbons are burnt at and below stoichiometric conditions. The reactions operating in this sequence can be classified into different categories; chain initiation or *fuel breakdown* reactions, *chain branching* reactions, *chain propagating* reactions and *chain terminating* reactions [32, 33]. The fuel breakdown reactions, creating intermediates and radicals initiates the reacting system. One example of such a reaction is the initiation step for methane breakdown in the high-temperature regime,

$$CH_4 + M \longrightarrow CH_3 + H + M, \tag{3.18}$$

producing a fast reacting H radical and a methyl (CH_3) radical. Reactions where reactants dissociate and thereby creates a radical are highly endothermic and hence very slow [32]. Once the H radical has been created it can for example abstract another H atom from a fuel molecule, or it can enter the H_2/O_2 system of reactions creating O, H and OH, building up a pool of radicals.
The expansion of this radical pool is achieved through chain branching reactions. The chain branching reaction is any reaction that creates two radicals for every one radical consumed, effectively increasing the number of radicals. These reactions and their expansion of the radical pool is necessary in order to move the system into a non-thermal explosive state. A typical and essential chain branching reaction is

$$H + O_2 \longrightarrow O + OH, \tag{3.19}$$

where one H radical is consumed and two new, O and OH, are produced. Because of the multiplication effect of the branching steps they do not need to occur rapidly in order to determine the progression of the system, and their activation energies are often higher than other non-branching (chain propagating) radical reactions [32].
The chain propagating reactions will create one radical for every radical consumed, hence they do not expand the radical pool but is simply progressing the combustion process. An example of such a reaction is

$$CH_3 + OH \longrightarrow CH_3O + H. \tag{3.20}$$

The final category of reactions are the chain terminating reactions. This type of reaction reduces the size of the radical pool by recombining radicals to form more stable molecules, either when two radicals recombine forming one stable molecule or through reactions between one radical and one molecule producing one stable species or a radical of lower reactivity. The recombination reactions, a type of terminating reactions, are exothermic and the energy created must be removed by either a third body species or through wall interaction in order for the reaction to progress. This mean that due to the third body dependence the recombination reactions in a gaseous state are slower than other types of reactions except at higher densities (higher pressures) [32]. A typical chain terminating reaction is

$$\mathrm{H} + \mathrm{H} + \mathrm{M} \longrightarrow \mathrm{H_2} + \mathrm{M}. \tag{3.21}$$

Chain terminating reactions are effectively slowing down the rate of the combustion due to the elimination of radicals.

3.5 Reaction pathways

When fuel and oxidizer reacts a sequence of reactions are created where for example the carbon and hydrogen in the fuel is rearranged into final products. A possible sequence of the carbon-containing species in a methane-air oxidation process is schematically shown in Figure 3.1.

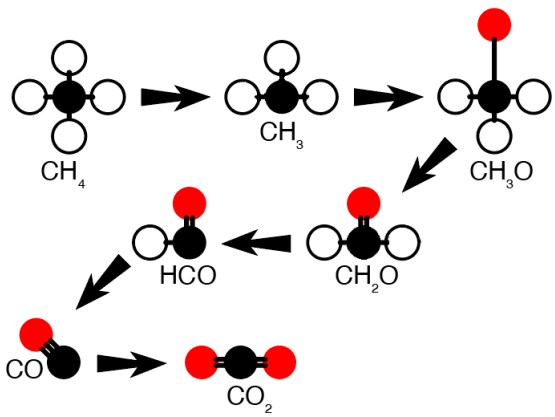

Figure 3.1: A reaction pathway showing the following sequence of species: $CH_4 \rightarrow CH_3 \rightarrow CH_3O \rightarrow CH_2O \rightarrow HCO \rightarrow CO \rightarrow CO_2$.

The sequence of species in Figure 3.1 is known as a *reaction pathway* and presents one theoretical, and often simplified, description of the transformation

of a fuel molecule into final products. This pathway is often used to highlight the main oxidation pathway taking into account the most probable reactions in the combustion process. In reality the reaction pathway can be, and often is, much more complex than the sequence presented in Figure 3.1. The complexity of the pathway increases with increasing size and structural complexity of the fuel molecule due to more intermediate species and reactions available.

3.6 Reaction mechanism

By combining the uni-, bi- and termolecular reactions into a sequence a complete description of the chemical kinetics of a reacting system can be achieved. Such a set of reactions is known as a *reaction mechanism* [33]. In theory it could include all possible species and reactions representing the combustion process. In reality the number of species and reactions present are lower due to limited importance of some of them, limitations in computational time it takes to solve such a system and limitations in the knowledge of which species and reactions need to be included. This means that each reaction mechanism has a limitation in its range of conditions where it has a high accuracy in its prediction of relevant flame parameters. An example of the reduced methane-air reaction mechanism [25] developed as a part of this thesis is presented in Table 3.1.

Table 3.1: Methane-air reaction mechanism Z42 [25].
Units: s, mole, cm^3, cal, K.

Reaction	A	n	E_a
$CH_4(+M) \rightarrow CH_3 + H(+M)^1$			
kf	6.30E+14	0	104000
kf_0	1.00E+17	0	86000
$CH_3 + H(+M) \rightarrow CH_4(+M)^1$			
kf	5.20E+12	0	-1310
kf_0	8.25E+14	0	-19310
$CH_4 + H \rightarrow CH_3 + H_2$	2.20E+04	3	8750
$CH_3 + H_2 \rightarrow CH_4 + H$	9.57E+02	3	8750
$CH_4 + OH \rightarrow CH_3 + H_2O$	1.60E+06	2.1	2460
$CH_3 + H_2O \rightarrow CH_4 + OH$	3.02E+05	2.1	17422
$CH_3 + O_2 \rightarrow CH_3O + O$	5.00E+13	0	25652
$CH_3 + O \rightarrow CH_2O + H$	6.80E+13	0	0
$CH_3 + OH \rightarrow CH_2 + H_2O$	7.60E+06	2.0	5000
$CH_3O + H \rightarrow CH_2O + H_2$	2.00E+13	0	0

Continued on next page

Reaction	A	n	E_a
$CH_3O + M \rightarrow CH_2O + H + M$	2.40E+13	0	28812
$CH_2O + H \rightarrow HCO + H_2$	9.00E+13	0	3991
$CH_2O + OH \rightarrow HCO + H_2O$	3.00E+13	0	1195
$CH_2 + O \rightarrow CO + H_2$	3.00E+13	0	0
$CH_2 + OH \rightarrow CH + H_2O$	1.13E+07	2.0	3000
$CH + O \rightarrow CO + H$	5.70E+13	0	0
$CH + OH \rightarrow HCO + H$	3.00E+13	0	0
$CH + O_2 \rightarrow HCO + O$	3.30E+13	0	0
$CH + CO_2 \rightarrow HCO + CO$	8.40E+13	0	200
$HCO + H \rightarrow CO + H_2$	4.00E+13	0	0
$HCO + M \rightarrow CO + H + M$	1.60E+14	0	14700
$CO + OH \rightarrow CO_2 + H$	1.51E+07	1.3	-758
$CO_2 + H \rightarrow CO + OH$	1.57E+09	1.3	21000
$H + O_2 \rightarrow OH + O$	1.55E+14	0	16800
$OH + O \rightarrow H + O_2$	1.20E+13	0	690
$O + H_2 \rightarrow OH + H$	1.80E+10	1	8826
$OH + H \rightarrow O + H_2$	8.00E+09	1	6760
$H_2 + OH \rightarrow H_2O + H$	1.17E+09	1.3	3626
$H_2O + H \rightarrow H_2 + OH$	5.09E+09	1.3	18588
$OH + OH \rightarrow O + H_2O$	6.00E+08	1.3	0
$O + H_2O \rightarrow OH + OH$	5.90E+09	1.3	17029
$H + O_2 + M \rightarrow HO_2 + M$[1]	1.60E+18	-0.8	0
$H + HO_2 \rightarrow OH + OH$	1.50E+14	0	1004
$H + HO_2 \rightarrow H_2 + O_2$	2.50E+13	0	700
$OH + HO_2 \rightarrow H_2O + O_2$	2.00E+13	0	1000
$HO_2 + HO_2 \rightarrow H_2O_2 + O_2$	8.00E+13	0	0
$H_2O_2 + M \rightarrow OH + OH + M$	1.30E+17	0	45500
$OH + OH + M \rightarrow H_2O_2 + M$	9.86E+14	0	-5070
$H_2O_2 + OH \rightarrow H_2O + HO_2$	1.00E+13	0	1800
$H_2O + HO_2 \rightarrow H_2O_2 + OH$	2.86E+13	0	32790
$OH + H + M \rightarrow H_2O + M$	2.20E+22	-2	0
$H + H + M \rightarrow H_2 + M$	1.80E+18	-1	0

[1]efficiencies = CH_4:6.5 CO:0.75 CO_2:1.5 H_2O:6.5 N_2:0.4 O_2:0.4

Using equations 3.2 and 3.10 gives

$$\frac{d[X_k]}{dt} = \dot{w}_k, k = 1, \ldots, N. \tag{3.22}$$

Equation 3.22 forms a set of non-linear first-order ordinary differential equations (ODE) describing the rate of change of concentrations for all N species as a function of time. Because of the large difference in rate of change between reactions the time-scales in a reaction mechanism can vary significantly. This means that the equations can become numerically stiff and will need advanced numerical routines in order to solve them [32].

3.7 Reaction mechanism classification

A reaction mechanism can be classified into different categories depending on its level of chemical complexity. Several classifications exists but here the three categories *detailed*, *global* and *reduced* reaction mechanism will be used and presented.

3.7.1 Detailed reaction mechanism

A detailed reaction mechanism is a mechanism that aim at, in detail, describe the chemical kinetics as rigorously as possible, and include all species and reactions that are necessary [33, 38]. This (often) requires a large set of species and reactions, describing the breakdown and oxidation of the fuel without the use of any simplifications, global reactions and without lumping several reactions into artificial ones. For simple fuel molecules, like hydrogen, this requires roughly ten species and 20-30 reactions but for larger fuels, like n-dodecane (n-$C_{12}H_{26}$) [39], many hundreds of species and thousands of reactions are needed. Even simple alkanes, such as methane, require up to one hundred species and several hundred reactions in order to fully describe the chemical kinetics. Trying to solve a system with that many species and reactions will require a significant computational capacity. Hence even though detailed reaction mechanisms increase our understanding of the chemical kinetic process they are, due to their high computational cost, mostly applicable in zero- and one-dimensional simulations.

3.7.2 Global reaction mechanism

In direct opposition to the detailed reaction mechanism stands the global reaction mechanism [33]. Its purpose is to model the overall chemical kinetic process, from fuel breakdown to final products, using only a handful of species and reactions. The chemical process is modelled without using any detailed description of the chemical kinetics, often excluding radicals and intermediate species and lacking the use of elementary reactions. The upside of this method is a reaction mechanism that is small, often using between one to five reactions, and not requiring a high computational capacity. The low computational

cost meant that global reaction mechanisms where the first to be used in three-dimensional reacting flow simulations [14–18, 40]. The downside of the highly simplified description of the chemistry in a global reaction mechanism is its limited predictability of flame parameters [10, 11, 20].

3.7.3 Reduced reaction mechanism

The third class of reaction mechanisms is the reduced reaction mechanism. Several different definitions for when a reaction mechanism is classified as reduced exists. If the mechanism has an unbroken reaction pathway, although in a reduced form, from the fuel breakdown through to intermediate products and down to final species production it is often named a *skeletal* reaction mechanism. If however the reaction pathway uses one or more artificial reactions, where one large molecule is broken down to several smaller intermediates in one step, short-cutting the correct reaction pathway, it is often named simply a reduced reaction mechanism. Here both types of reaction mechanisms will be referred to as reduced reaction mechanisms.
The number of reactions in a reduced reaction mechanisms can for example vary between 10% [25] to 0.005% [20, 41, 42] of that of a corresponding detailed reaction mechanism. The benefit of the reduced reaction mechanism is that it can achieve a high predictability without a high computational cost [11, 25, 42, 43]. This is due to the fact that the reduced reaction mechanism incorporates the most important species and reactions for the selected flame parameters modelled, and for a certain range of conditions. This enables a high level of predictability, but at the same time removing species and reactions of lesser importance, keeping the computational cost to a minimum. The combination of a high predictability and a relatively low computational cost has made the reduced reaction mechanisms attractive options for three-dimensional combustion flow simulations [11, 12, 20–22, 25].

3.8 Analysing a reaction mechanism

There are a number of methods to analyse the structure of a reaction mechanism. Two of the most common approaches are the *sensitivity analysis* [28,33] and the *reaction flow analysis* [28]. What type of method used to analyse and understand the chemical kinetics depends on what flame parameters the reaction mechanism is modelled to predict, and what type of information about the chemistry that the user demand.

3.8.1 Sensitivity analysis

A detailed reaction mechanism can consist of thousands of elementary reactions but the importance of each reaction to a certain flame parameter can vary greatly. Many reactions have a relatively low impact on the time-dependent solution of the system of ODE's whereas others have a very high impact where small variations in their rates greatly affect certain flame parameters. Reactions displaying a high impact on the results requires that the rate coefficients, determined by the rate parameters A, n and E_a, have a high level of accuracy. On the contrary, reactions displaying a low impact demand a far less accurate determination of their rate parameters. One way of determining the relative impact of reactions on a certain flame parameter is to conduct a *sensitivity analysis* where the relative impact, or sensitivity, of reactions to predefined flame parameters is calculated.

Figure 3.2 shows the relative normalized sensitivities of the 14 most important reactions on the laminar burning velocity, for a reduced kerosene-air reaction mechanism [42] at an equivalence ration of ϕ=1.0 and initial gas temperature and pressure of T=400 K and p=1 atm.

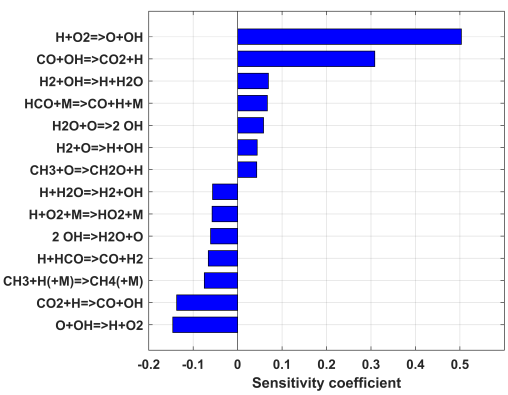

Figure 3.2: Sensitivity analysis showing the seven reactions with the highest sensitivities and the seven with the lowest, for the laminar burning velocity of a kerosene-air mixture, at p=1 atm, T=400 K and ϕ=1.0, modelled using the Z77 kerosene-air reaction mechanism [42].

Some reactions in Figure 3.2 have a high positive sensitivity, indicating a strong influence to increase the laminar burning velocity whereas other reactions have a strong negative sensitivity and hence an opposite effect on the burning velocity. The majority of the reactions with positive sensitivities are chain branching, increasing the size of the radical pool and promoting an increase in

the burning velocity. The chain terminating reactions, which reduces the size of the radical pool, are on the other hand dominating the number of reactions with negative sensitivities.

3.8.2 Reaction path analysis

Another option for analysing individual reactions in a reaction mechanism is to determine the characteristic reaction pathways. This is done through a *reaction path analysis* [28] which show (major) reaction pathways and the main reactants for each pathway, for a given set of conditions. A reaction flow analysis investigates the formation and consumption of species, either at specific times in the time-dependent solution or at specific locations in a spatially dependent steady-state problem [28, 44, 45]. Reaction flow analyses enables the creation of *reaction path diagrams*, exemplified in Figure 3.3. Figure 3.3 shows the reaction pathways of the Z42 reaction mechanism at the point in the flame where the temperature gradient is at its peak, corresponding to a temperature of 1200 K. The pathways are here displayed at the peak in temperature gradient because that often provides the most varied and diverse pathways. At lower or higher temperatures the possible reaction pathways, especially for reduced reaction mechanisms, are generally fewer, producing less diverse reaction path diagrams.

The reaction pathways shown in Figure 3.3 are illustrated together with the most important reactants for each pathway. Normally a criteria is set for the minimum effect a reaction pathway has to have in order for it to be displayed in the diagram. This means that the diagram will not necessarily display all possible reaction routes but only the most important ones at the selected condition.

3.9 Key flame parameters

The goal for any reaction mechanism, whether it is global, detailed or reduced, is to model a set of flame parameters. This choice of parameters, and the ranges of conditions where they should be accurately modelled, depends on what application, or at which conditions, the reaction mechanism is to be used at. Examples of flame parameters are the *flame temperature*, T, the *laminar burning velocity*, s_L, the *ignition delay time*, τ_{ig}, the *extinction strain rate*, σ_{ext} and the *concentrations of major species*, in hydrocarbon combustion often defined as CO_2, H_2O, CO and H_2. Graphs illustrating these flame parameters for a kerosene-air mixture are shown in Figures 3.4 and 3.5.

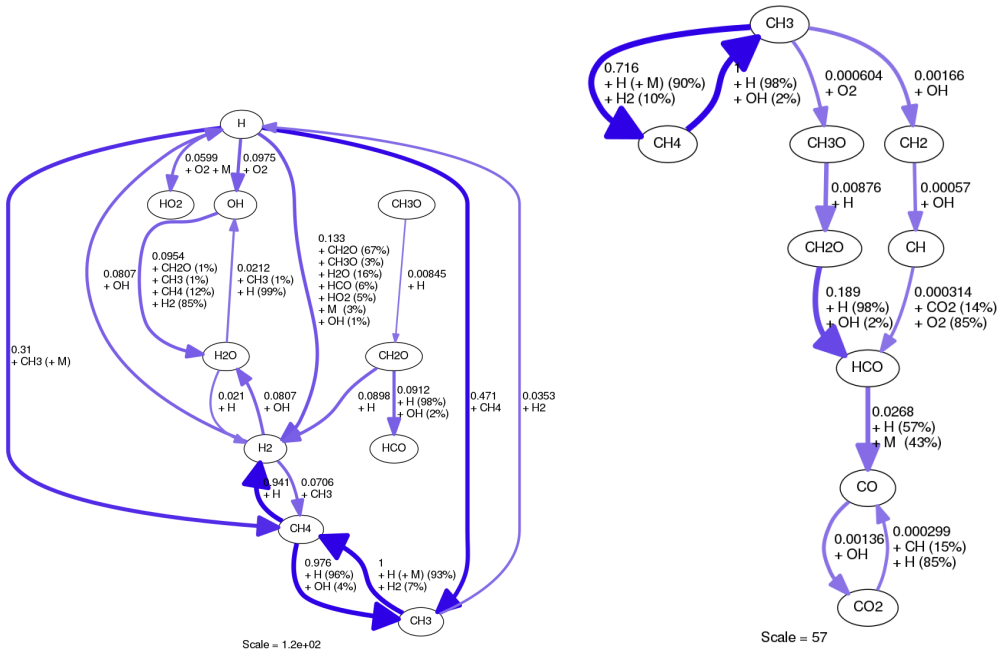

(a) (b)

Figure 3.3: Reaction pathway diagrams for a methane-air flame simulated at ϕ=1.0, p=1 atm and T=300 K, using the Z42 reaction mechanism [25]. In (a) pathways of species including H atoms are shown and in (b) pathways of species with C atoms.

3.9.1 Laminar burning velocity

The laminar burning velocity is defined as "*the velocity at which unburned gases move through the combustion wave in the direction normal to the wave surface*" [32]. For a given set of reactants the burning velocity depends on the equivalence ratio and initial gas pressure and temperature [33]. For a combustion LES of a premixed system the laminar burning velocity is a key flame parameter needed in the modelling, and one that a reaction mechanism need to be able to predict with a high accuracy [33]. The combustion process of a premixed flame is controlled by transport processes, mainly the combination of heat conduction and diffusion of radicals in front of the flame front.

The laminar burning velocity is modelled using a flame in a one-dimensional premixed set-up at laminar flow conditions. For most hydrocarbons the laminar burning velocity of a alkane-air mixture at ambient temperatures and pressures is in the range of 40 cm/s [32]. Figure 3.4(a) show laminar burning velocity

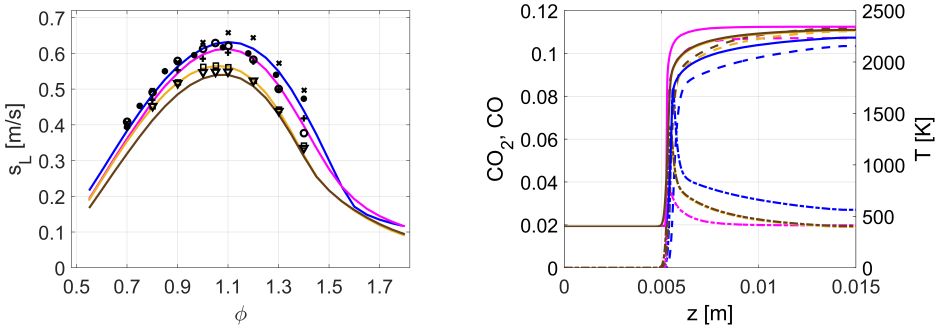

(a) (b)

Figure 3.4: Figures showing flame parameters for a set of reaction mechanisms and experimental data, for a kerosene-air mixture at an initial condition of p=1 atm and T=400 K. (a) shows the laminar burning velocity versus the equivalence ratio, ϕ, and (b) the one-dimensional profiles of the temperature (solid line; right ordinate) and CO and CO_2 mole fractions (dot-dashed and dashed lines, respectively; left ordinate) at ϕ=1.0. Legend, reaction mechanisms: blue - Z77 [42], magenta - S6664 [39], orange - HC247 [46,47] ($C_{11}H_{22}$), brown - HC277 [46,47] ($C_{12}H_{23}$). Legend, experimental data, laminar burning velocity: $\bigtriangledown$ - Xu et al. [47], $\circ$ - Ji et al. [48], $\square$ - Xu et a. [47], $\times$ - Kumar et al. [49], $\bullet$ - Kumar et al. [50], $+$ - Hui et al. [51].

predictions versus the equivalence ratio, ϕ, for four reaction mechanisms together with experimental data.

3.9.2 Flame temperature

The flame temperature, the solid lines in the one-dimensional flame profile in Figure 3.4(b), with the temperature displayed on the right ordinate, is another key flame parameter. The increase in temperature during combustion will produce a volumetric expansion that in turn will affect the flow. An increase in pressure, increased forces on the investigated geometry and ablation of combustor material are all effects that can originate from the combustion process and the subsequent increase in temperature. The temperature is also important to have well predicted in order to get the correct reaction rates due to the highly temperature-dependent Arrhenius reaction rate expression.

3.9.3 Species concentrations

A reaction mechanism should ideally be able to predict the concentrations of the major species. One reason is that a majority of the positive net heat released

from the reaction process occur in the later stages of the combustion pathways, i.e. where the major species are being formed. A correct formation of these major species is needed in order to get a correct flame temperature, both in magnitude and spatially. Moreover, major species are important when determining the completeness of the combustion process, and some species are also considered key pollutants. If a combustion process is incomplete, meaning that some of the fuel is not being converted into CO_2 and H_2O then the reaction mechanism will need to be capable of predicting this. Figure 3.4(b) shows one-dimensional flame profiles of CO and CO_2, with the mole fractions on the left ordinate.

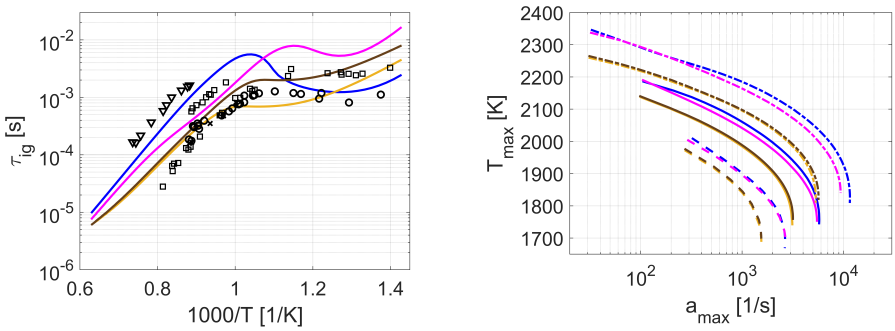

(a) (b)

Figure 3.5: Figures showing flame parameters for a set of reaction mechanisms and experimental data, for a kerosene-air mixture. (a) show the ignition delay times at p=20 atm and ϕ=1.0 and (b) the extinction strain rate at p=1 atm (dashed), p=3 atm (solid) and p=10 atm (dot-dashed). Legend, reaction mechanisms: blue - Z77 [42], magenta - S6664 [39], orange - HC247 [46, 47] ($C_{11}H_{22}$), brown - HC277 [46, 47] ($C_{12}H_{23}$). Legend, experimental data: $\times$ - Zhang et al. [52], $\circ$ - Vasu et al. [53], $\bigtriangledown$ - Zhu et al. [54], $\square$ - Vasu et al. [55].

3.9.4 Ignition delay time

It is possible to set up a fully premixed fuel-air mixture in an enclosed vessel and keeping it at a fixed temperature. If the ongoing exothermic reactions in that vessel exceeds the endothermic reactions the system will eventually move to a thermally explosive state [28, 32]. Hence an explosive state occurs when insufficient heat is removed from the system so that the reaction process becomes self-heating. The enclosed vessel can be modelled in a zero-dimensional set-up using either a constant pressure or a constant volume assumption. The time it takes to move the system from the initial temperature into this explosive

state is known as the ignition delay time. This time is highly dependent on the initial temperature and generally speaking, the higher the initial temperature, the faster the system will move into the explosive state and hence the shorter the ignition delay time will be. Exceptions to this can be found for large hydrocarbon fuels, such as $C_{12}H_{23}$, that, at lower temperatures can have an increased ignition delay time even though the temperature is increasing. This is known as the Negative Temperature Coefficient (NTC) effect [28, 33] and can be seen in Figure 3.5(a). The NTC behaviour is a consequence of changes in reaction pathways for fuel and fuel products occurring as the temperature increases, and it is highly dependent on the O_2 addition to the first fuel product [47].
There exists several definitions of when the system is considered to be ignited, which defines the ignition delay time, both in experiments and in simulations. Often the experiments use a peak in pressure to determine the ignition delay time, or measurements of excited OH^* emissions [56]. Simulations sometimes use a pre-defined temperature rise or peak OH^* concentrations as the definition of ignition delay time. If a reaction mechanism lacks the OH^* species it is possible to define the ignition delay time as the time when the OH concentration has reached 5% of its peak value, which often occurs at approximately the same time as the peak in OH^*. The prediction of when the OH^* peaks corresponds to a temperature increase of between 200 and 400 K [43], and this temperature definition of the ignition delay time can be used when simulating reaction mechanisms that do not contain the OH species. It should also be noted that experiments of ignition delay times have large uncertainties, often in the range of 30% or more [56].

3.9.5 Extinction strain rate

In order to take into account the kinetic-diffusion coupling, and the corresponding interaction between the flow and the chemistry, one-dimensional premixed [57, 58] or non-premixed [59] models of opposed-jet flows can be simulated [3]. Two opposing jets are flowing along a stagnation streamline, and the combustion is present at the point where the two jets meet. By increasing the velocities of the jets the turbulence originating from the increasing flow velocities eventually causes the flame to extinguish, resulting in a simulated result of the extinction strain rate. Extinction of flames occurs when a flame front is submitted to external perturbations, and heat loss or strong aerodynamic stretch decrease the reaction rate to values insufficient to sustain a flame [3]. The flow velocity at which the flame becomes extinct in the simulation is determined by the inherent chemical modelling of the reaction mechanism. A reaction mechanism with a too high extinction prediction will result in a flame that could survive artificially high flow speeds. Conversely, a too low extinction prediction

by the reaction mechanism will result in a flame that becomes extinct where in the real world a flame would still be present. Figure 3.5(b) show results of extinction strain rate simulations where the maximum flame temperature is decreasing as the strain rate, coupled to the flow velocities of the jets, increase until eventually the strain becomes too high and the flame becomes extinct.

Chapter 4

H_2/O_2 and $C_1/H/O$ kinetics

The following chapter presents a detailed description of key species and reactions present in the H_2/O_2 chemistry, and a reduced set of species and reactions present in the $C_1/H/O$ chemistry. These two sets of chemistries are of high importance in any hydrocarbon oxidation, hence it is necessary to model them with a high degree of accuracy when developing hydrocarbon reaction mechanisms. The model development methodology presented in Chapter 5 for creating reduced reaction mechanisms relies on detailed modelling of the H_2/O_2 chemistry, and a semi-detailed modelling of the $C_1/H/O$ chemistry, and this chapter provides a guide as to what species and reactions to include.

4.1 The H_2/O_2 system

One essential and critical set of reactions for any hydrogen, hydrocarbon or oxygenated hydrocarbon fuel is the reactions contained within the H_2/O_2 reaction system. Besides containing the obvious species H_2 and O_2 this system also produces the radicals H, O, OH, HO_2 and H_2O_2, all of which play essential roles for the overall characteristics and performance of any hydrogen, hydrocarbon or oxygenated hydrocarbon combustion process.
Any reaction mechanism modelling a fuel must contain at least one initiation reaction in order to start to breaking down the fuel and to initiate a pool of radicals. If the fuel in question is hydrogen the two most important initiation reactions at most conditions are [32, 60, 61]

$$H_2 + M \longrightarrow H + H + M \tag{4.1}$$

and

$$H_2 + O_2 \longrightarrow HO_2 + H. \tag{4.2}$$

Reaction

$$H_2 + HO_2 \longrightarrow H_2O_2 + H \tag{4.3}$$

increase in importance when the pressure increases and the temperature decreases [32]. Reaction 4.1 is the most probable initiation reaction at high temperatures whereas reaction 4.2 prevails at lower temperatures.

The initiation reactions provide the system with radicals that can then initiate further fuel breakdown. Note that reactions 4.1, 4.2 and 4.3 are not essential when modelling hydrocarbon or oxygenated hydrocarbon fuels, since those fuels will have their own dedicated carbon containing initiation reactions that will create the initial pool of radicals. Once the initiation reactions has provided the system with radicals these radicals (often H radicals) further propagate via chain branching reactions, effectively increasing the size of the radical pool. Important reactions creating radicals in the H_2/O_2 reaction system are [32]

$$H + O_2 \longrightarrow O + OH, \tag{4.4}$$

$$O + H_2 \longrightarrow H + OH, \tag{4.5}$$

$$O + H_2O \longrightarrow OH + OH, \tag{4.6}$$

$$H_2 + OH \longrightarrow H_2O + H. \tag{4.7}$$

Reactions 4.4-4.7 will here be referred to as *hydrogen subsystem I*, and is sometimes referred to as *hydrogen-oxygen shuffle reactions* [60]. Note that there is no chemical barrier that prevents hydrogen subsystem I from increasing the radical pool infinitely and hence reaching an explosive state. Reaction 4.4 is endothermic and its importance for the build-up of the radical pool increases at higher temperatures and lower pressures, whereas reaction 4.5 is exothermic. Since the hydrogen subsystem I contains important chain branching and propagating reactions it contains key reaction pathways in the oxidation of any hydrogen, hydrocarbon or oxygenated hydrocarbon fuel.

The H atoms produced in the system can react with an oxygen molecule via reaction 4.4, or via the competing reaction

$$H + O_2 + M \longrightarrow HO_2 + M. \tag{4.8}$$

Reaction 4.8, being a third body reaction, is pressure sensitive and its rate decreases at elevated temperatures or at low pressures. At low temperatures or elevated pressures reaction 4.8 can be more active than reaction 4.4, effectively

competing for the H radicals in the system. The HO_2 radical is relatively non-reactive, therefore called metastable. It can accumulate in large concentrations, and for any reaction mechanism the H_2/O_2 chemistry must, in order to be complete, contain reactions for HO_2 oxidation. HO_2 can be consumed by the radicals H, O and OH through reactions [32]

$$HO_2 + H \longrightarrow H_2 + O_2, \tag{4.9}$$

$$HO_2 + H \longrightarrow OH + OH, \tag{4.10}$$

$$HO_2 + H \longrightarrow H_2O + O, \tag{4.11}$$

$$HO_2 + O \longrightarrow O_2 + OH, \tag{4.12}$$

$$HO_2 + OH \longrightarrow H_2O + O_2. \tag{4.13}$$

Reactions 4.9-4.13 will be referred to as *hydrogen subsystem II*. HO_2 may also recombine, forming hydrogen peroxide via reaction

$$HO_2 + HO_2 \longrightarrow H_2O_2 + O_2. \tag{4.14}$$

The hydrogen peroxide is then consumed by reactions with radicals OH and H, or via a third body M according to

$$H_2O_2 + OH \longrightarrow H_2O + HO_2, \tag{4.15}$$

$$H_2O_2 + H \longrightarrow H_2O + OH, \tag{4.16}$$

$$H_2O_2 + H \longrightarrow HO_2 + H_2, \tag{4.17}$$

$$H_2O_2 + M \longrightarrow OH + OH + M. \tag{4.18}$$

Reactions 4.14-4.18 will be referred to as *hydrogen subsystem III*. Note that reaction 4.8 terminates the chain branching and propagating of hydrogen subsystem I at especially elevated pressures, but also creates new chain branching pathways, via reaction 4.10 or reactions 4.14 and 4.18. Both of these sequences, reaction pathways 4.8 $\rightarrow$ 4.10 and 4.8 $\rightarrow$ 4.14 $\rightarrow$ 4.18, are exothermic. This

means that even though reaction 4.8 inhibits the chain branching and propagation of hydrogen subsystem I the highly exothermic nature of some of the reaction sequences can still move the reaction system into an explosive state. Even slow reactions can move a system to become explosive as long as they are exothermic enough.

Finally the size of the radical pool of H, O and OH is controlled through third body chain terminating reactions. Some of the most important third-body recombination reactions are:

$$H + H + M \longrightarrow H_2 + M, \tag{4.19}$$

$$O + O + M \longrightarrow O_2 + M, \tag{4.20}$$

$$H + O + M \longrightarrow OH + M, \tag{4.21}$$

$$H + OH + M \longrightarrow H_2O + M. \tag{4.22}$$

Reactions 4.19-4.22 will be referred to as *hydrogen subsystem IV*. Reactions 4.21 and 4.22 has been shown to be necessary to include whereas 4.19 and 4.20 are of less importance [60].

Without hydrogen subsystem I the most important chain branching and propagating reactions would be missing, whereas hydrogen subsystems II and IV both affects the chemical characteristics at elevated pressures or at lower temperatures. Hydrogen subsystem III completes the HO_2 sequence and also provides a separate chain branching pathway via reactions 4.14 and 4.18. All four subsystems needs to be included into any hydrogen, hydrocarbon or oxygenated hydrocarbon fuel reaction mechanism although not all reactions are needed, especially not in hydrogen subsystems II, III and IV.

During the initial phase of an ignition sequence the hydrogen fuel is consumed without much heat released. During this period the radical concentrations are increasing, forming an increasingly expanding radical pool. It is not until significant radical recombination takes place that the heat of the system starts to increase, and this heat in turn will then further feed the necessary temperature increase that hydrogen subsystem I needs in order to move the system into an explosive regime [60].

4.2 The $C_1/H/O$ system

Now that the H_2/O_2 subsystem has been described the next subsystem to focus on is the $C_1/H/O$ subsystem. Whilst the H_2/O_2 subsystem is limited in size

due to the relative simplicity of the H_2 fuel molecule the C_1/H/O subsystem could in theory expand to a much greater subsystem. In order to prevent a large number of species and reactions in the C_1/H/O subsystem it should be developed in a much more reduced format than the H_2/O_2 subsystem. This means minimizing the number of reactions responsible for the low- and medium-temperature chemistries, and to limit the size the carbon species to C_1-species only.

Presented below are the chemical pathways describing the high-temperature oxidation of methane. Several detailed mechanisms modelling this fuel has been published [62–65]. The initiation of high-temperature methane oxidation starts with the H-abstraction reaction,

$$CH_4 + M \longrightarrow CH_3 + H + M. \tag{4.23}$$

The presence of the H atom then builds an initial radical pool, via the H_2/O_2 subsystem. These radicals then continue to abstract H from the methane molecule, exemplified by

$$CH_4 + H \longrightarrow CH_3 + H_2 \tag{4.24}$$

and

$$CH_4 + OH \longrightarrow CH_3 + H_2O. \tag{4.25}$$

The reaction rates of 4.24 and 4.25 are generally fast, with reaction 4.24 being the fastest [32]. The methyl radical is then consumed (mainly) through oxidation with O_2 [32] via

$$CH_3 + O_2 \longrightarrow CH_3O + O, \tag{4.26}$$

with reactions between the methyl radical and O and OH representing other reaction pathways for the methyl oxidation. The main oxidation pathway of the formed methoxy radical, CH_3O, is through the fast H-abstraction reaction

$$CH_3O + M \longrightarrow CH_2O + H + M. \tag{4.27}$$

The subsequent oxidation of formaldehyde, CH_2O, proceeds through H-abstraction reactions with the radicals H, OH, O and CH_3, exemplified by

$$CH_2O + H \longrightarrow HCO + H_2 \tag{4.28}$$

and

$$CH_2O + OH \longrightarrow HCO + H_2O, \tag{4.29}$$

whereas HCO decomposes mainly through

$$HCO + M \longrightarrow CO + H + M. \tag{4.30}$$

CO is then converted into CO_2 through the dominant reaction

$$CO + OH \longrightarrow CO_2 + H. \tag{4.31}$$

Reaction 4.31 is responsible for most of the produced CO_2 for any hydrocarbon-air mixture at high temperatures [32]. This conversion is delayed until the original fuel have been consumed [66] and reaction 4.31 closes the reaction pathway from CH_4 to CO_2.

Chapter 5

Reaction mechanism development

There are several ways of producing reduced reaction mechanisms. The most common ones uses a top-down approach where a reduced reaction mechanism is derived from a detailed one. Instead of this top-down approach a new bottom-up approach, where different parts of the chemistry is divided into blocks of varying chemical complexity, will be presented in this thesis.

5.1 The top-down approach

The top-down approach starts off with a detailed reaction mechanism and then by various optimization, reduction and/or lumping techniques reduces the size of that detailed reaction mechanism, creating a smaller version of the original mechanism. The reduction attempts to find the most important reaction pathways, with or without lumping of reactions, without losing too much accuracy on the pre-defined combustion parameters that the reaction mechanism aim to predict. One advantage of this approach is that it is easy to implement and sometimes demand less knowledge in chemical kinetics by the user compared to when a reaction mechanism is developed from the ground up, step by step. Another advantage is that, *in theory*, the reduced reaction mechanism only incorporates the most important species and reactions resulting in a good compromise between mechanism size and predictability. Which reactions that are included can however vary significantly when starting from different detailed mechanisms due to the fact that the fundamental understanding of the underlying chemistry, i.e. which species and reactions to include initially, is not complete.

Various reduction techniques using the top-down approach have been developed. Examples of reduction techniques are the *sensitivity based approaches*

[38, 67–70]. In order to predict a small number of important species often a large number of intermediate species need to be included in the simulation. Many species however exhibits a weak coupling to the species of interest and can therefore be removed without significant loss in accuracy on the chemical model [33]. The *connectivity method* presented by Turányi et al. [68] identifies such redundant species. By characterising the effect of a change in concentration for each species on the concentration of the important ones it is possible to determine which species are redundant [33]. Reduction methods using *directed relation graphs* (DRGs) [71–73] have much in common with the connectivity method. DRGs are based on identifying groups of species that are internally coupled, without a strong coupling to pre-selected important species. This weak coupling to pre-selected important species means the identified groups of species are not necessary for the accurate simulation of the species profiles of the pre-selected ones [33]. Various *optimization techniques* [74–78] exists as well. These are based on minimising an objective function which is subjected to a set of constraints. Such constraints can be a pre-defined number of species and/or reactions included in the reaction mechanism. Another target could be pre-specified target errors, minimising the reaction mechanism whilst still satisfying these targets.
All of these reduction techniques require a detailed reaction mechanism as input for the reaction mechanism reduction. However, for reaction mechanisms of large and complex fuels, often including several fuel isomers, the above mentioned reduction techniques may not create a reduced reaction mechanism small enough for combustion CFD. In that case the use of *lumping techniques*, where large species are broken down into several smaller ones in one single reaction, effectively short-cutting a large number of reactions, can be used. These lumping techniques can be performed using strict mathematical approaches [79] or by using a chemical approach [80] where the parameters for the lumping reactions are derived from experiments [33]. Adaptive reduction schemes have been discussed as well [33] where the original detailed reaction mechanism can change over time throughout the simulation, creating a reduced reaction mechanism suited to the current conditions. Such techniques can however quickly become computationally expensive since a reaction mechanism reduction must be carried out a significant number of times.

One drawback of a top-down reduction approach is that the original detailed reaction mechanisms are not designed to be reduced, they are designed to describe the chemical kinetic process as accurately as possible. Because of this it is not certain that reduction of a detailed reaction mechanism will produce an accurate enough, or small enough, reduced reaction mechanism.

Another drawback of the top-down reduction approach is that sometimes the reduced reaction mechanism still incorporates too many species and reactions,

making it too computationally expensive. Reducing the mechanism even further could then result in a reaction mechanism with poor predictability.

5.2 The bottom-up approach

Instead of *reducing* an already existing detailed reaction mechanism it is possible to *develop* a reduced reaction mechanism from the ground-up, using a bottom-up approach. By building a chemistry model from the ground up, using existing chemical kinetic knowledge, each part of the reaction mechanism can have its own level of chemical complexity. Also, since the chemistry is built from a clean sheet certain key reaction rates can be modified in order to incorporate some of the effects of missing reactions. This bottom-up approach will remove the dependence on detailed reaction mechanisms but is still limited by the current chemical knowledge when choosing which species and reactions to include. The approach will rely more on experimental data, as demonstrated by another bottom-up development strategy by Wang et al. [46] and Xu et al. [47].

A schematic image of the model development methodology presented here is shown in Figure 5.1. Each part of the chemistry is represented by a box, where the boxes are of varying sizes depending on the importance of the individual chemistry in each box for the overall reaction mechanism.

5.3 The block structure modelling methodology

The bottom-up development methodology proposed here divides the chemistry into blocks that can then be combined to create reduced reaction mechanisms for different fuels. These blocks will be of varying chemical complexity depending on what parts of the chemistry they contain, and depending on what chemical parameters are to be predicted. Since radicals, such as O, H, OH, CH_3 and HO_2, are essential in the combustion process the chemistry controlling these radicals, and the blocks containing the majority of this chemistry, will have a high level of chemical complexity. This means for example that the block containing the H_2/O_2 chemistry will have a higher complexity, and hence be more chemically correct, than the blocks containing C_2 species. If the ignition delay time is a primary target the block controlling the fuel breakdown needs to have a relatively high chemical complexity, especially for larger hydrocarbon fuels operating at lower temperatures.

5.3.1 The H_2/O_2 block

It has been well established [32] that a large part of the combustion process of any hydrocarbon fuel is controlled through the creation and consumption of

Figure 5.1: Schematic image of the block structure modelling methodology. The methodology is used to create reduced ethylene-air [43], propane-air [11], kerosene-air [20,41,42] and Jet Propellant 10-air (JP-10-air) [81] reaction mechanisms.

the radical pool [32], and some key radicals in this pool are the O, H, OH and HO_2 species. A large part of the reactions controlling these species are found in the H_2/O_2 chemistry, meaning that this part of the modelling, or this block, is essential for any hydrocarbon combustion modelling. Having a well-predicted modelling of this radical pool demands the inclusion of most, if not all, of the reactions and reaction pathways in Section 4.1. When all these reactions and their corresponding species are included the end result is a detailed hydrogen-air reaction mechanism. Another important characteristic in this block is the production of the final species H_2O, which is an overall exothermic process. This process will play a key role in determining the overall combustion characteristic due to the effects on the temperature increase.

5.3.2 The C_1/H/O block

Other key species in any hydrocarbon combustion are the C_1 species, such as CH_3, CH_2O, HCO, CO and CO_2. These species are to a large degree described within the C_1/H/O chemistry. Since CH_4 in terms of concentration is one of the main intermediate species in oxidation of larger hydrocarbons [32, 46, 47], and since it is present ahead of smaller C_1 radicals in the reaction chain, it can be used as a fuel molecule for the C_1 species block. Like the H_2/O_2 block the C_1/H/O chemistry also contain highly exothermic pathways producing final species.

The number of possible species, reactions and reaction pathways is considerably higher in this block compared to the H_2/O_2 block due to the more complex molecular structure of CH_4 compared to H_2. A result of this increase in molecular complexity is that the size of the C_1/H/O block could potentially be at least one order of magnitude larger than that of the H_2/O_2 block. However, since the most important radicals are mainly controlled within the H_2/O_2 block the C_1/H/O block could in theory be reduced without the loss of the main description of the chemical process and without a loss in reaction mechanism predictability. The main reactions and reaction pathways needed in the C_1/H/O block are described in Section 4.2.

It is within the C_1/H/O block that a first significant reduction of species and reactions can begin and a reduced reaction mechanism can start to take form. By coupling the chemistries described in Sections 4.1 and 4.2 a reduced methane-air reaction mechanism can be produced [25], shown in Table 3.1.

5.3.3 The C_2 intermediates block

When moving towards more complex fuel molecules the number of possible species, reactions and reaction pathways becomes larger. The influence of the C_2 block on the radical pool production/consumption, and therefore the overall combustion process, is smaller compared to the H_2/O_2 and C_1/H/O blocks. This means that the chemical complexity for the C_2 block can be further reduced compared to that of the C_1/H/O block. The high concentration of the C_2H_4 species in the oxidation of larger hydrocarbon molecules [32, 46, 47] is one of the main reasons to include the C_2 block. Even though the chemical complexity for the C_2 block can be relatively low, and the reduction in species and reactions is extensive, this block still contributes with important features to the combustion process, such as the inclusion of the important C_2H_4 species. It also serves as a bridge between initial fuel breakdown products of larger fuel molecules and the underlying H_2/O_2 and C_1/H/O blocks.

5.3.4 Additional C_x blocks

Even though CH_4 and C_2H_4 are some of the main intermediate hydrocarbons in the oxidation of larger hydrocarbon fuels, so are also C_3H_6, C_4H_{10} and n-C_4H_{10}, [32, 46, 47]. It could therefore be useful to also include one block containing C_3 species and one containing C_4 species. As with the C_2 block the chemical complexity in the C_3 and C_4 blocks can be relatively low and the blocks themselves serve the dual purposes of adding key important intermediate hydrocarbons as well as acting as a bridge between initial fuel breakdown products and the underlying C_2 and C_1 blocks. However, since the main goal with reduced reaction mechanism development is to produce high-performing reaction mechanisms but still using as few species and reactions as possible these larger C_x blocks would ideally be omitted if possible. It has been proven that it is possible to create high-performing reaction mechanisms without adding blocks with carbon number higher than two [11, 20, 41–43, 81].

5.3.5 The fuel breakdown block

The chemical complexity and size of the block controlling the fuel breakdown reactions varies significantly depending on the chosen fuel. It also depends if the reaction mechanism is designed to predict the sometimes complex ignition behaviours accompanying some large hydrocarbons. For simpler alkanes and alkenes, such as CH_4 and C_2H_4, the main fuel breakdown reactions are generally already included in the C_1/H/O and C_2 blocks. For alkanes and alkenes operating at elevated temperatures often only thermal decomposition reactions breaking bonds between carbon atoms (C-C bond breaking) in the fuel molecule are needed. This type of fuel breakdown results in global reactions that in one single step produces a set of C_1 and/or C_2 species which then couples to an underlying reduced reaction mechanism [11,20,41,42,46,47,81,82]. A C-C bond break for propane could be

$$C_3H_8 \longrightarrow CH_3 + C_2H_5. \tag{5.1}$$

Reaction 5.1 then couples to the C_2 intermediate block through the C_2H_5 species and to the C_1/H/O block through the CH_3 species. For large fuel molecules, with carbon numbers of roughly five or higher, the simple thermal decomposing reactions may not be enough to predict the complex ignition characteristics associated with these fuels [41, 46, 47, 82]. A large fuel molecule with its many possible intermediate species and reaction pathways demand a more rigorous strategy for the modelling of its initial oxidation, including more oxygen-containing fuel products and with a larger set of fuel and fuel product reactions. An example

of the complex reaction pathways of large hydrocarbons is schematically shown in Figure 5.2.

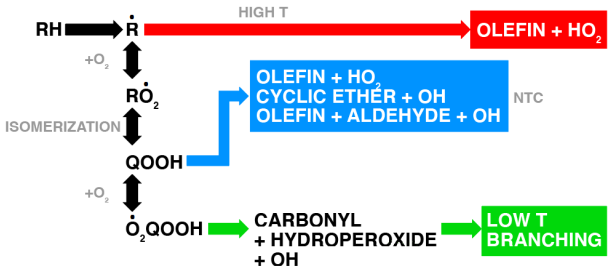

Figure 5.2: Simplified reaction scheme for paraffin auto-ignition, adopted from [83, 84].

It has been shown that a large fuel molecule with its extensive chemical complexity can be effectively modelled, even for ignition delay time with a NTC behaviour, by just expanding the chemistry describing the fuel and initial fuel products [42, 81, 85].

5.3.6 Reaction rate coefficients

Having knowledge about which reactions to include, and which major reaction pathways are important, is not sufficient to complete the modelling. The corresponding reaction coefficients (A, n, E_a) also need to be determined. For elementary reactions such coefficients can be found in the literature, and often different detailed reaction mechanisms have the same, or similar, coefficient values for one particular reaction.

Assigning appropriate reaction coefficients to non-elementary reactions can however be challenging. The C-C bond breaking reactions for example are mostly associated with high-temperature chemistry. For such C-C bond breaking reactions the idea is often that these bonds are broken via thermal decomposition and a high activation energy is therefore an appropriate choice [20, 41, 42, 46, 47, 81, 82].

When the reactions and their reaction coefficients have been chosen additional adjustments of the coefficients might still be needed. Since the majority of the chemistry is controlled through the production and consumption of radicals these are the species whose reactions should be adjusted initially.

5.3.7 Limitations of the block structure methodology

As with any development technique there are limitations to what this bottom-up block structure methodology can model. At more extreme conditions or when

using exotic fuel mixture compositions the block structure methodology may need to add so many additional species and reactions that the result will be a (semi-)detailed reaction mechanism.

Another limitation is that it demands a high level of chemical kinetic knowledge in order to determine which species and reactions, and which blocks, need to be included. When using existing automated reduction techniques the level of chemical kinetic knowledge required is generally not as high.

The validation of the reaction mechanisms developed using the block structure methodology rely on experimental data, hence the availability of these data can become a limiting factor. This is true for all users of bottom-up development principles [20, 41–43, 46, 47, 81, 85, 86].

5.3.8 Summary of the block structure methodology

The bottom-up development methodology presented here divides the chemistry into blocks, with individual chemical complexity of each block dependent on the importance of that block on the overall combustion process. This will create one block with a high chemical complexity and a large number of reactions (H_2/O_2 block), blocks with reduced number of reactions but still with a relatively high chemical complexity (C_1/H/O block and in certain cases the fuel breakdown block), and less important blocks with lower chemical complexity (C_2 and C_x blocks). The blocks are then combined to form one coherent reduced reaction mechanism with a high predictability but a low number of species and reactions and hence a relatively low computational cost.

Two main features of the block structure modelling methodology presented here are that it

- makes it possible to adjust the level of chemical complexity in each block depending on the importance of the underlying chemistry;
- enables the use of one single set of reactions in the underlying H_2/O_2, C_1/H/O and C_2 blocks irrespective of what alkane or alkene is being modelled [11, 20, 25, 41–43, 81].

By following the block structure development methodology several reduced reaction mechanisms have been developed. The developed reaction mechanisms include mechanisms for methane-air [25] and ethylene-air combustion [43] as well as propane-air [11], kerosene-air ($C_{12}H_{23}$-air) [20, 41, 42] and JP-10-air [81] combustion.

Chapter 6

Combustion modelling

There are three methods for simulating turbulent combustion [3]; Direct Numerical Simulation (DNS), Reynolds Averaged Navier-Stokes (RANS) and Large Eddy Simulation (LES). The DNS method, where all spatial and temporal scales are resolved [87, 88] is limited to canonical problems due to the vast computational costs associated with solving the equations on such large ranges of scales that combustion flow normally entails. The engineering alternative to DNS is RANS [4, 89] which is based on the ensemble or time-averaged flow equations. The averaging essentially removes all dynamic and intrinsic coupling between the flow and the chemistry in the underlying reactive Navier-Stokes equations and the effects of the turbulence are transformed into Reynolds stress and flux terms, and mean reaction rates [4, 89, 90]. RANS is capable of capturing gross features of combustion but its lack of temporal resolution hinders the method from predicting unsteady phenomena such as flame-stabilization, cycle-to-cycle variations, combustion instabilities, thermoacoustic instabilities and self-ignition, with a high degree of accuracy. The third alternative, LES, is based on the idea of spatial scale separation. LES divides the flow into two regimes of the reacting equations using a low-pass filtering with a cut-off length scale based on the grid size, Δ. The first regime, composing the large-scale eddies, is simulated and solved for using space-time accurate schemes, whereas the second regime, composing the scales from Δ down to the Kolmogorov scale, is modelled using subgrid models [6]. Figure 6.1 illustrates on which scales the different modelling options can operate. As LES has predominantly been used in this work it is described in greater detail below.

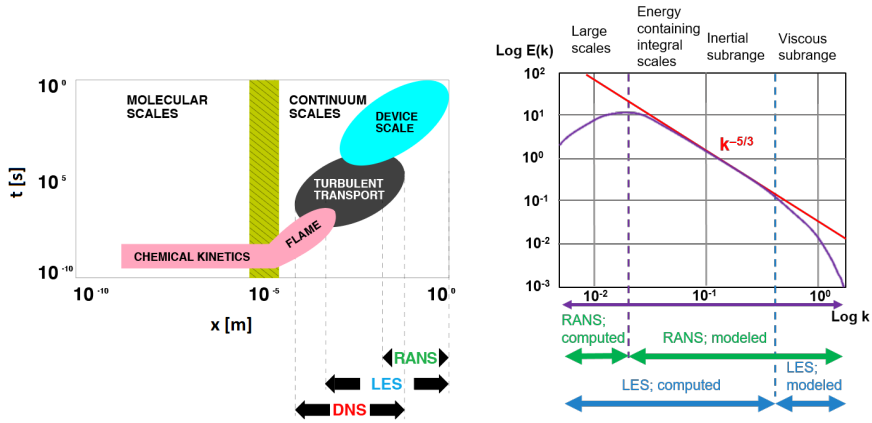

(a) (b)

Figure 6.1: Spatial and temporal scales and processes in reactive flows in (a), and the energy cascade in (b). Indications where each modelling approach (DNS, LES and RANS) can be applied is shown in both (a) and (b).

6.1 Large Eddy Simulation

The LES approach [6] adopted in the presented research is based on low-pass filtering of the governing reactive Navier-Stokes equations, eq. 2.7. Each dependent variable is decomposed to $f = \tilde{f} + f''$, where $\tilde{f}$ is the resolved part and f'' is the fluctuating part whose effects are modelled by the subgrid models. The resolved part, $\tilde{f}$, is commonly expressed using a Favre filter such that $\tilde{f} = \overline{\rho f}/\bar{\rho}$. The filtering is applied to $\tilde{f}$ (resolved part) through the filter $\bar{f} = G * f$ where $G = G(\mathbf{x}, \Delta)$, with a filter width of Δ. Filtering the reactive Navier-Stokes equations, eq. 2.7, will result in the following equations:

$$\begin{cases} \partial_t(\bar{\rho}) + \nabla \cdot (\bar{\rho}\tilde{\mathbf{v}}) = 0, \\ \partial_t(\bar{\rho}\tilde{\mathbf{v}}) + \nabla \cdot (\bar{\rho}\tilde{\mathbf{v}} \otimes \tilde{\mathbf{v}}) = -\nabla\bar{p} + \nabla \cdot \left(2\mu\tilde{\mathbf{D}} - \frac{2}{3}\mu(\nabla \cdot \tilde{\mathbf{v}})\mathbf{I} - \mathbf{B}\right), \\ \partial_t(\bar{\rho}\tilde{E}) + \nabla \cdot (\bar{\rho}\tilde{\mathbf{v}}\tilde{E}) = \nabla \cdot \left(- \bar{p}\tilde{\mathbf{v}} + 2\mu\tilde{\mathbf{D}}\tilde{\mathbf{v}} - \frac{2}{3}\mu(\nabla \cdot \tilde{\mathbf{v}})\tilde{\mathbf{v}} + \varkappa\nabla\tilde{T} - \mathbf{b_E}\right), \\ \partial_t(\bar{\rho}\tilde{Y}_i) + \nabla \cdot (\bar{\rho}\tilde{\mathbf{v}}\tilde{Y}_i) = \nabla \cdot \left(\frac{\mu}{Sc_i}\nabla\tilde{Y}_i - \mathbf{b}_i\right) + \overline{\dot{w}}_i. \end{cases} \tag{6.1}$$

Here the bar is denoting the filtered quantities and the tilde the Favre averaged ones. The total energy is expressed as $\tilde{E} = \tilde{e}_{in} + \frac{1}{2}\tilde{\mathbf{v}}^2 + k$ where k is the subgrid kinetic energy, $k = \frac{1}{2}(\bar{\mathbf{v}}^2 - \tilde{\mathbf{v}}^2)$. $\mathbf{B}$ is the subgrid stress tensor, $\mathbf{B} = \bar{\rho}(\widetilde{\mathbf{v} \otimes \mathbf{v}} - \tilde{\mathbf{v}} \otimes \tilde{\mathbf{v}})$. The flux vectors $\mathbf{b}_E$ and $\mathbf{b}_i$ are expressed using $\mathbf{b}_E = \bar{\rho}(\widetilde{\mathbf{v}E} - \tilde{\mathbf{v}}\tilde{E})$ and $\mathbf{b}_i = \bar{\rho}(\widetilde{\mathbf{v}Y_i} - \tilde{\mathbf{v}}\tilde{Y}_i)$, respectively [91].

6.1.1 Subgrid flow modelling

To describe the effects of the unresolved flow on the resolved flow using the resolved variables, and to close the filtered reacting LES equations, eq. 6.1, a subgrid model is required [6]. The subgrid models can in LES be described as either *functional* or *structural* models [6]. Functional subgrid models, the most widely used class, aim to emulate the cascade of kinetic energy from large scales to small scales. This type of subgrid models includes the frequently used Smagorinsky (SMG) model [92,93] and the Wall-Adapting Local Eddy (WALE) model [94], where the latter is missing an approximation of k, required for modelling the subgrid turbulence chemistry interactions. Another useful functional model is the One-Equation Eddy Viscosity Model (OEEVM) [95–97]. Structural subgrid models are intended to mimic the structure of the subgrid stress tensor and flux vectors instead of the effects of these on the resolved flow. Examples of structural models are the Scale Similarity model [98] and the Approximate Deconvolution Model (ADM) [99,100].

6.1.2 Modelling of filtered reaction rates

A second model required to close the filtered reacting flow equations, eq. 6.1, is the one for the filtered species reaction rates, $\overline{\dot{w}}_i$. This model is commonly denoted a Turbulence Chemistry Interaction (TCI) model due to the highly non-linear nature of the species reaction rates, rates depending on composition and temperature, and to the fact that most reactions are confined to thin reacting structures at small unresolved scales. Different approaches especially designed for LES have been proposed, including *flamelet* models, *finite rate chemistry* models and *linear eddy* models [3]. Another class of models are the Probability Density Function (PDF) models. PDF model is a collection name for several different models that share the feature of expressing the filtered reaction rate in terms of a multi-variable PDF, $\mathfrak{P} = \mathfrak{P}(\rho, T, Y_i, \mathbf{x}, t)$, that provides most of the statistical information of interest regarding the flow at $\mathbf{x}$ and t [101–103].

The finite rate chemistry models do not assume anything about the flow or the flame structure but instead attempts to solve the species equations using models for the filtered reaction rates, $\overline{\dot{w}}_i$. A number of finite rate chemistry models are available, some of which will be described briefly below.

- The Eddy Dissipation Concept (EDC) [104], based on the model by Magnussen et al. [105], uses the assumption that the combustion takes place in regions of fine structure and with high vorticity and chemical activity. These in turn are embedded in regions with lower vorticity and chemical activity. The filtered reaction rates, $\overline{\dot{w}}_i$, are represented as weight averages of the reaction rates within the fine structures and surroundings, so that

$\overline{\dot{w}}_i = \gamma^* \omega_i^* + (1-\gamma^*)\omega_i^0$. γ^* is the reacting volume fraction, and ω_i^* and ω_i^0 the reaction rates in the fine structures and surroundings, respectively. In general $\omega_i^* \gg \omega_i^0$ meaning that ω_i^0 can be neglected. Here γ^* is estimated as $\gamma^* = 1.02(\nu/\Delta v')^{3/4}$ and τ^* as $\tau^* = 1.24(\nu/\Delta v'^3)^{1/2}$, with ν being the molecular viscosity and v' the subgrid velocity fluctuations.

- The Thickened flame model (TFM) [106] is based on the assumption that the flame can be thickened by decreasing the quasi-laminar reaction rates by a factor F, and increasing the diffusivity by the same factor to preserve the laminar burning velocity. The factor $F = \Delta/\delta_v$, where Δ is the filter width and δ_v the laminar flame thickness. The increase in flame area due to turbulence is allowed for by pre-multiplying the quasi-laminar reaction rates, $\overline{\dot{w}}_i$, and diffusivities, D_i, by the subgrid wrinkling factor Ξ, so that $\overline{\dot{w}}_i = \Xi \dot{w}_i / F$ and $D_i = F\Xi D_i$.

- The Partially Stirred Reactor model (PaSR) [107,108], based on the same assumptions as the EDC model, uses theoretical estimates and DNS data to estimate γ^*. The fine structures are lumped together so that $\gamma^* \approx \tau_c/(\tau^* + \tau_c)$ where the chemical time scale $\tau_c \approx \delta_v / s_L$ represents the overall combustion reaction. The modelling of τ^* is based on the observation that the fine structure area-to-volume ratio is given by the dissipative length scale $l_D = (\nu/(v'/\Delta))^{1/2})$. The velocity that influences the fine structures is the Kolmogorov velocity, v_η, such that $\tau^* = l_D/v_\eta$. This can then be reformulated as $\tau^* = \sqrt{\tau_\Delta \tau_\eta}$ where the shear time-scale τ_Δ is written as $\tau_\Delta = \Delta/v'$. The filtered reaction rates can then be written as

$$\overline{\dot{w}_i(\rho, Y_i, T)} = \gamma^* \dot{w}_i(\rho, Y_i^*, T^*) + (1-\gamma^*)\dot{w}_i(\rho, Y_i^0, T^0). \tag{6.2}$$

  Here $(1-\gamma^*)\dot{w}_i(\rho, Y_i^0, T^0)$ is small and usually neglected.

Several other models exists, such as the Fractal Model (FM) [109–111], or the Quasi-Laminar (QL) model which does not take into account the effects of the subgrid turbulence.

In the present work only the finite rate chemistry model have been used, using both the EDC [25] and PaSR [11, 20, 21] models, both of which have shown to produce good predictions for a variety of applications [10, 11, 13, 20, 22, 25, 112, 113].

Chapter 7

Mechanism performances

The block structure methodology was implemented to develop reduced reaction mechanisms for methane-air, Z42 [25], ethylene-air, Z66 [43], propane-air, Z66 [11] and kerosene-air combustion, Z65 [41] and Z77 [42]. In this chapter a selection of results for these reaction mechanisms will be presented and compared to experimental data and detailed reaction mechanisms, and for methane and propane also global reaction mechanisms. The simulations will focusing on flame parameters presented in Section 3.9. These parameters are the laminar burning velocity, s_L, ignition delay time, τ_{ig}, flame temperature, T_{max}, and major species concentrations (here CO and CO_2). The flame parameters are sampled using zero- and laminar one-dimensional simulations performed using Cantera [114]. The extinction strain rate, σ_{ext}, will not be included in this section because that flame parameter has not been a development target for any of the reduced reaction mechanisms developed using the block structure methodology.

7.1 Laminar burning velocity

The laminar burning velocity is, for wide ranges of equivalence ratios and temperature and pressure conditions, an indicator if a reaction mechanism can be considered well-developed. Results for all four fuels will be presented below. Initially presented at standard conditions, defined for methane, ethylene and propane as p=1 atm and T=300 K, and for kerosene as p=1 atm and T=400 K. The higher temperature for kerosene is because the kerosene fuel is not in gaseous phase at 300 K. The kerosene mixture is represented by either $C_{12}H_{23}$ [41,42,47] (Z65, Z77, HC277), N-$C_{12}H_{26}$ [39] (S6664) or a mixture composition with an average molecular structure close to $C_{12}H_{23}$ [115] (R5591). All simulations will, if possible, run from ϕ=0.5 to ϕ=1.8, covering fuel-air mixtures from lean to rich.

Laminar burning velocities for fuel-air mixtures of small alkanes, methane and propane, are shown in Figures 7.1(a) and (b), respectively. Here results from the Z42 [25] and Z66 [11] reaction mechanisms are plotted together with experimental data and results from both detailed and global reaction mechanisms. For methane-air flames Z42 matches both the experimental data and the predictions by the two detailed reaction mechanisms (GRI 3.0 [62], SD270 [64]) over the complete range of equivalence ratios. The two global reaction mechanisms (WD2 [8], JL4 [7]) both have decent predictions up to stoichiometric mixtures. At higher equivalence ratios the simple chemical description of these reaction mechanisms result in substantial overpredictions in the laminar burning velocity. For propane, Z66 matches both the experimental data and detailed reaction mechanism predictions. The results from the two global reaction mechanisms again overpredict the velocity at fuel rich conditions. The individual differences of the respective detailed mechanisms and Z42 and Z66 can be considered to be within uncertainty limits of the experimental data. Due to the poor predictability of global reaction mechanisms none will be included when simulating ethylene-air and kerosene-air mixtures.

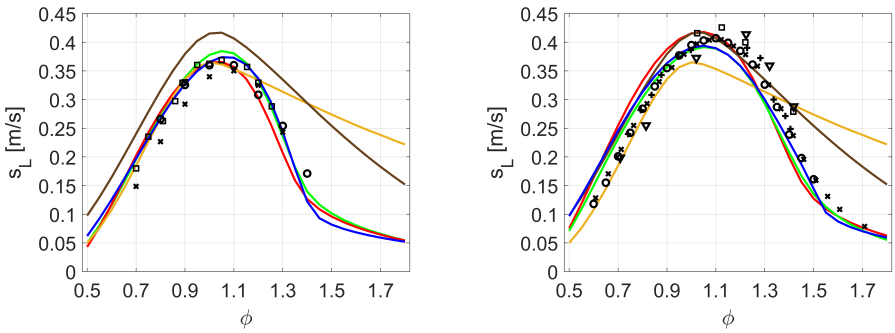

Figure 7.1: Laminar burning velocities for CH_4 in (a) and C_3H_8 in (b), at standard conditions. Legend, reaction mechanisms, for CH_4: blue - Z42 [25], red - SD270 [64], green - GRI 3.0 [62], orange - WD2 [8], brown - JL4 [7]. For C_3H_8: blue - Z66 [11], red - SD270 [64], green - USC C_1-C_4 [65], orange - WD2 [8], brown - JL4 [7]. Legend, experimental data, for CH_4: $\circ$ - Goswami et al. [116], $\square$ - Park et al. [117], $\times$ - Lowry et al. [118]. For C_3H_8: $\circ$ - Bosschaart et al. [119], $\times$ - Dirrenberger et al. [120], $\bigtriangledown$ - Huzayyin et al. [121], $+$ - Vagelopoulos et al. [122], $\square$ - Jomaas et al. [123].

Ethylene-air flames, displayed in Figure 7.2(a), show similar behaviour as the smaller alkanes above, and the Z66 reaction mechanism matches both the experimental data and the detailed reaction mechanisms [124, 125] (Aramco

1.3 [124], USC C_2-C_3 [125]). Note the different amplitude in laminar burning velocity of ethylene compared to methane and propane. This difference in laminar burning velocity is generic when comparing small alkanes to small alkenes. For the kerosene-air mixture, Figure 7.2(b), two reduced reaction mechanisms developed using the block structure methodology is shown, the smaller Z65 [41] and the slightly larger Z77 [42]. Two detailed reaction mechanisms (S6664 [39], R5591 [115]) are used for comparison, and one reduced reaction mechanism (HC277 [46,47]), also developed using a bottom-up development approach. Note that R5591 [115] did not converge for all equivalence ratios. The experimental data sets can be divided into two different levels, one with a maximum value of 60 cm/s or higher, and one at around 55 cm/s. All reaction mechanisms matches one of the two sets of experimental data.

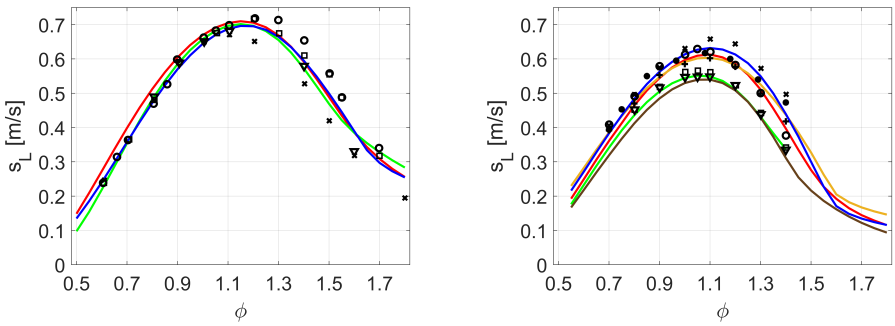

Figure 7.2: Laminar burning velocities for C_2H_4 in (a) and kerosene in (b), at standard conditions. Legend, reaction mechanisms, for C_2H_4: blue - Z66 [43], red - Aramco 1.3 [124], green - USC C_2-C_3 [125]. For kerosene: blue - Z77 [42], orange - Z65 [41], red - S6664 [39], green - R5591 [115], brown - HC277 [46, 47] ($C_{12}H_{23}$). Legend, experimental data, for C_2H_4: ∘ - Jomaas et al. [126], × - Kochar et al. [127], □ - Egolfopoulos et al. [128], ▽ - Hassan et al. [129]. For kerosene: ▽ - Xu et al. [47], ∘ - Ji et al. [48], □ - Xu et al. [47], × - Kumar et al. [49], • - Kumar et al. [50], + - Hui et al. [51].

The laminar burning velocity for all hydrocarbons is to a large degree determined by the high-temperature chemistry described in the H_2/O_2 and $C_1/H/O$ blocks. Once these blocks have been properly developed they have the possibility to model the laminar burning velocities for several alkane and alkene fuels using the same set of reactions. Figures 7.1 and 7.2 show that the reduced reaction mechanisms developed using the block structure methodology is capable of predicting the laminar burning velocities at standard conditions for a wide range of equivalence ratios and for C_1 to C_{12} hydrocarbon fuels. Figure 7.1

also clearly show the limitations of global reaction mechanisms. A too simple description of the chemistry will result in poor predictions at conditions other than fuel lean.

7.1.1 Sensitivity analysis

In order to investigate the most important reactions for the laminar burning velocities for individual reaction mechanisms sensitivity analyses are performed. The analyses are made at standard conditions and ϕ=1.0. To limit the analysis only the smallest (methane) and largest (kerosene) fuels will be shown. For methane, shown in Figure 7.3, Z42 [25], containing 18 species and 42 irreversible reactions, is compared to SD270 [64], containing 58 species and 270 reversible reactions. Even with a large difference in number of species and reactions both reaction mechanisms show strong similarities in their sensitivity analyses, indicating that both reaction mechanisms rely on the same chemistry to determine the laminar burning velocity. Reactions with negative sensitivities present in both reaction mechanisms are $H+O_2+M \rightarrow HO_2+M$, $CH_3+H+M \rightarrow CH_4+M$, $CH_4+H \rightarrow CH_3+H_2$ and $H+HCO \rightarrow CO+H_2$. Similar reactions with positive sensitivities are $H+O_2 \rightarrow O+OH$, $CO+OH \rightarrow CO_4+H$, $CH_3+O \rightarrow CH_2O+H$ and $HCO + M \rightarrow CO + H + M$. Generally all reactions with a high negative sensitivity reduces the size of the radical pool or reduce the concentration of H atoms, effectively reducing the rate of progress of the reacting system. Conversely, reactions with high positive sensitivities expands the radical pool or the H atom concentration, speeding up the rate of reaction of the system. Even though Z42 only contain 30% of the number of species and 8% of the number of reactions of the detailed reaction mechanism both mechanisms show strong similarities in key reactions and simulation results. This show that it is possible for a reduced reaction mechanism to predict the laminar burning velocity as long as certain key reactions are present.

The sensitivity analyses of kerosene is shown in Figure 7.4. Here the Z77 [42] reaction mechanism, containing 30 species and 77 irreversible reactions, is compared to a S6664 [39] containing 798 species and 6664 reversible and irreversible reactions. Even though Z77 contain less than 4% of the number of species and less than 1% of the number of reactions present in S6664 both mechanisms show strong similarities in their sensitivity analyses. Four of the reactions with the highest negative sensitivities and six of the reactions with the highest positive sensitivities are the same between the two reaction mechanisms. Several of these reactions are also identical to the reactions in the sensitivity analyses for methane. This shows that the chemistry important for predicting the laminar burning velocity is more or less the same regardless of the size of the alkane fuel. This in turn means that as long as key species and reactions

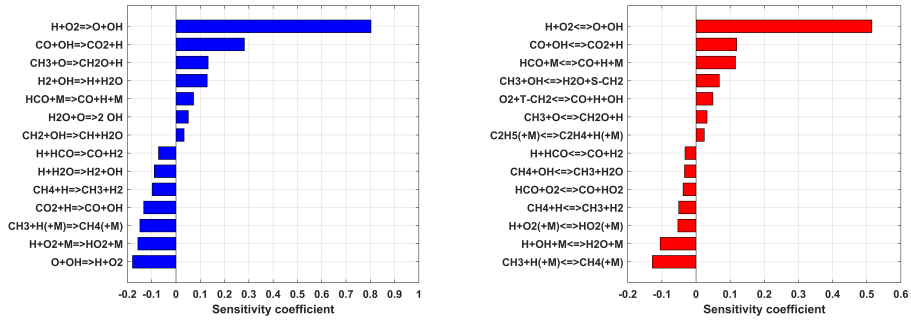

(a) (b)

Figure 7.3: Sensitivity analysis for the laminar burning velocity of a methane-air mixture at standard conditions and ϕ=1.0. Z42 [25] is shown in (a) and SD270 [64] in (b).

are present in the H_2/O_2 and $C_1/H/O$ blocks the reaction mechanism will be capable of predicting the laminar burning velocity for a wide range of alkane fuel sizes. The consequence of this is that there is a lowest number of species and reactions needed in the H_2/O_2 and $C_1/H/O$ blocks, enabling a much higher degree of reduction for the other blocks. Hence, the possible level of reduction increases as the fuel molecular size increases.

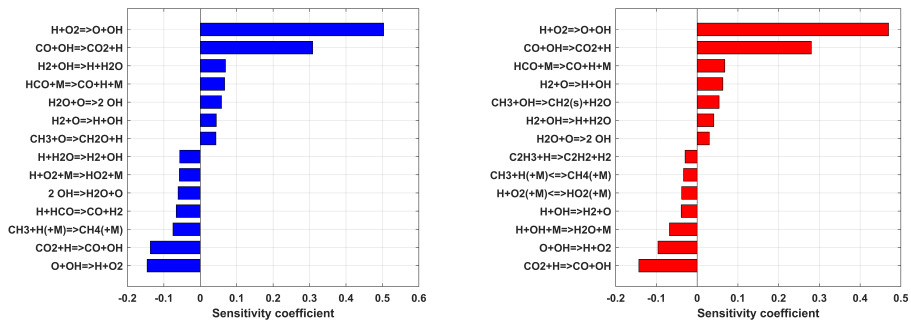

(a) (b)

Figure 7.4: Sensitivity analysis for the laminar burning velocity of a kerosene-air mixture at standard conditions and ϕ=1.0. Z77 [42] is shown in (a) and S6664 [39] in (b).

7.1.2 Computational cost

The main limitations for the use of reaction mechanisms in LES or DNS is the computational cost they require. In this section time requirements of all reaction mechanisms in Figures 7.1 and 7.2 are presented, for simulations of laminar burning velocities at standard conditions and equivalence ratios between 0.5 and 1.8 (0.5 to 1.4 for R5591 [115]). Unsurprisingly the reaction mechanisms requiring the least amount of time are the global reaction mechanisms WD2 [8] and JL4 [7]. However, considering their limited predictability the low computational cost can not be considered a large enough compensation. The reduced reaction mechanisms developed using the block structure methodology requires far less computational time than detailed reaction mechanisms. The time needed for Z42 [25] for a methane-air mixture is between 9% and 7% of the time needed for the reference detailed reaction mechanisms. For Z66 [11] and a propane-air mixture it is between 13% and 3%, and for Z66 [43] and an ethylene-air mixture between 4% and 0.1%. For the largest fuel, kerosene, the reference reaction mechanisms consists of two detailed, S6664 [39] and R5591 [115], and one reduced reaction mechanism, HC277 [46, 47]. The time needed for the smaller Z65 [41] reaction mechanism compared to the three reference reaction mechanisms is 13%, 0.2% and 0.02%, and for the slightly larger Z77 [42] 43%, 0.6% and 0.08%. The relatively low computational cost for the reduced kerosene-air reaction mechanisms compared to the other fuels is probably due to the higher initial gas temperature of 400 K. Savings in computational cost for all four fuels using the reduced reaction mechanisms is profound. Without this considerably lower computational cost the reduced reaction mechanisms would not be suitable for three-dimensional LES or DNS. The simulation times for each reaction mechanism presented in Figures 7.1 and 7.2 are listed in Table 7.1, which also displays the number of species and reactions for each reaction mechanism.

Table 7.1: Time it takes to compute the laminar burning velocity at standard conditions for all reaction mechanisms in Figures 7.1 and 7.2.

Reaction mechanism	Fuel	$N_{species}$	$N_{reactions}$	total time
Z42 [25]	CH_4	18	42	5 min
SD270 [64]	CH_4	58	270	72 min
GRI 3.0 [62]	CH_4	53	325	57 min
WD2 [7]	CH_4	6	2	0.8 min
JL4 [8]	CH_4	7	4	1.6 min
Z66 [43]	C_2H_4	23	66	6 min

Continued on next page

Reaction mechanism	Fuel	$N_{species}$	$N_{reactions}$	Time
Aramco 1.3 [124]	C_2H_4	253	1542	6008 min
USC C_2-C_3 [125]	C_2H_4	75	529	148 min
Z66 [11]	C_3H_8	25	66	13 min
SD270 [64]	C_3H_8	58	270	99 min
USC C_1-C_4 [65]	C_3H_8	111	784	518 min
WD2 [7]	C_3H_8	6	2	0.9 min
JL4 [8]	C_3H_8	7	4	1.4 min
Z65 [41]	$C_{12}H_{23}$	24	65	0.3 min
Z77 [42]	$C_{12}H_{23}$	30	77	1 min
HyChem [46, 47]	$C_{12}H_{23}$	50	277	2.3 min
R5591 [115]	$C_{12}H_{23}$	231	5591	167 min
S6664 [39]	N-$C_{12}H_{26}$	798	6664	1226 min

7.1.3 Effects of temperature and pressure

The laminar burning velocity is strongly affected by variations in initial gas temperature and pressure. Ideally, for most real-world applications, any reaction mechanism should be capable of predicting the increasing or decreasing laminar burning velocities resulting from changes in these conditions.

To illustrate the effects of increasing initial gas temperature or pressure methane-air and kerosene-air mixtures have been simulated at elevated conditions. By increasing the temperature of the initial fuel-air mixture an increase in the laminar burning velocity is achieved, exemplified in Figure 7.5. Both methane, Figure 7.5(a), and kerosene, Figure 7.5(b), show gradual increases in laminar burning velocities as the temperature increases. All reaction mechanisms are able to predict an increase in laminar burning velocities, and their mutual relations are similar to that of the standard conditions in Figures 7.1(a) and 7.2(b).

If an increase in initial gas temperature results in increasing laminar burning velocities an increase in initial gas pressure has the opposite effect. The higher the pressure the lower the laminar burning velocity. Figures 7.6(a) and (b) illustrate how the increase in pressure affects the laminar burning velocities of methane-air and kerosene-air mixtures, respectively. Z42 and Z65/Z77 together with the detailed reaction mechanisms capture the effect of an increase in pressure. Same as for the increase in temperature the mutual relations between these mechanisms are similar to what they are at the standard conditions in Figures 7.1(a) and 7.2(b). The global reaction mechanisms however are unable to capture the effect of an increase in pressure, with only modest decreases in the predicted velocities. Because of the low predictability of global reaction

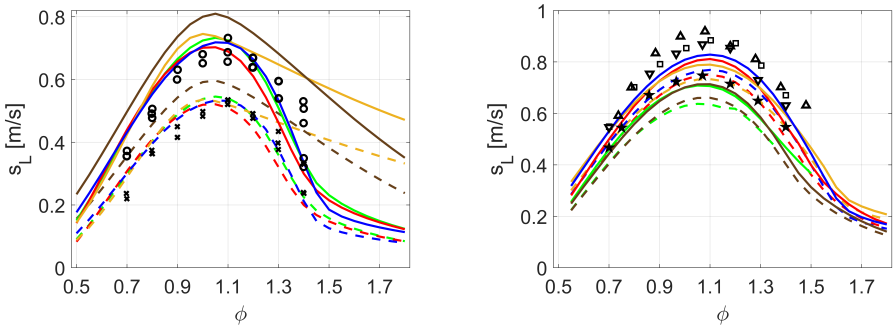

Figure 7.5: Laminar burning velocities at p=1 atm and elevated initial gas temperatures, for CH_4 in (a) and kerosene in (b). Dashed lines for CH_4 corresponds to T=373 K and solid lines to T=443 K. Dashed lines for kerosene corresponds to T=450 K and solid lines to T=470 K. Legend, reaction mechanisms, for CH_4: blue - Z42 [25], red - SD270 [64], green - GRI 3.0 [62], orange - WD2 [8], brown - JL4 [7]. For kerosene: blue - Z77 [42], orange - Z65 [41], red - S6664 [39], green - R5591 [115], brown - HC277 [46,47] ($C_{12}H_{23}$). Legend, experimental data, for CH_4 at T=373 K: $\circ$ - Hu et al. [130]. At T=443 K: $\times$ - Hu et al. [130]. For kerosene at T=450 K: $\star$ - Kumar et al. [50]. At T=470 K: $\bigtriangledown$ - Kumar et al. [50], $\square$ - Kumar et al. [49], $\bigtriangleup$ - Chong et al. [131].

mechanisms these will not be included in comparisons of the other flame parameters. Comparisons between global, reduced and detailed reaction mechanisms, for a wide range of fuels have been presented in several publications [10–12,20]. Note that, as in Figure 7.2(b), R5591 [115] did not provide a solution for all equivalence ratios.

Most real world applications operate at elevated temperatures and pressures making it crucial that the effect of this is accurately modelled by the reaction mechanisms. Figures 7.5 and 7.6 show that the chosen species and reactions in the H_2/O_2 and $C_1/H/O$ blocks are capable of capturing the impact an increase in temperature or pressure has on the chemical kinetics. Since the reaction mechanisms developed using the block structure methodology all share the same species and reactions in their corresponding H_2/O_2 and $C_1/H/O$ blocks similar temperature and pressure dependencies on the laminar burning velocities can be seen for all these reaction mechanisms [11,25,41–43]. The results in Figures 7.5 and 7.1.3 verifies that the chemical kinetics necessary to capture the temperature and pressure effects on the laminar burning velocity is all present in the H_2/O_2 and $C_1/H/O$ blocks.

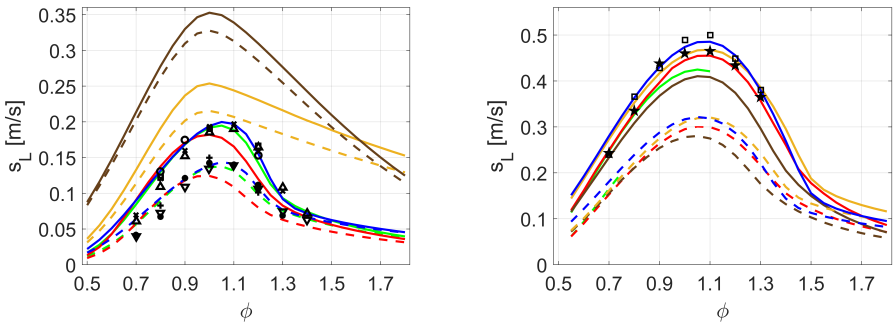

Figure 7.6: Laminar burning velocities at elevated initial gas pressures, for CH_4 at T=300 K in (a) and kerosene at T=400 K in (b). Solid lines for CH_4 corresponds to p=5 atm and dashed lines to p=10 atm. Solid lines for kerosene corresponds to p=3 atm and dashed lines to p=10 atm. Legend, reaction mechanisms, for CH_4: blue - Z42 [25], red - SD270 [64], green - GRI 3.0 [62], orange - WD2 [8], brown - JL4 [7]. For kerosene: blue - Z77 [42], orange - Z65 [41], red - S6664 [39], green - R5591 [115], brown - HC277 [46,47] ($C_{12}H_{23}$). Legend, experimental data, for CH_4 at 5 atm: $\circ$ - Goswami et al. [116], $\times$ - Lowry et al. [118], $\square$ - Gu et al. [132], $\triangle$ - Rozenchan et al. [133]. At 10 atm: $*$ - Lowry et al. [118], $+$ - Gu et al. [132], $\triangledown$ - Rozenchan et al. [133]. For kerosene at 3 atm: $\star$ - Hui et al. [51], $\square$ - Ji et al. [48].

7.2 Ignition delay time

Unlike the laminar burning velocity which relies heavily on the H_2/O_2 and $C_1/H/O$ blocks (see Sections 7.1 and 7.1.1) the ignition delay time also requires a sophisticated modelling of the fuel breakdown block. Nowhere is this more clear than for the Z77 reaction mechanism [42] whose main difference compared to its parent reaction mechanism Z65 [41] lies in the fuel breakdown modelling. Of the six reduced reaction mechanisms developed as part of this thesis [11,20,25,41–43] only two, modelling either ethylene-air [43] or kerosene-air [42] combustion, used the ignition delay time as a development target. Hence, these two reaction mechanisms produce more accurate ignition predictions than the other four. As described in Section 3.9.4 there are several possible definitions of when the fuel-air mixture has reached an explosive state. The ignition delay time results illustrated here uses either a certain value of the OH concentration (ethylene-air [43]) or a pre-defined value in the temperature increase (kerosene-air [41,42]) as the definition. For ethylene-air the reduced reaction mechanism Z66 is compared to two detailed reaction mechanisms (Aramco 1.3 [124] and USC C_2-C_3 [125])

and experimental data [56, 134, 135]. Shown in Figure 7.7 are the comparative results at ϕ=1.0 and pressures of either p=1.1 atm in (a) or 10.2 atm in (b), with an initial gas temperature range of between 1050 K and 1330 K. All three reaction mechanisms show predictions within the range of the experimental data, with an exception of USC C_2-C_3 [125] at lower temperatures and at p=10 atm. However, the results from the detailed reaction mechanisms come at a high computational cost compared to Z66, as indicated by the simulation times seen in Table 7.1.

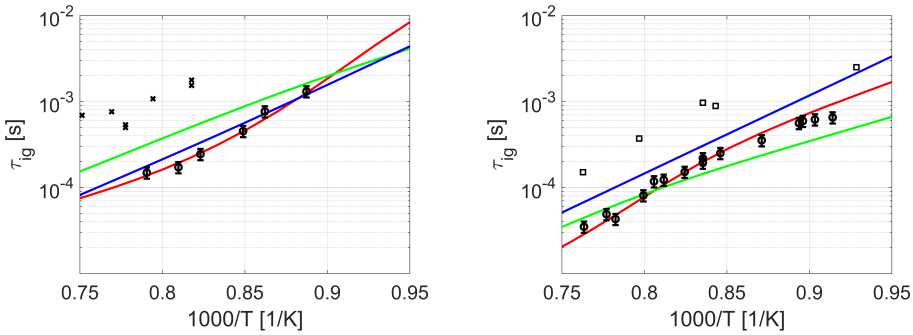

Figure 7.7: Ignition delay time for ethylene-air mixtures, at ϕ=1.0 and around p=1.0 atm in (a) and 10.0 atm in (b). Legend, reaction mechanisms: blue - Z66 [43], red - Aramco 1.3 [124], green - USC C_2-C_3 [125]. Legend, experimental data: ○ - Kopp et al. [56], × - Kalitan et al. [135], □ - Saxena et al. [134].

The complex NTC behaviour of large hydrocarbon fuel molecules represents a challenge for all chemical kinetic modelling, not least for reduced reaction mechanisms. The NTC behaviour also necessitates the use of a wider simulated temperature range, typically ranging from approximately 800 K to 1300 K, in order to capture the NTC ignition behaviour below approximately 1000 K. Figure 7.8 show the ignition delay time for a kerosene-air mixture at ϕ=1.0, and at p=10 atm in (a) and 20 atm in (b). The most obvious result here is the inability of two of the reaction mechanisms [41, 82] (orange, Z65 [41], and magenta, Jetsurf [82], lines) to capture the NTC behaviour. This is because these two reaction mechanisms only incorporates the high-temperature kinetics, limiting their predictable range to higher temperatures. Outside of the high-temperature regime these two reaction mechanisms overpredicts the ignition delay time by several orders of magnitudes. The range of predictions of the reaction mechanisms capable of reproducing a NTC behaviour is wide. Uncertainty in ignition delay time measurements is large, illustrated by the experimental data in Figure 7.8(b) where the differences in uncertainty can be one order of magnitude.

Given these large uncertainties all four reaction mechanisms capable of capturing the NTC behaviour (Z77, HC277, S6664, R5591) can be viewed as having acceptable modelling predictions. The large difference in ignition delay time predictions between Z65 and Z77 illustrate the flexibility of the block structure methodology. By adding a more accurate fuel breakdown block, increasing the number of species and reactions by only a handful, the overall predictability of Z77 is greatly improved compared to Z65. Since the species and reactions in the underlying H_2/O_2 and $C_1/H/O$ blocks are kept intact between Z65 and Z77 both will have similar predictive capabilities of the laminar burning velocity, temperature and species profiles [42] whose parameters mainly dependent on the chemistry in these blocks.

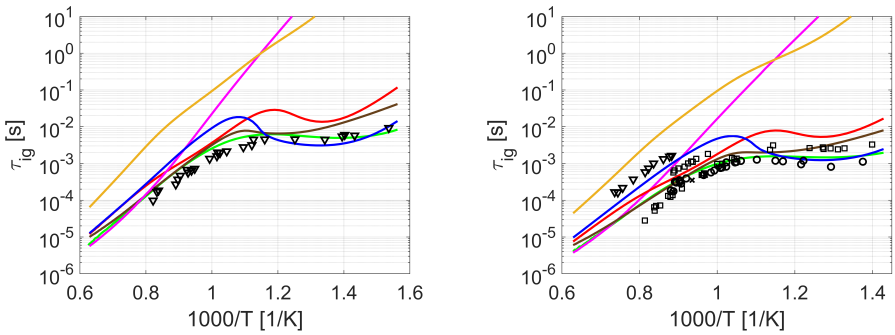

Figure 7.8: Ignition delay time for kerosene-air mixtures, at ϕ=1.0 and p=10 atm in (a) and p=20 atm in (b). Legend, reaction mechanisms: blue - Z77 [42], orange - Z65 [41], red - S6664 [39], green - R5591 [115], brown - HC277 [46, 47] ($C_{12}H_{23}$), magenta - Jetsurf [82]. Legend, experimental data, for 10 atm: $\bigtriangledown$ - Zhang et al. [52]. For 20 atm: $\times$ - Zhang et al. [52], $\circ$ - Vasu et al. [53], $\bigtriangledown$ - Zhu et al. [54], $\square$ - Vasu et al. [55].

Figures 7.7 and 7.8 show that it is possible for a reduced reaction mechanism to model the ignition delay time accurately. Even large fuel molecules such as kerosene, with its complex NTC behaviour, can be modelled as long as the underlying H_2/O_2 and $C_1/H/O$ blocks together with an extensive fuel breakdown block is used. Figures 7.7 and 7.8 also show that the modelling capabilities of the reduced reaction mechanisms is not limited to ambient pressures but can be used over a wide pressure range.

7.3 Flame temperature

The flame temperature is one of the most important flame parameters a reaction mechanism must be able to predict. The temperature is often displayed as either the maximum temperature for a specific equivalence ratio, Figure 7.9(a), or as the temperature profile over the one-dimensional simulation domain, Figure 7.9(b). Here Figure 7.9(b) is complemented with mole fraction profiles of the fuel (C_2H_4) and CO_2. Figure 7.9 illustrates the results of temperature predictions for an ethylene-air flame at standard conditions using the Z66 [43] reaction mechanism together with two detailed reaction mechanisms, Aramco 1.3 [124] and USC C_2-C_3 [125], and experimental data [136]. Note how the shape of the CO_2 concentration profile follows that of the temperature in Figure 7.9(b), highlighting the importance of the exothermic reaction, reaction 4.31 in Section 4.2, which forms CO_2.

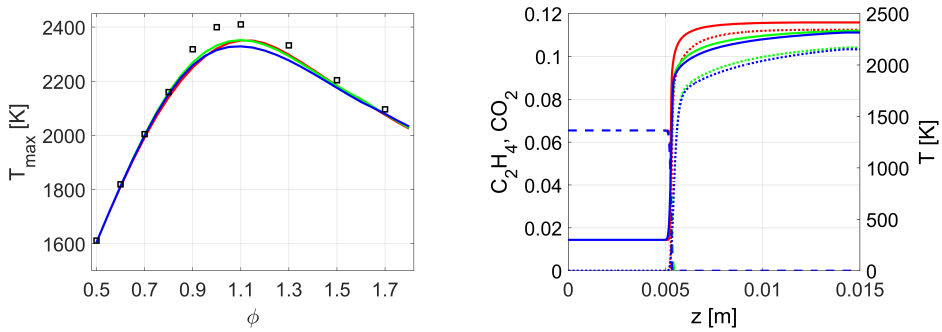

(a) (b)

Figure 7.9: Temperature displayed using maximum temperature, T_{max}, versus equivalence ratio in (a) and temperature profiles at one specific equivalence ratio (ϕ=1.0) in (b). Also in (b) are the profiles of the mole fractions of the fuel (C_2H_4), dashed lines, and CO_2, dotted lines. Legend, reaction mechanisms: blue - Z66 [43], red - Aramco 1.3 [124], green - USC C_2-C_3 [125]. Legend, experimental data: □ - Law et al. [136]

Similar results for maximum and profile temperature, with similar predictability, can be seen for all reduced reaction mechanisms presented here, spanning C_1 to C_{12} fuel species [11, 25, 41, 42].

7.4 Species profiles

Species mole fraction profiles for a propane-air mixture simulated at standard conditions, Figure 7.10, are shown for three different equivalence ratios, ϕ=0.6,

1.0 and 1.4. The Z66 [11] reaction mechanism is compared to SD270 [64] and USC C_1-C_4 [65]. Irrespective of which equivalence ratio investigated the difference between the reaction mechanisms is small and the reduced reaction mechanism is capable of predicting similar species mole fraction profiles as the reference reaction mechanisms. The drop in propane concentration is abrupt, indicating a fast fuel breakdown for all reaction mechanisms. At fuel lean conditions, 7.10(a), the CO mole fraction reaches its peak shortly after the disappearance of the fuel, and then reduces as most of the CO is converted to CO_2. A similar feature can be seen at stoichiometric conditions, Figure 7.10(b), with the difference that not all CO is being converted to CO_2, and a significant amount of CO is present at the end of the domain. At fuel rich conditions, Figure 7.10(c), the roles of CO and CO_2 are reversed, with CO mole fraction being higher at the end of the domain. Due to the lack of sufficient amounts of oxygen in the fuel-air mixture at fuel rich conditions a complete conversion of CO to CO_2 is prevented, highlighting the insufficient combustion taking place. As seen i Figure 7.9(c) this insufficient combustion results in lower maximum temperatures compared to stoichiometric conditions even though the fuel concentration remains high.

Accurate major species predictability can be seen for all reduced reaction mechanisms presented here [11, 25, 41–43].

7.5 Summary, reaction mechanisms

Illustrated in this section are key results for the reduced reaction mechanisms developed using the block structure methodology. Section 7.1 show that all these reaction mechanisms manages to accurately predict the laminar burning velocity at standard conditions for a wide range of hydrocarbon fuels. Despite their considerably smaller size than the corresponding reference detailed reaction mechanisms the reduced reaction mechanisms show excellent predictability. All of these reduced reaction mechanisms use the same species and reactions in their H_2/O_2 and $C_1/H/O$ blocks. As seen in Section 7.1.1 the species and reactions present in these blocks are essential for the modelling of the laminar burning velocity, both for detailed and reduced reaction mechanisms. Once a proper set of species and reactions are chosen for these blocks flame parameters such as temperature, Section 7.3, and species profiles, Section 7.4, will also be modelled with high accuracy. Added to the temperature and species profiles are the capabilities to capture the temperature and pressure effects on the laminar burning velocities, presented in Section 7.1.3, which are also mainly determined by the chemistry in the H_2/O_2 and $C_1/H/O$ blocks. One flame parameter requiring an extended level of chemical modelling is the ignition delay time, shown in Section 7.2. The inability of the smallest kerosene-air reaction mechanism

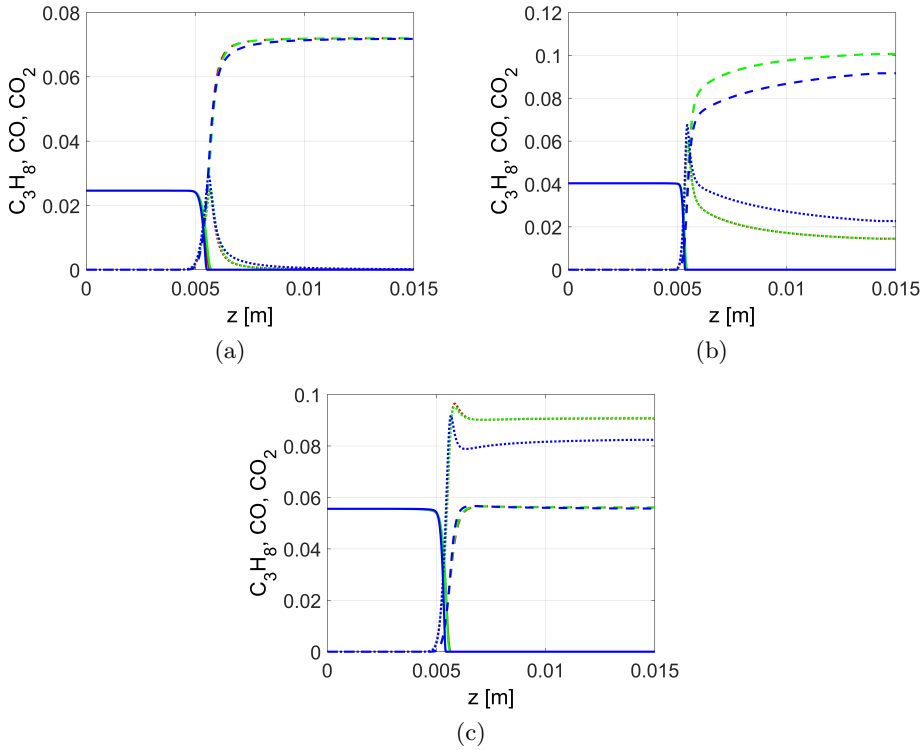

Figure 7.10: Profiles of the mole fractions of the fuel (C_3H_8), solid lines, CO, dotted lines, and CO_2, dashed lines, simulated at standard conditions and ϕ=0.6 in (a), ϕ=1.0 in (b) and ϕ=1.4 in (c). Legend, reaction mechanisms, for C_3H_8: blue - Z66 [11], red - SD270 [64], green - USC C_1-C_4 [65].

Z65, with its simple description of the fuel breakdown, to model ignition delay times illustrates this. The improved Z77 reaction mechanism, with the addition of an extended fuel breakdown modelling effectively demonstrates the model flexibility of the block structure methodology. Z77 adds a set of species and reactions to the fuel breakdown block resulting in vastly improved modelling capability, keeping the same species and reactions in the H_2/O_2 and $C_1/H/O$ blocks. Another key reaction mechanism characteristic important in higher order simulations is to have a low computational cost. Section 7.1.2 show the cost for a range of detailed, global and reduced reaction mechanisms for the laminar burning velocities. Substantial cost savings is achieved with the developed reduced reaction mechanisms presented here, and as seen in the subsequent result sections these cost savings come at little or no reduction in model accuracy.

7.6 LES and reduced reaction mechanisms

The goal of the reaction mechanism development methodology presented in Chapter 5 is to create reaction mechanisms small enough for finite rate combustion LES yet with a high level of chemical complexity. This chapter will present a selection of results from finite rate combustion LES' [11, 20, 21] with reduced mechanisms using kerosene [20], methane and ethylene [21] and propane [11] as fuel.

7.6.1 Annular gas turbine combustor

Figure 7.11 show an annular multi-burner generic aero-engine combustor [20]. The use of a reduced reaction mechanism with more detailed reaction pathways than is present in a global reaction mechanism means that the flame structure and topology can be more accurately modelled. The flame can now be represented by several layers of different species, shown as iso-surfaces of $C_{12}H_{23}$,C_2H_4 and HCO in Figure 7.11, instead of the otherwise more crude assumption that the fuel molecule transitions directly into CO and CO_2. Figure 7.11(c) show instantaneous CO (top) and CO_2 (bottom). Because CO is present earlier in the reaction pathway, exemplified in Figure 3.1, it is present further upstream in the combustor, and the conversion of CO to CO_2 occur further downstream. Figure 7.11(d) show instantaneous OH (top) and C_2H_2 (bottom). OH is often indicative of the post-flame region and is here present further downstream in the combustor.

The improvements in flame topology, heat release positioning and the burning velocity achieved by using a high-performing reduced reaction mechanism can also improve thermoacoustics and pressure predictions. Pressure on the surface of the inner and outer liners is shown in Figure 7.12 [20] where a high pressure region (dark colours) is present opposed to a low pressure region (light colours). The opposed positioning of the high and low pressure regions on the inner liner show that an azimuthal pressure wave is present whereas the pressure regions on the outer liner is more scattered.

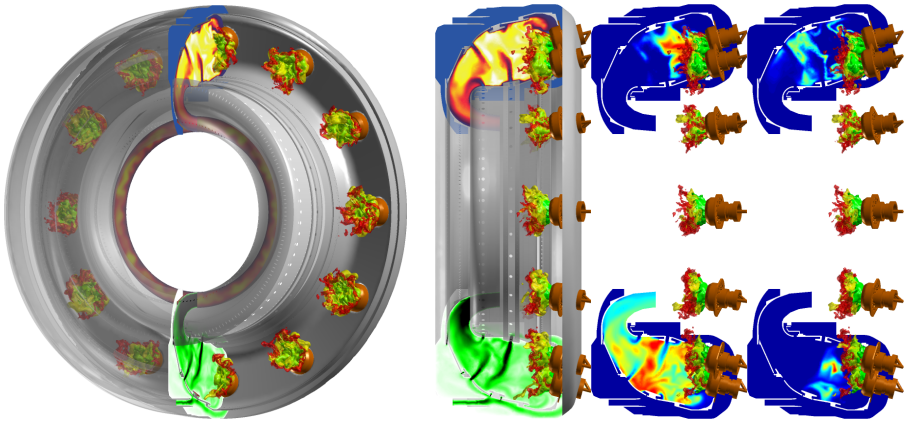

(a) (b) (c) (d)

Figure 7.11: Instantaneous distributions of temperature (top) and velocity magnitude (bottom) in (a) and (b), with Iso-surfaces of $C_{12}H_{23}$ in green, C_2H_4 in yellow and HCO in red. Instantaneous distributions of CO (top) and CO_2 (bottom) in (c) and OH (top) and C_2H_2 (bottom) in (d), together with the same Iso-surfaces as in (a) and (b).

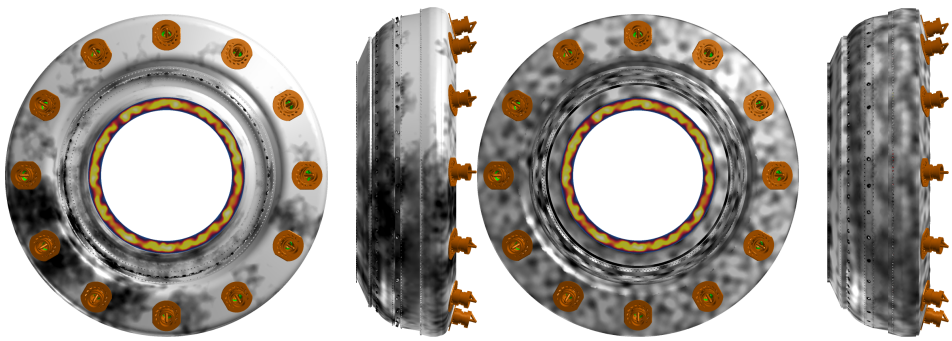

(a) (b) (c) (d)

Figure 7.12: Contours of the pressure fluctuations on the inner flame tube wall seen from the bottom in (a) and side in (b), and on the outer flame tube wall seen from the bottom in (c) and side in (d).

7.6.2 Model annular gas turbine combustor

The following premixed model annular combustor is used to illustrate the differences in flame structure, distribution and topology, and combustion dynamics when using two hydrocarbon fuels with significant different fuel properties [21]. The two fuels, the alkane CH_4 and alkene C_2H_4, show significant differences in their laminar burning velocities (compare Figures 7.1(a) and 7.2(a)), with C_2H_4 burning roughly twice as fast as CH_4. Other flame parameters such as ignition delay time and maximum flame temperature also differ between the two fuels, with C_2H_4 burning at a higher temperature and ignites faster. The effect of the higher burning velocity and faster ignition of C_2H_4 compared to CH_4 is clearly seen when comparing the flames in Figure 7.13, visualized as volumetric rendered heat-release, Q. The faster burning of C_2H_4, Figure 7.13(a), result in smaller, more regular and compact flames, with less wrinkling and little flame-flame interaction. In contrast the CH_4 flames, Figure 7.13(b), are more irregular, have wider topologically overlapping regions and extend further into the combustor. Because of burning further downstream the flames will interact more with the turbulence, with a more pronounced turbulence-chemistry interaction, which in turn increases the flame area making the CH_4 flames more susceptible to acoustic perturbations [21]. Different pressure distributions of the two fuels are seen in the circular pressure images (extracted at the marked height A). The C_2H_4 flames are governed by azimuthal modes, as shown by varying regions of low and high pressures in the circular image in Figure 7.13(a), and the CH_4 flames by longitudinal modes [21].

Figure 7.14 compare instantaneous and time-averaged side-views of experimental OH* chemiluminescence and LES-based volumetric renderings of Q, for the two fuels. The LES captures the differences in flame topology of the two cases, and the experimental and predicted flame heights are for C_2H_4 $\sim$30 mm and $\sim$27 mm, respectively, and for CH_4 $\sim$45 mm in both experiments and simulations. Figure 7.14 clearly show that both the instantaneous and time-averaged C_2H_4 and CH_4 simulated cases are qualitatively similar to the experiments.

To capture the differences between the C_2H_4 and CH_4 flames the chemical modelling, i.e. the reaction mechanisms, must have a high level of predictability for a range of flame parameters. The ability of the LES to capture the differences in acoustic perturbations, the flame structure, distribution and topology, and combustion dynamics between the two cases can only be achieved by using high performing reaction mechanisms [21].

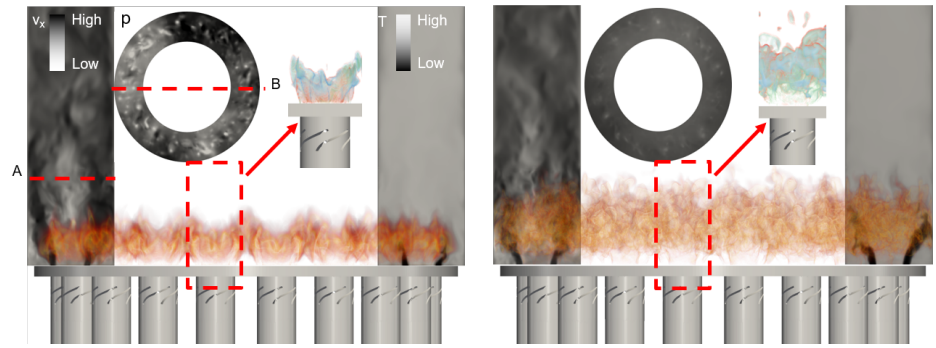

(a) (b)

Figure 7.13: Instantaneous LES predictions of the C_2H_4 flames in (a), and CH_4 flames in (b). Left section in each image show the axial velocity, v_x, and right section the temperature, T, extracted at the marked position B. Circular images show the pressure, extracted at the marked position A. Flames are visualized as volumetric renderings of the heat-release, Q. Inserts of individual flames show C_2H_3/CH_3 in green, CH_2O in blue and HCO in red.

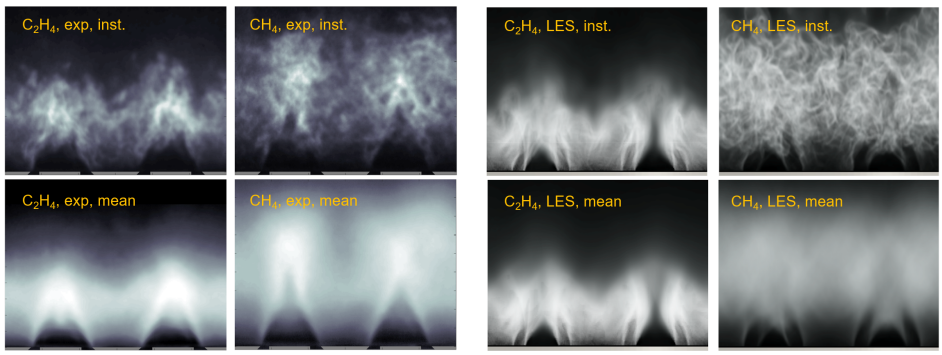

(a) (b)

Figure 7.14: Side-views of instantaneous (top row) and time-averaged (bottom row) experimental OH* chemiluminescence images (left) and LES-based images (right) for the two cases.

7.6.3 Bluff body stabilized flame

LES results for a triangular flame holder in a straight channel, using a premixed propane-air mixture, are shown in Figure 7.15 [11]. The intrinsic flame topology, shown using one- and two-dimensional plots as well as tree-dimensional volumetric renderings [137] links the results for the one-dimensional laminar flame to the three-dimensional LES. The use of a reduced reaction mechanism produces a more accurate image of the flame topology, and in the laminar simulation three flame regions can be identified: a preheat layer, an inner layer and an oxidation layer. These one-dimensional results, Figure 7.15(a), are then compared to scatter plots of the same species, Figure 7.15(b), from the LES.

By following key reaction pathways in the propane-air combustion a set of species are chosen to represent the flame. C_2H_5 is chosen because it is a direct result from C-C bond breaking of the propane molecule (see reaction 5.1), HCO is a good indicator of where the heat release will be present spatially and CO indicates where an exothermal pathways leading to CO_2 starts. Added to these is also the OH radical, a key radical in any hydrocarbon combustion but also an indicator of the start of the post-flame region in the inner layer.

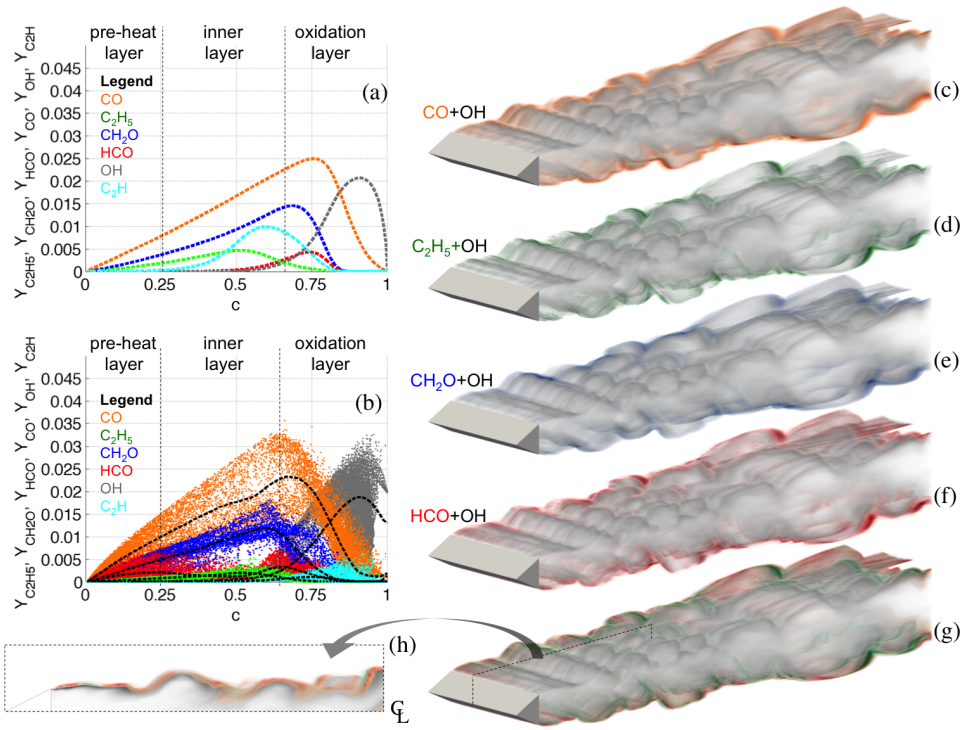

Figure 7.15: Showing laminar flame profiles in (a) and statistics of turbulent flame profiles in (b), at p_0=101 kPa and T_0=288 K. Black dashed lines in (b) correspond to conditional averages of the species. Volumetric renderings of OH together with (c) CO, (d) C_2H_5, (e) CH_2O and (f) HCO, and with a combined volumetric rendering (g) of all those intermediates and radicals. (h) shows a slice through the computational domain in (g). The colour maps for the volumetric rendering ranges from semi-transparent white to the opaque colour of the species, Y_k, matching the range $0.98Y_{k,peak}$ to $0.02Y_{k,peak}$ and the mapping relating the concentrations with hue and opacity is linear.

Chapter 8

Concluding remarks

A novel technique for development of reduced reaction mechanisms is developed based on a bottom-up approach. The technique divides different parts of the chemical kinetics into blocks of varying chemical complexity and creates a reduced reaction mechanism by combining blocks into one coherent mechanism. The development technique enables different chemical complexity depending on the importance of each block to the overall modelling. It also enables the use of a single set of reactions in the underlying H_2/O_2 and $C_1/H/O$ blocks irrespective of what hydrocarbon fuel is to be modelled. Using the development technique reduced reaction mechanisms for methane-air [25], ethylene-air [43], propane-air [11], kerosene-air [20, 41, 42] and JP-10-air [81] combustion are created.

Finite rate combustion LES' were made with the OpenFOAM [138] 2.2.2 software, using reduced reaction mechanisms and with LES-PaSR [11, 20, 21] or LES-EDC [25] turbulence-chemistry interaction modelling. By using improved reduced reaction mechanisms instead of global ones more accurate results are produced [11, 20] and the improved modelling of the chemistry is able to better predict flame position [11, 20, 21, 25] and topology [11, 20, 21, 25], OH^* chemiluminescence [21], velocity, pressure and temperature data [11], flame-flame interactions [21], pressure fluctuations [11, 21] and more.

8.1 Outlook

The introduction of more accurate reaction mechanisms in combustion LES has enabled more accurate simulation results. Even so, the field of combustion LES is still at an early stage [3]. There are several areas where future research need to be improved, both for reaction mechanisms and their use in combustion LES. When it comes to the reaction mechanisms one obvious first task is to create

reaction mechanisms for a wider range of fuels. Apart from the mechanisms presented here reduced reaction mechanisms are needed for the complete range of C_2 to C_{18} alkanes and alkenes, but also alcohols and biofuels. For the latter the underlying $C_1/H/O$ and C_2 blocks may well need to be expanded compared to the ones presented here in order to capture the subtle effects of large hydrogenated fuels. Also, since most biodiesels are multi-component fuels several fuel molecules needs to be modelled using one single reaction mechanism, and several fuel breakdown blocks will need to be included.

A second task worth pursuing is to create a fixed set of H_2/O_2, $C_1/H/O$ and C_2 blocks for a range of alkanes, all with the same reactions but also the same reaction rate coefficients. Then only the fuel breakdown block would differ between different reaction mechanisms.

A third future research area is to continue to work on improving the turbulence-chemistry interaction models to better take into account the wider range of species and reaction time scales accompanying these improved reaction mechanisms [139].

Bibliography

[1] British Petroleum. BP statistical review of world energy 2019. https://www.bp.com/content/dam/bp/business-sites/en/global/corporate/pdfs/energy-economics/statistical-review/bp-stats-review-2019-full-report.pdf, 2019.

[2] G. Kalghatgi, H. Levinsky, and M. Colket. Future transportation fuels. *Progress in Energy and Combustion Science*, 69:103 – 105, 2018.

[3] T. Poinsot and D. Veynante. *Theoretical and Numerical Combustion.* Edwards, 2 edition, 2005.

[4] S.B. Pope. *Turbulent Flows.* Cambridge University Press, New York, 2000.

[5] S. Menon and C. Fureby. *Computational Combustion.* John Wiley & Sons, 2010.

[6] P. Sagaut. *Large Eddy Simulation for Incompressible Flows.* Springer Verlag, Heidelberg, 2001.

[7] W.P. Jones and R.P. Lindstedt. Global reaction schemes for hydrocarbon combustion. *Combustion & Flame*, 73:222, 1988.

[8] C.K. Westbrook and F.L. Dryer. Simplified reaction mechanisms for the oxidation of hydrocarbon fuels in flames. *Combustion Science and Technology*, 27:31, 1981.

[9] B. Franzelli, E. Riber, M. Sanjosé, and T. Poinsot. A two-step chemical scheme for kerosene–air premixed flames. *Combustion & Flame*, 157:1364 – 1373, 2010.

[10] C. Fureby. A comparative study of subgrid models, reaction mechanisms and combustion models in LES of supersonic combustion. *AIAA – 2019–4273*, page 4273, 2019.

[11] N. Zettervall, K. Nordin-Bates, E. Heimdahl Nilsson, and C. Fureby. Large eddy simulation LES of a premixed bluff body stabilized flame using global and skeletal reaction mechanisms. *Combustion & Flame*, 179:1–22, 2016.

[12] G. Bulat, E. Fedina, C. Fureby, W. Meier, and U. Stopper. Reacting flow in an industrial gas turbine combustor: LES and experimental analysis. *Proceedings of the Combustion Institute*, 35:3175, 2015.

[13] N. Zettervall and C. Fureby. A computational study of ramjet, scramjet and dual-mode ramjet combustion in combustor with a cavity flameholder. *AIAA – 2018–1146*, 2018.

[14] C. Fureby and C. Löfström. Large-eddy simulations of bluff body stabilized flames. *Proceedings of the Combustion Institute*, 25:1257, 1994.

[15] F.F. Grinstein and K. Kailasanath. Three-dimensional numerical simulations of unsteady reactive square jets. *Combustion & Flame*, 100:2–10, 1995.

[16] G. Staffelbach, L.Y.M. Gicquel, and T. Poinsot. Highly parallel large eddy simulations of multiburner configurations in industrial gas turbines. In *Complex Effects in Large Eddy Simulations*, volume 56, pages 325 – 336. Springer, Berlin, 2007.

[17] G. Staffelbach, L. Gicquel, G. Boudier, and T. Poinsot. Large eddy simulation of self-excited azimuthal modes in annular combustors. *Proceedings of the Combustion Institute*, 32:2909, 2009.

[18] F.F. Grinstein and C. Fureby. LES studies of the flow in a swirl gas combustor. *Proceedings of the Combustion Institute*, 30:1791 – 1798, 2005.

[19] C. Fureby. LES of a multi-burner annular gas turbine combustor. *Flow, Turbulence & Combustion*, 84:543–564, 2010.

[20] N. Zettervall, E. Fedina, K. Nordin-Bates, E. Heimdal Nilsson, and C. Fureby. Combustion LES of a multi-burner annular aero-engine combustor using a skeletal reaction mechanism for jet-A air mixtures. *AIAA – 2015–4020*, 2015.

[21] N. Zettervall, N.A. Worth, M. Mazur, J.R. Dawson, and C. Fureby. Large eddy simulation of CH_4-air and C_2H_4-air combustion in a model annular gas turbine combustor. *Proceedings of the Combustion Institute*, 37:5223 – 5231, 2019.

[22] K. Danel, N. Zettervall, and C. Fureby. A combined experimental and computational study of jet engine combustion–baseline engine operation. *AIAA – 2019–4328*, 2019.

[23] A. Vincent-Randonnier, V. Sabelnikov, A. Ristori, N. Zettervall, and C. Fureby. An experimental and computational study of hydrogen–air combustion in the LAPCAT II supersonic combustor. *Proceedings of the Combustion Institute*, 37:3703 – 3711, 2019.

[24] Ekaterina Fedina. *Post-Detonation Afterburning of High Explosives*. PhD thesis, Lund University, 2017.

[25] A. Larsson, N. Zettervall, T. Hurtig, E.J.K. Nilsson, A. Ehn, P. Petersson, M. Alden, J. Larfeldt, and C. Fureby. Skeletal methane–air reaction mechanism for large eddy simulation of turbulent microwave-assisted combustion. *Energy & Fuels*, 31:1904 – 1926, 2017.

[26] A. Ehn, P. Petersson, J. Zhu, Z.S. Li, M. Aldén, E. Nilsson, J. Larfeldt, A. Larsson, T. Hurtig, N. Zettervall, and C. Fureby. Investigations of microwave stimulation of a turbulent low-swirl flame. *Proceedings of the Combustion Institute*, 2016.

[27] E.S. Oran and J.P. Boris. *Numerical Simulation of Reactive Flow*. Cambridge University Press, UK, 2 edition, 2001.

[28] J. Warnatz, U. Maas, and R.W. Dibble. *Combustion*. Springer, Germany, 2 edition, 1999.

[29] L.F. Richardson. *Weather prediction by numerical processes*. Cambridge University Press, Cambridge, 1922.

[30] R. Borghi. On the structure of turbulent flames. *Journal de Chimie Physique et de Physico-Chimmie Biologique*, 81:83–96, 1984.

[31] F.A. Williams. *Combustion Theory*. Benjamin Cummins, Menlo Park California, 1985.

[32] I. Glassman and R.A. Yetter. *Combustion*. Academic Press, Elservier, 4 edition, 2010.

[33] F. Battin-Leclerc, J.M. Simmie, and E. Blurock. *Cleaner Combustion. Developing Detailed Chemical Kinetic Models. Series: Green Energy and Technology*. Springer International Publishing AG, New York, 2013.

[34] S. Arrhenius. Quantitative relationship between the rate a reaction proceed and its temperature. *The Journal of Physical Chemistry*, 4:226–248, 1889.

[35] S. Arrhenius. On the reaction rate of the inversion of non-refined sugar upon souring. *Zeitschrift für Physikalische Chemie*, 4:226–248, 1889.

[36] F.A. Lindemann, S. Arrhenius, I. Langmuir, N.R. Dhar, J. Perrin, and W.M. Lewis. Discussion on the radiation theory of chemical action. *Transactions of the Faraday Society*, 17:598 – 606, 1922.

[37] M. Quack and J. Troe. Specific rate constants of unimolecular processes ii. adiabatic channel model. *Berichte der Bunsengesellschaft für physikalische Chemie*, 78:240 – 252, 1974.

[38] T. Turanyi. Reduction of large reaction mechanisms. *New journal of chemistry*, 14:795 – 803, 1990.

[39] S.M. Sarathya, C.K. Westbrook, M. Mehl, W.J. Pitz, C. Togbe, P. Dagaut, H. Wang, M.A. Oehlschlaeger, U. Niemann, K. Seshadri, P.S. Veloo, C. Ji, F.N. Egolfopoulos, and T. Luf. Comprehensive chemical kinetic modeling of the oxidation of 2-methylalkanes from C7 to C20. combustion and flame. *Combustion & Flame*, 158:2338 – 2357, 2011.

[40] S. Olovsson. Combustion calculations on a premixed system with a bluff body flameholder. *AIAA Journal*, 92:3470, 1992.

[41] N. Zettervall, C. Fureby, and E.J.K. Nilsson. Small skeletal kinetic mechanism for kerosene combustion. *Energy & Fuels*, 30:9801–9813, 2016.

[42] N. Zettervall, C. Fureby, and E.J.K. Nilsson. A reduced chemical kinetic reaction mechanism for kerosene-air combustion. *Fuel*, 269:117446, 2020.

[43] N. Zettervall, C. Fureby, and E.J. Nilsson. Small skeletal kinetic reaction mechanism for ethylene–air combustion. *Energy & Fuels*, 31:14138–14149, 2017.

[44] J. Warnatz. The structure of laminar alkane-, alkene-, and acetylene flames. *Symposium (International) on Combustion*, 18:369 – 384, 1981.

[45] R.J. Kee, F.M. Rupley, J.A. Miller, M.E. Coltrin, J.F. Grcar, E. Meeks, H.K Moffat, A.E. Lutz, G. Dixon-Lewis, M.D. Smooke, J. Warnatz, G.H. Evans, R.S. Larson, R.E. Mitchell, L.R. Petzold, W.C. Reynols, M. Caracotsios, W.E. Stewart, P. Glarborg, C. Wang, C.L. McLellan, O. Adigun, W.G. Houf, C.P. Chou, S.F. Miller, P. Ho, P.D. Young, and D.J. Young. CHEMKIN release 4.0.2. reaction design, 2005.

[46] H. Wang, R. Xu, K. Wang, C.T. Bowman, D.F. Davidson, R.K. Hanson, K. Brezinsky, and F.N. Egolfopoulos. A physics-based approach to modeling real-fuel combustion chemistry - I. evidence from experiments, and thermodynamic, chemical kinetic and statistical considerations. *Combustion & Flame*, 193:502 – 519, 2018.

[47] R. Xu, K. Wang, S. Banerjee, J. Shao, T. Parise, Y. Zhu, S. Wang, A. Movaghar, D.J. Lee, R. Zhao, X. Han, Y. Gao, T. Lu, K. Brezinsky, F.N. Egolfopoulos, D.F. Davidson, R.K. Hanson, C.T. Bowman, and H. Wang. A physics-based approach to modeling real-fuel combustion chemistry - II. reaction kinetic models of jet and rocket fuels. *Combustion & Flame*, 193:520 – 537, 2018.

[48] C. Ji, E. Dames, Y.L. Wang, H. Wang, , and F.N. Egolfopoulos. Propagation and extinction of premixed C5–C12n-alkane flames. *Combustion & Flame*, 157:277 – 287, 2010.

[49] K. Kumar and C.J. Sung. Laminar flame speeds and extinction limits of preheated n-decane/O2/N2 and n-dodecane/O2/N2 mixtures. *Combustion & Flame*, 151:209 – 224, 2007.

[50] K. Kumar, C.J. Sung, and X. Hui. Laminar flame speeds and extinction limits of conventional and alternative jet fuels. *Fuel*, 90:1004 – 1011, 2011.

[51] X. Hui and C.J. Sung. Laminar flame speeds of transportation-relevant hydrocarbons and jet fuels at elevated temperatures and pressures. *Fuel*, 109:191 – 200, 2013.

[52] C. Zhang, B. Li, F. Rao, P. Li, and X. Li. A shock tube study of the autoignition characteristics of RP-3 jet fuel. *Proceedings of the Combustion Institute*, 35:3151 – 3158, 2015.

[53] S.S. Vasu, D.F. Davidson, Z. Hong, V. Vasudevan, and R.K. Hanson. n-dodecane oxidation at high-pressures: Measurements of ignition delay times and OH concentration time-histories. *Proceedings of the Combustion Institute*, 32:173 – 180, 2009.

[54] Y. Zhu, S. Li, D.F. Davidson, and R.K. Hanson. Ignition delay times of conventional and alternative fuels behind reflected shock waves. *Proceedings of the Combustion Institute*, 35:241 – 248, 2015.

[55] S.S. Vasu, D.F. Davidson, and R.K. Hanson. Jet fuel ignition delay times: Shock tube experiments over wide conditions and surrogate model predictions. *Combustion & Flame*, 152:125 – 143, 2008.

[56] M.M. Kopp N.S. Donato, E.L. Petersen, W.K. Metcalfe, S.M. Burke, and H.J. Curran. Oxidation of ethylene–air mixtures at elevated pressures, part 1: experimental results. *Journal of Propulsion and Power*, 30:790 – 798, 2014.

[57] A.T. Holley, Y. Dong, M.G. Andac, and F.N. Egolfopoulos. Extinction of premixed flames of practical liquid fuels: Experiments and simulations. *Combustion & Flame*, 144:448–460, 2006.

[58] A.T. Holley, X.Q. You, E. Dames, H. Wang, and F.N. Egolfopoulos. Sensitivity of propagation and extinction of large hydrocarbon flames to fuel diffusion. *Proceedings of the Combustion Institute*, 32:1157–1163, 2009.

[59] C. Liu, R. Zhao, R. Xu, F.N. Egolfopoulos, and H. Wang. Binary diffusion coefficients and non-premixed flames extinction of long-chain alkanes. *Proceedings of the Combustion Institute*, 36:1523–1530, 2017.

[60] A.L. Sanchez and F.A. Williams. Recent advances in understanding of flammability characteristics of hydrogen. *Progress in Energy and Combustion Science*, 41:11, 2014.

[61] J.V. Michael, J.W. Sutherland, L.B. Harding, and A.F. Wagner. Initiation in H2/O2: Rate constants for H2 + O2 → H + HO2 at high temperature. *Proceedings of the Combustion Institute*, 28:1471, 2000.

[62] G.P. Smith, D.M. Golden, M. Frenklach, N.W. Moriarty, B. Eiteneer, M. Goldenberg, C.T. Bowman, R.K. Hanson, S. Song, W.C. Gardiner Jr., V.V. Lissianski, and Z. Qin. http://www.me.berkeley.edu/gri_mech.

[63] C-W. Zhou, Y. Li, U. Burke, C. Banyon, K.P. Somers, S. Khan, J.W. Hargis, T. Sikes, E.L. Petersen, M. AlAbbad, A. Farooq, Y. Pan, Y. Zhang, Z. Huang, J. Lopez, Z. Loparo, S.S. Vasu, and H.J. Curran. An experimental and chemical kinetic modeling study of 1,3-butadiene combustion: Ignition delay time and laminar flame speed measurements. *Combustion & Flame*, 197:423–438, 2018.

[64] Mechanical and University of California Aerospace Engineering (Combustion Research). Chemical-kinetic mechanisms for combustion applications. http://combustion.ucsd.edu.

[65] H. Wang, X. You, A.V. Joshi, S.G. Davis, A. Laskin, F. Egolfopoulos, and C.K. Law. USC Mech Version II. high-temperature combustion reaction model of H2/CO/C1-C4 compounds. http://ignis.usc.edu/USC_Mech_II.htm, 2007.

[66] C.K. Westbrook and F.L. Dryer. Chemical kinetic modeling of hydrocarbon combustion. *Progress in Energy and Combustion Science*, 10:1, 1984.

[67] T. Turanyi. Kinal — a program package for kinetic analysis of reaction mechanisms. *Computers & chemistry*, 14:253 – 254, 1990.

[68] T. Turanyi. Sensitivity analysis of complex kinetic systems. tools and applications. *Journal of mathematical chemistry*, 5:203 – 248, 1990.

[69] A.S. Tomlin, M.J. Pilling, T. Turányi, J.H. Merkin, and J. Brindley. Mechanism reduction for the oscillatory oxidation of hydrogen: sensitivity and quasi-steady-state analyses. *Combustion & Flame*, 91:107 – 130, 1992.

[70] T. Nagy and T. Turányi. Reduction of very large reaction mechanisms using methods based on simulation error minimization. *Combustion & Flame*, 156:417 – 428, 2009.

[71] T. Lu and C.K. Law. A directed relation graph method for mechanism reduction. *Proceedings of the Combustion Institute*, 30:1333 – 1341, 2005.

[72] T. Lu and C.K. Law. Linear time reduction of large kinetic mechanisms with directed relation graph: n-heptane and iso-octane. *Combustion & Flame*, 144:24 – 36, 2006.

[73] T. Lu and C.K. Law. On the applicability of directed relation graphs to the reduction of reaction mechanisms. *Combustion & Flame*, 146:472 – 483, 2006.

[74] I.P Androulakis. Kinetic mechanism reduction based on an integer programming approach. *AIChE Journal*, 46:361 – 371, 2000.

[75] K. Edwards, T. F. Edgar, and V.I. Manousiouthakis. Kinetic model reduction using genetic algorithms. *Computers & chemical engineering*, 22:239 – 246, 1998.

[76] I. Banerjee and M.G. Ierapetritou. Development of an adaptive chemistry model considering micromixing effects. *Chemical Engineering Science*, 58:4537 – 4555, 2003.

[77] L. Elliott, D.B. Ingham, A.G. Kyne, N.S. Mera, M. Pourkashanian, and C.W. Wilson. Genetic algorithms for optimisation of chemical kinetics reaction mechanisms. *Progress in Energy and Combustion Science*, 30:297 – 328, 2004.

[78] L. Elliott, D.B. Ingham, A.G. Kyne, N.S. Mera, M. Pourkashanian, and C.W. Wilson. Reaction mechanism reduction and optimization using genetic algorithms. *Industrial & engineering chemistry research*, 44:658 – 667, 2005.

[79] H. Huang, M. Fairweather, J.F. Griffiths, A.S. Tomlin, and R.B. Brad. A systematic lumping approach for the reduction of comprehensive kinetic models. *Proceedings of the Combustion Institute*, 30:1309 – 1316, 2005.

[80] E. Ranzi, T. Faravelli, P. Gaffuri, and A. Sogaro. Low-temperature combustion: automatic generation of primary oxidation reactions and lumping procedures. *Combustion & Flame*, 102:179 – 192, 1995.

[81] N. Zettervall. Reduced chemical kinetic reaction mechanism for JP-10-air combustion. *Energy & Fuels*, 000:000–000, 2020. https://doi.org/10.1021/acs.energyfuels.0c02971.

[82] X. You, F.N. Egolfopoulos, and H. Wang. Detailed and simplified kinetic models of n-dodecane oxidation: The role of fuel cracking in aliphatic hydrocarbon combustion. *Proceedings of the Combustion Institute*, 32:403 – 410, 2009.

[83] H.J. Curran, P. Gaffuri, W.J. Pitz, and C.K. Westbrook. A comprehensive modeling study of n-heptane oxidation. *Combustion & Flame*, 114:149 – 177, 1998.

[84] H.J. Curran, P. Gaffuri, W.J. Pitz, and C.K. Westbrook. A comprehensive modeling study of iso-octane oxidation. *Combustion & Flame*, 129:253 – 280, 2002.

[85] Y. Chang, M. Jia, Y. Li, Y. Zhang, M. Xie, H. Wang, and R.D. Reitz. Development of a skeletal oxidation mechanism for biodiesel surrogate. *Proceedings of the Combustion Institute*, 35:3037–3044, 2015.

[86] Y. Chang, M. Jia, Y. Li, Y. Liu, M. Xie, H. Wang, and R.D. Reitz. Development of a skeletal mechanism for diesel surrogate fuel by using a decoupling methodology. *Combustion & Flame*, 162:3785 – 3802, 2015.

[87] M. Tanahashi, M. Sato, M. Shimura, and T. Miyauchi. DNS and combined laser diagnostics of turbulent combustion. *Journal of Thermal Science and Technology*, 3:391–409, 2008.

[88] J.B. Bell, M.S. Day, J.F. Grcar, M.J. Lijewski, J.F. Driscoll, and S.A. Filatyev. Numerical simulation of a laboratory-scale turbulent slot flame. *Proceedings of the Combustion Institute*, 31:1299–1307, 2007.

[89] D.B. Spalding. Mathematical models of turbulent flames; a review. *Combustion Science and Technology*, 13:3–25, 1976.

[90] W. Jones and J.H. Whitelaw. Calculation methods for reacting turbulent flows: a review. *Combustion & Flame*, 48:1–26, 1982.

[91] C. Fureby. Comparison of flamelet and finite rate chemistry LES for premixed turbulent combustion. *AIAA–2007-1413, 45th AIAA Aerospace Sciences Meeting and Exhibit, 8 - 11 January 2007, Reno, Nevada*, 2007.

[92] J. Smagorinsky. General circulation experiments with the primitive equations.{I}: The basic experiment. *Monthly Weather Review*, 91:99–165, 1963.

[93] M. Germano, U. Piomelli, P. Moin, and W.H. Cabot. A dynamic subgrid–scale eddy viscosity model. *Physics of Fluids A: Fluid Dynamics*, 3:1760–1765, 1991.

[94] F. Nicoud and F. Ducros. Subgrid-scale stress modelling based on the square of the velocity gradient tensor. *Flow, Turbulence and Combustion*, 62:183–200, 1999.

[95] A. Yoshizawa and K. Horiuti. A statistically-derived subgrid-scale kinetic energy model for the large-eddy simulation of turbulent flows. *Journal of the Physical Society of Japan*, 54:2834–2839, 1985.

[96] W.W. Kim and S. Menon. An unsteady incompressible Navier–Stokes solver for large eddy simulations of turbulent flows. *International Journal for Numerical Methods in Fluids*, 31:983–1017, 1999.

[97] U. Schumann. Subgrid scale model for finite difference simulations of turbulent flows in plane channels and annuli. *Journal of Computational Physics*, 18:376–404, 1975.

[98] J. Bardina, J. Ferziger, and W. Reynolds. Improved subgrid-scale models for large-eddy simulation. *In 13th Fluid and PlasmaDynamics Conference*, page 1357, 1980.

[99] S. Stolz and N.A. Adams. An approximate deconvolution procedure for large-eddy simulation. *Physics of Fluids*, 11:1699–1701, 1999.

[100] N.A. Adams and S. Stolz. A subgrid-scale deconvolution approach for shock capturing. *Journal of Computational Physics*, 178:391–426, 2002.

[101] C. Dopazo and E. O'Brien. Statistical treatment of non-isothermal chemical reactions in turbulence. *Combustion Science & Technology*, 13:99–122, 1973.

[102] C. Dopazo. Recent developments in pdf methods. *Turbulent Reactive Flows*, 13:375–474, 1993.

[103] S. Pope. Computations of turbulent combustion: Progress and challanges. *Proceedings of the Combustion Institute*, 23:591–612, 1975.

[104] C. Fureby. Large eddy simulation modelling of combustion for propulsion applications. *Philosophical Transactions of the Royal Society A: Mathematical, Physical and Engineering Sciences*, 367:2957–2969, 2009.

[105] B.F. Magnussen. On the structure of turbulence and generalized eddy dissipation concept for chemical reactions in turbulent flow. *19th AIAA Aerospace Meeting*, 1981.

[106] P.J. O'Rourke and F.V. Bracco. Two scaling transformations for the numerical computation of multidimensional unsteady laminar flames. *Journal of Computational Physics*, 33:185, 1979.

[107] V. Sabelnikov and C. Fureby. LES combustion modelling for high Re flames using a multi-phase anology. *Combustion & Flame*, 160:83–96, 2013.

[108] E. Baudoin, K.J Nogenmyr, X.S. Bai, and C. Fureby. Comparison of LES models applied to a bluff body stabilized flame. *AIAA – 2009–1178*, 2009.

[109] E. Giocomazzi, C. Bruno, and B. Favini. Fractal modelling of turbulent mixing. *Combustion Theory and Modelling*, 3:637–655, 1999.

[110] E. Giocomazzi, C. Bruno, and B. Favini. Fractal modelling of turbulent mixing. *Proceedings of the Combustion Institute*, 4:391–412, 2000.

[111] V. Battaglia E. Giacomazzi and C. Bruno. The coupling of turbulence and chemistry in a premixed bluff-body flame by LES. *Combustion & Flame*, 138:320–355, 2004.

[112] M. Chapuis, E. Fedina, C. Fureby, K. Hannemann, S. Karl, and J. Martinez Schramm. A computational study of the HyShot II combustor performance. *Proceedings of the Combustion Institute*, 34:2101, 2013.

[113] C. Fureby. A comparative study of flamelet and finite rate chemistry LES for a swirl stabilized flame. *ASME Journal Engineering for Gas Turbines & Power*, 134(041503 (13 pages)), 2012. http://dx.doi.org/10.1115/1.4004718.

[114] Cantera. www.cantera.org/docs/ sphinx/html/index.html, 2016.

[115] E. Ranzi, A. Frassoldati, A. Stagni, M. Pelucchi, A. Cuoci, and T. Faravelli. Reduced kinetic schemes of complex reaction systems: fossil and biomass-derived transportation fuels. *International Journal of Chemical Kinetics*, 46:512–542, 2014.

[116] M. Goswami, S.C. Derks, K. Coumans, W.J. Slikker, M.H. de Andrade Oliveira, R.J. Bastiaans, C.C.M.Luijtena, L.P.H. de Goey, and A.A. Konnov. The effect of elevated pressures on the laminar burning velocity of methane+ air mixtures. *Combustion & Flame*, 160:1627–1635, 2013.

[117] O. Park, P.S. Veloo, N. Liu, and F.N. Egolfopoulos. Combustion characteristics of alternative gaseous fuels. *Proceedings of the Combustion Institute*, 33:887–894, 2011.

[118] W. Lowry, J. de Vriesand M. Krejci, E. Petersen, Z. Serinyel, W. Metcalfe, H. Curran, and G. Bourque. Laminar flame speed measurements and modeling of pure alkanes and alkane blends at elevated pressures. *Journal of Engineering for Gas Turbines and Power*, 133, 2011.

[119] K.J. Bosschaart and L.P.H. De Goey. The laminar burning velocity of flames propagating in mixtures of hydrocarbons and air measured with the heat flux method. *Combustion & Flame*, 136:261–269, 2004.

[120] P. Dirrenberger, H. Le Gall, R. Bounaceur, O. Herbinet, P.A. Glaude, A. Konnov, and F. Battin-Leclerc. Measurements of laminar flame velocity for components of natural gas. *Energy & fuels*, 25:3875–3884, 2011.

[121] A.S. Huzayyin, H.A. Moneib, M.S. Shehatta, and A.M.A. Attia. Laminar burning velocity and explosion index of LPG–air and propane–air mixtures. *Fuel*, 87:39–57, 2008.

[122] C.M. Vagelopoulos and F.N. Egolfopoulos. Direct experimental determination of laminar flame speeds. *In Symposium (international) on combustion*, 27:513–519, 1998.

[123] G. Jomaas, X.L. Zheng, D.L. Zhu, and C.K. Law. Experimental determination of counterflow ignition temperatures and laminar flame speeds of

C2–C3 hydrocarbons at atmospheric and elevated pressures. *Proceedings of the Combustion Institute*, 30:193–200, 2005.

[124] W.K. Metcalfe, S.M. Burke, S.S. Ahmed, and H.J. Curran. A hierarchical and comparative kinetic modeling study of C1-C2 hydrocarbon and oxygenated fuels. *International Journal of Chemical Kinetics*, 45:638–675, 2013.

[125] H. Wang and A. Laskin. A comprehensive kinetic model of ethylene and acetylene oxidation at high temperatures. Progress Report for an AFOSR New World Vista Program, 1998.

[126] G. Jomaas, X.L. Zheng, D.L Zhu, and C.K. Law. Experimental determination of counterflow ignition temperatures and laminar flame speeds of C2–C3 hydrocarbons at atmospheric and elevated pressures. *Proceedings of the Combustion Institute*, 30:193–200, 2005.

[127] Y. Kochar, J. Seitzman, T. Lieuwen, W. Metcalfe, S. Burke, H. Curran, W. Lowry, E. Petersen, and G. Bourque. Laminar flame speed measurements and modeling of alkane blends at elevated pressures with various diluents. *In ASME 2011 Turbo Expo: Turbine Technical Conference and Exposition*, pages 129–140, 2011.

[128] F.N. Egolfopoulos, D.L. Zhu, and C.K. Law. Experimental and numerical determination of laminar flame speeds: Mixtures of C2-hydrocarbons with oxygen and nitrogen. *Symposium (International) on Combustion*, 23, 1991.

[129] M.I. Hassan, K.T. Aung, O.C. Kwon, and G.M. Faeth. Properties of laminar premixed hydrocarbon/air flames at various pressures. *Journal of Propulsion and Power*, pages 479–488, 1998.

[130] E. Hu, X. Li, X. Meng, Y. Chen, Y. Cheng, Y. Xie, and Z. Huang. Laminar flame speeds and ignition delay times of methane–air mixtures at elevated temperatures and pressures. *Fuel*, 158:1–10, 2015.

[131] C.T. Chong and S. Hochgreb. Measurements of laminar flame speeds of liquid fuels: Jet-A1, diesel, palm methyl esters and blends using particle imaging velocimetry (PIV). *Proceedings of the Combustion Institute*, 33:979 – 986, 2011.

[132] X.J. Gu, M.Z. Haq, M. Lawes, and R. Woolley. Laminar burning velocity and markstein lengths of methane–air mixtures. *Combustion & Flame*, 29:41–58, 2000.

[133] G. Rozenchan, D.L. Zhu, C.K. Law, and S.D. Tse. Outward propagation, burning velocities, and chemical effects of methane flames up to 60 atm. *Proceedings of the Combustion Institute*, 29:1461–1470, 2002.

[134] S. Saxena, M.S.P. Kahandawala, and S.S. Sidhu. A shock tube study of ignition delay in the combustion of ethylene. *Combustion & Flame*, 158:1019–1031, 2011.

[135] D.M. Kalitan, J.M. Hall, and E.L. Petersen. Ignition and oxidation of ethylene-oxygen-diluent mixtures with and without silane. *Journal of Propulsion and Power*, 21:1045–1056, 2005.

[136] C.K. Law, A. Makino, and T.F. Lu. On the off-stoichiometric peaking of adiabatic flame temperature. *Combustion & Flame*, 145:808–819, 2006.

[137] A. Watt and M. Watt. *Advanced Animation and Rendering Techniques: Theory and Practice*. Addison-Wesley, USA, 1992.

[138] OpenFOAM. www.openfoam.org, 2009.

[139] A.J. Aspden, N. Zettervall, and C. Fureby. An a priori analysis of a DNS database of turbulent lean premixed methane flames for LES with finite-rate chemistry. *Proceedings of the Combustion Institute*, 37:2601–2609, 2019.

Chapter 9

Acknowledgements

This work was financially supported by the Swedish Defence Research Agency FOI, the Swedish Defence Materiel Administration FMV, Siemens Energy, foreign partners, the EU project STRATOFLY, and the EFFECT 1 and EFFECT 2 projects sponsored by the Swedish Energy Agency. The work has been carried out at FOI, with the assistance of the Department of Combustion Physics at Lund University, Sweden.

I would like to express my deepest gratitude to everybody who has supported me during this work. In particular,

To my supervisors:
Associate Prof. Elna Johanna Kristina Nilsson. Your deep knowledge in detailed chemical kinetics, and your patience, your eye for details and your will to listen to my ideas has pushed my research to a level it would otherwise not have achieved.
Prof. Fureby. Early on you saw the potential and need for this research, and you let me investigate, explore and test all my ideas. My curiosity and ideas was always encouraged, no matter how different or strange they seemed at the time. Without your insights and forward thinking this research would not have been possible. You always believed in me, often more than I did myself.

To my colleagues:
My colleagues in the CFD&C group at FOI, Grindsjön, thank you for all your support. Thank you for all your patience and your unrestrained will to help me, no matter how small or big the issue has been. Thank you Ekaterina Fedina and Kevin Nordin-Bates for your assistance to pretty much all questions related to combustion that I have had. Thank you Ekaterina Fedina for proofreading this thesis. Thank you Niklas Wikström for helping me with software issues,

mesh issues and anything code related. Thank you all for helping me in difficult times and when my mood was low.

To my family:
My mother, thank you for unlimited love, support, and for always believing in me.
My father, thank you for unlimited love, support, your will to listen to my thoughts and ideas of my research, for proofreading this thesis and for always believing in me.
My brother, thank you for unlimited love, support, and for the help with some of the graphics and the image on the cover page for this thesis.
Azizam Cariz, thank you for supporting me, for all your love and always believing in me.

Chapter 10

Author Contributions

Paper I:
Large Eddy Simulation of a premixed bluff body stabilized flame using global and skeletal reaction mechanisms

N. Zettervall, K. Nordin-Bates, E. J. K. Nilsson, C. Fureby (2017)
Combustion & Flame, vol. 179, pp. 1–22

The increasing computational capacity in recent years has spurred the growing use of combustion Large Eddy Simulation (LES) for engineering applications. The modeling of the subgrid stress and flux terms is well-established in LES, whereas the modeling of the filtered reaction rate terms is under intense development. The significance of the reaction mechanism is well documented, but only a few computational studies have so far been conducted with the aim of studying the influence of the reaction mechanism on the predicted flow and flame. Such an investigation requires the availability of well documented, thoroughly tested, and accurate reaction mechanisms suitable for use in practical engineering simulations. Global and detailed reaction mechanisms are available for many fuel mixtures, whereas skeletal reaction mechanisms suitable for LES are in rather short supply. This research attempts to close this gap by using combustion LES to examine a well-known bluff-body stabilized premixed propane–air flame using two well-known global reaction mechanisms and a novel skeletal reaction mechanism, developed as part of this study. These reaction mechanisms are studied for laminar flames, and comparison with experimental data and detailed reaction mechanisms demonstrates that the skeletal mechanism shows improved agreement with respect to all parameters studied, in particular the lami-

nar flame speed and the extinction strain rate. The LES results reveal that the choice of the reaction mechanism does not significantly influence the instantaneous or time-averaged velocity, whereas the instantaneous and time-averaged species and temperature are influenced. The agreement with the experimental data increases with increased fidelity of the reaction mechanism, and the skeletal reaction mechanism provides a more realistic basis for e.g. emission predictions.

N. Zettervall developed and analysed the propane-air reaction mechanism Z66, set-up and conducted the majority of the zero- and one-dimensional chemical kinetic simulations, and the analysis of these simulations. N. Zettervall also co-wrote the paper with the co-authors, focusing on the combustion chemistry section and Appendix 1.

Paper II: Skeletal Methane–Air Reaction Mechanism for Large Eddy Simulation of Turbulent Microwave-Assisted Combustion

A. Larsson, N. Zettervall, T. Hurtig, E. J. K. Nilsson, A. Ehn, P. Peterson, M. Alden, J. Larfeldt, C. Fureby (2017)
Energy & Fuels, vol. 31, pp. 1904–1926

Irradiating a flame via microwave radiation is a plasma-assisted combustion (PAC) technology that can be used to modify the combustion chemical kinetics in order to improve flame stability and to delay lean blow-out. One practical implication is that combustion engines may be able to operate with leaner fuel mixtures and have an improved fuel flexibility capability including biofuels. Furthermore, this technology may assist in reducing thermoacoustic instabilities, which is a phenomenon that may severely damage the engine and increase NO_X production. To further understand microwave-assisted combustion, a skeletal kinetic reaction mechanism for methane-air combustion is developed and presented. The mechanism is detailed enough to take into account relevant features, but sufficiently small to be implemented in large eddy simulations (LES) of turbulent combustion. The mechanism consists of a proposed skeletal methane-air reaction mechanism accompanied by subsets for ozone, singlet oxygen, chemionization, and electron impact reactions. The baseline skeletal methane-air mechanism contains 17 species and 42 reactions, and it predicts the ignition delay time, flame temperature, flame speed, major species, and most minor species well, in addition to the extinction strain, compared to the detailed GRI 3.0 reaction

mechanism. The amended skeletal reaction mechanism consists of 27 species and 80 reactions and is developed for a reduced electric field E/N below the critical field strength (of ∼125 Td) for the formation of a microwave breakdown plasma. Both laminar and turbulent flame simulation studies are carried out with the proposed skeletal reaction mechanism. The turbulent flame studies consist of propagating planar flames in homogeneous isotropic turbulence in the reaction sheets and the flamelets in eddies regimes, and a turbulent low-swirl flame. A comparison with experimental data is performed for a turbulent low-swirl flame. The results suggest that we can influence both laminar and turbulent flames by nonthermal plasmas, based on microwave irradiation. The laminar flame speed increases more than the turbulent flame speed, but the radical pool created by the microwave irradiation significantly increases the lean blow-out limits of the turbulent flame, thus making it less vulnerable to thermoacoustic combustion oscillations. Apart from the experimental results from low-swirl flame presented here, experimental data for validation of the simulated trends are scarce, and conclusions build largely on simulation results. Analysis of chemical kinetics from simulations of laminar flames and LES on turbulent flames reveal that singlet oxygen molecule is of key importance for the increased reactivity, accompanied by production of radicals such as O and OH.

N. Zettervall developed and analysed the methane-air reaction mechanism Z42, set-up and conducted some of the zero- and one-dimensional chemical kinetic simulations, as well as the three-dimensional LES of the low-swirl burner with and without microwave assisted combustion. N. Zettervall helped analyse the LES results of the low-swirl burner and co-wrote the paper with the co-authors, focusing mainly on the section with the low-swirl burner results.

Paper III:
Combustion LES of a Multi-Burner Annular Aero-engine Combustor using a Skeletal Reaction Mechanism for Jet-A Air Mixtures

N. Zettervall, E. Fedina, K. Nordin-Bates, E. Heimdal Nilsson, C. Fureby (2015)
51st AIAA/SAE/ASEE Joint Propulsion Conference
Orlando, Florida
AIAA - 4020

In this study we describe combustion simulations of a single sector and a

fully annular generic multi-burner aero-engine combustor. The objectives are to facilitate the understanding of the flow, mixing and combustion processes to help improve the combustor design and the design process, as well as to show that it is now feasible to perform high-fidelity reacting flow simulations of full annular gas turbine combustors with realistic combustion chemistry. For this purpose we use a carefully validated finite rate chemistry Large Eddy Simulation (LES) model together with a range of reaction mechanisms for kerosene-air combustion. The influence of the chemical reaction mechanism on the predictive capability of the LES model, and on the resulting understanding of the combustion dynamics has recently been proved very important and here we extend this for kerosene-air combustion. As part of this work a separate study of different kerosene-air reaction mechanism is comprised, and based on this evaluation the most appropriate reaction mechanisms are used in the subsequent LES computations. A generic small aircraft or helicopter aero-engine combustor is used, and modeled both as a conventional single sector configuration and more appropriately as a fully annular multi-burner configuration. The single-sector and fully annular multi-burner LES predictions are similar but with the fully annular multi-burner configuration showing different combustion dynamics and mean temperature and velocity profiles. For the fully annular multi-burner combustor azimuthal pressure fluctuations are clearly observed, resulting in successive reattachment-detachment of the flames in the azimuthal direction.

N. Zettervall developed and analysed the kerosene-air reaction mechanism Z57, set-up and conducted a majority of the zero- and one-dimensional chemical kinetic simulations, as well as the annular three-dimensional LES. N. Zettervall co-wrote the paper with the co-authors, focusing mainly on the combustion chemistry section and the section containing the LES results.

Paper IV: Small Skeletal Kinetic Mechanism for Kerosene Combustion

N. Zettervall, E. J. K. Nilsson, C. Fureby (2016)
Energy & Fuels, vol. 30(11), pp. 9801–9813

The development and validation of a new skeletal mechanism for kerosene combustion, suitable for reacting direct-, large-eddy, and Reynolds averaged Navier-Stokes Simulations, are presented. The mechanism consists of 65 irreversible reactions between 22 species and is built on a global fuel breakdown approach to produce a subset of C_2 intermediates. A more detailed set of reactions for $H/O/C_1$

chemistry largely determines the combustion characteristics. The mechanism is validated for combustion characteristics related to ignition, flame propagation, and flame extinction over a wide range of pressure, temperature, and equivalence ratios. Agreement with experiments and a more complex reference mechanism are excellent for laminar burning velocities and extinction strain rate, while ignition delays are overpredicted at stoichiometric and rich conditions. Concentration profiles for major stable products are in agreement with reference mechanism, and also a range of intermediate species and radicals shows sufficient agreement. The skeletal mechanism shows an overall good performance in combination with a numerical stability and short computation time, making it highly suitable for combustion Large Eddy Simulation (LES).

N. Zettervall developed and analysed the kerosene-air reaction mechanism Z65, set-up and conducted the majority of the zero- and one-dimensional chemical kinetic simulations, parts of the analysis and co-wrote the paper with the co-authors, focusing mainly on the mechanism development and mechanism validation sections.

Paper V:
Small Skeletal Kinetic Reaction Mechanism for Ethylene-Air Combustion

N. Zettervall, C. Fureby, E. J. K. Nilsson (2017)
Energy & Fuels, vol. 31, pp. 14138–114149

Ethylene is a fuel considered for high-speed ram- and scramjet combustion applications, mainly because of the short ignition delay time resulting from its high reactivity. Further research and development on these combustion systems would benefit from simulations of large eddy (LES) type, which allow some chemical detail to accurately predict combustion characteristics and pollutant formation. In the present work, a chemical kinetic mechanism suitable for LES is presented, consisting of 66 irreversible reactions between 23 species. The mechanism is extensively validated for combustion characteristics related to ignition and flame propagation over a wide range of pressure, temperature, and equivalence ratios that previously published mechanism of this size have not covered. Agreement with a detailed reference mechanism is good for ignition delay, flame temperature, and laminar burning velocities. In addition, overall concentration profiles of major stable products are in overall good agreement with a reference mechanism. The skeletal mechanism shows an overall good performance in combination with a numerical stability and short computation time, making it highly

suitable for combustion LES.

N. Zettervall developed and analysed the ethylene-air reaction mechanism Z66, set-up and conducted the zero- and one-dimensional chemical kinetic simulations, collected all experimental data, made a majority of the plots, parts of the analysis and wrote a majority of the paper.

Paper VI: Large eddy simulation of CH_4-air and C_2H_4-air combustion in a model annular gas turbine combustor

N. Zettervall, N. A. Worth, M. Mazur, J. R. Dawson, C. Fureby (2019) Proceedings of the Combustion Institute, vol. 37, pp. 5223–5231

Combustion instabilities are one of the major challenges in developing and operating propulsion and power generating gas-turbine engines. More specifically, techniques for managing the increasingly stringent emissions regulations and efficiency demands have often given rise to thermo-acoustic instabilities, particularly for annular combustors operating in a lean premixed mode. In this paper, we combine experimental and computational methods to examine unsteady gas turbine combustion in a full annular model gas turbine combustor installed at NTNU, operating both methane- and ethylene-air blends. The experimental data consists of flame images, high-speed OH chemiluminescence images, as well as pressure and heat-release time-series at discrete locations for the ethylene-air case. The computational set-up consists of the 18 inlet tubes and swirlers, and the full annular combustor placed in a large external domain. The computational model consists of a compressible finite rate chemistry LES model using skeletal methane-air and ethylene-air combustion chemistry. The combustor is simulated in its self-excited state, without external forcing. From the experiments and simulations the methane and ethylene cases are found to behave differently: The ethylene-air flames are much smaller than the methane-air flames, resulting in different interaction between adjacent flames. The LES predictions show good qualitative agreement with the measurements in terms of instantaneous and time-averaged flame structure. Comparing measured and predicted time-series of pressure and heat-release also shows good quantitative agreement with respect to the dynamics and structure for the ethylene-air case. Investigating the predicted combustion dynamics using Proper Orthogonal Decomposition (POD) confirms the importance of the self-excited azimuthal mode on the behavior of the flame: the presence of nodes and anti-nodes of pressure induced fluctuations of the swirler mass-flow, which then, in turn, influence the heat-release. These*

events occur shifted in time.

N. Zettervall made the computational mesh, conducted the zero- and one-dimensional chemical kinetic simulations, as well as the three-dimensional LES, made all plots and all figures of the LES results, parts of the analysis and co-wrote the paper with the co-authors, focusing on the combustion chemistry section and the section containing the LES results.

Paper VII:
A reduced chemical kinetic reaction mechanism for kerosene-air combustion

N. Zettervall, C. Fureby, E. J. K. Nilsson (2020)
Fuel, vol. 269, pp. 117446

Development of a new reduced chemical kinetic reaction mechanism for kerosene-air combustion is presented. The new mechanism uses a modular based development technique and is a further development on previously presented kerosene-air mechanisms. The new mechanism consists of 30 species and 77 irreversible reactions and is developed to accurate reproduce key flame parameters yet being small enough to be used in finite rate Large Eddy Simulations (LES), Direct Numerical Simulations (DNS) and in Reynolds Average Navier-Stokes (RANS) simulations. The well-proven development technique uses a refined fuel break-down oxidation sub-mechanism, a simplified C_2 intermediate species sub-mechanism and a more detailed set of reactions for the $H/C_1/O$ chemistry. The mechanism has been modified to be able to predict ignition delay times for a wide range of temperatures, including in the negative temperature regime. The mechanism has been evaluated for combustion parameters related to flame propagation and ignition over a wide range of equivalence ratios, initial gas temperatures and pressures. Agreements to experimental data and a set of detailed and skeletal mechanisms are good for all target parameters. The proposed mechanism shows good agreement at a computational cost far below all tested reference mechanisms, making it highly suitable for use in combustion computational fluid dynamic (CFD) simulations.

N. Zettervall developed and analysed the kerosene-air reaction mechanism Z77, set-up and conducted the zero- and one-dimensional chemical kinetic simulations, collected all experimental data, made all plots, all of the analysis and wrote the majority of the paper.